2019-12

Conformance Control for SAGD Using Oil-in-Water Emulsions in Heterogeneous Oil Sands Reservoirs

Ni, Yidan

UNIVERSITY OF CALGARY

Conformance Control for SAGD Using Oil-in-Water Emulsions in Heterogeneous Oil Sands Reservoirs

by

Yidan Ni

A THESIS

SUBMITTED TO THE FACULTY OF GRADUATE STUDIES

IN PARTIAL FULFILMENT OF THE REQUIREMENTS FOR THE

DEGREE OF MASTER OF SCIENCE

GRADUATE PROGRAM IN CHEMICAL ENGINEERING

CALGARY, ALBERTA

DECEMBER, 2019

Abstract

Steam-Assisted Gravity Drainage (SAGD) is a widely used technology for heavy oil and bitumen recovery in Alberta, Canada. However, a SAGD conformance problem can arise due to the heterogeneity of oil sands reservoirs, such as the presence of high permeability zones and high water saturation zones. In particular, during a geomechanical dilation start-up process that has been developed and applied in SAGD start-up operations, the dilation fluid tends to flow into the high permeability zones, leaving the low permeability zones un-swept. Therefore, the high permeability zones must be temporarily and selectively blocked off so as to more effectively dilate the low permeability zones along a SAGD well-pair.

Laboratory permeability reduction tests in sandpacks using oil-in-water (O/W) emulsion injection showed that a permeability reduction of up to 99.97% can be achieved. Results of emulsion injection in parallel-sandpack tests demonstrated that good conformance control can be obtained by a suitable combination of interfacial tension (IFT), emulsion quality, emulsion slug size, and oil phase viscosity of an emulsion system. The reservoir simulation study was conducted to first match the laboratory test results and then to optimize SAGD conformance control operations using emulsion injection in heterogeneous oil sands reservoirs. A field-scale SAGD simulation model was established to show that emulsion injection before the dilation start-up process can build up communication between the injector and producer, resulting in more uniform steam chamber growth, lower cumulative Steam-to-Oil ratio (cSOR), and higher cumulative oil production.

Acknowledgements

I want to express sincere appreciation to my supervisor Dr. Mingzhe Dong for his great supervision and helpful instructions for my studies at the University of Calgary.

I am also grateful to my co-supervisor Dr. Ian G. Gates for his valuable suggestions regarding my thesis research.

I am also grateful for the support from Bitcan, PetroChina Canada and Natural Sciences and Engineering Research Council (NSERC) of Canada through an NSERC CRD grant.

Dedication

To my parents,

Thanks for their support and love

Table of Contents

List of Tables

List of Figures and Illustrations

List of Symbols and Abbreviations

Symbols

$RF_{high\ k}$	Retention factor for high permeability sandpack	Dimensionless
$RF_{low\ k}$	Retention factor for low permeability sandpack	Dimensionless
$RF_{new\ high\ k}$	Retention factor for high permeability sandpack after correlation	Dimensionless
$RF_{new\ low\ k}$	Retention factor for low permeability sandpack after correlation	Dimensionless
RF_{block}	Retention factor at each O/W emulsion property	Dimensionless
RF_{max}	Maximum retention factor	Dimensionless
RF_{2PV}	Retention factor after 2 PV of waterflooding	Dimensionless
CAP_{block}	Capture coefficient at each O/W emulsion property	Dimensionless
CAP_{max}	Maximum capture coefficient	Dimensionless
$CAP_{residual}$	Capture coefficient after 2PV of waterflooding	Dimensionless
L_b	Base emulsion slug size	PV
$L_{low\ k}$	Emulsion slug size entered into the low permeability sandpack	PV
$L_{hign\ k}$	Emulsion slug size entered into the high permeability sandpack	PV
$CAP_{residual\ high\ k}$	Capture coefficient after 2PV of waterflooding for high permeability sandpack	Dimensionless
$CAP_{residual\ low\ k}$	Capture coefficient after 2PV of waterflooding for low permeability sandpack	Dimensionless

Abbreviations

O/W emulsion	Oil-in water emulsion
SAGD	Steam-Assisted Gravity Drainage
CSS	Cyclic Steam Stimulation
CWE	Cold Water Equivalents
cSOR	Cumulative Steam-to-Oil Ratio
IFT	Interfacial Tension
RF	Retention Factor
CAP	Capture Coefficient
PV	Pore Volume
ΔP	Pressure Drop
cP	Centipoise

Chapter 1. Introduction and Literature Review

1.1 Background

Canada has heavy oil and bitumen (oil sands) reserves of 1.7 trillion barrels, which makes it the third-largest oil reserve country in the world, after Saudi Arabia and Venezuela. Specifically, the largest reserves of heavy oil and oil sands are located in Alberta, mainly in Athabasca, Cold Lake, and Peace River (Nasr and Ayodele, 2005). The viscosity of oil sands in Alberta can reach to million centipoise (cP), and it can be reduced to lower than 10 cP when the temperature is above 196℃ (Gates and Chakrabarty, 2008). The Athabasca oil sands has highest in-situ viscosity, which is about 5,000,000 cP, compared with 100,000 cP in Cold Lake and 200,000 cP in Peace River. Because the oil sands are not mobile in the reservoirs due to such extremely high viscosity. Therefore, viscosity reduction is the dominant mechanism for oil sands recovery. There are 2 common bitumen extraction techniques employed in the oil sands reservoirs: Mining and In-situ methods. Bitumen can only be extracted in-situ if the oil sands deposit is more than 200 meters below the surface, while mining operations are typically less than 75 meters below grade. Around 80% of bitumen is produced using in-situ method. Among the main thermal in-situ recovery techniques, such as Steam-Assisted Gravity Drainage (SAGD), steam flooding, and Cyclic Steam Stimulation (CSS), SAGD is recognized as a mainstream technology for producing oil from oil sands reservoirs. Viable SAGD production strongly depends on the development of the steam chamber since oil is essentially only produced from the heated zones. Therefore, a uniform and stable development of the steam chamber can conduct more heat to the cold bitumen, which eventually leads to higher cumulative oil production with less steam consumption.

1.2 SAGD Process

The concept of SAGD was introduced originally by Butler in the late 1970s, and the SAGD process was proposed by Butler and his colleagues thirty years ago (Butler, 1998). In this process, one injection well and one production well as a well pair are drilled in the pay zone, as shown in Figure 1.2.1. The producer is located parallel below the injector, with a vertical distance of 5 to 10 meters (Butler 1981). After few months of nonproductive steam circulation to preheat the areas between the well pair, steam is injected into the reservoir through the injection well and creates a steam chamber to heat the cold bitumen. Heated oil and condensate fluid will be drained by gravity force along the edge of the chamber to the producer (Butler 1987).

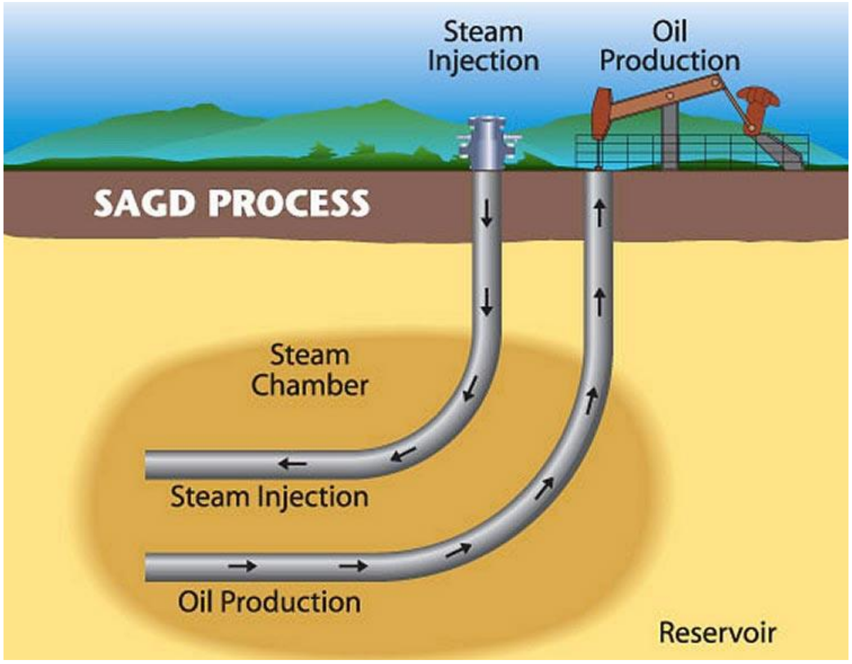

Figure 1.2.1. Schematic of SAGD Process (Courtesy of Canadian Centre for Energy Information).

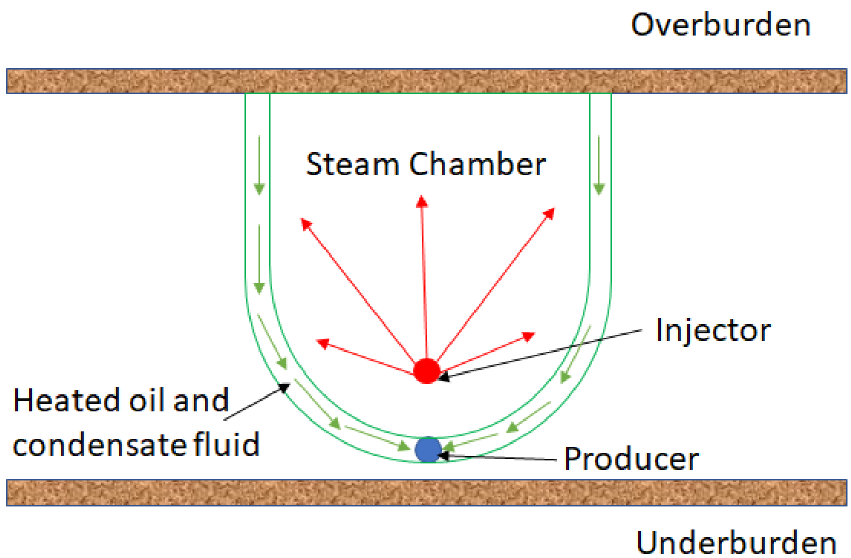

Figure 1.2.2. Schematic of SAGD steam chamber.

The development and characteristics of the steam chamber are important to show a successful SAGD production, because most of the oil is produced from the area near the vapor-liquid interface at the boundary of the steam chamber as shown in Figure 1.2.2. The steam chamber rises vertically at an early stage and begins to grow laterally once it touches the overburden of the reservoir (Ito and Ipek, 2005). The latent heat from the injected steam was transferred to heat the cold oil by both conduction and convection (Edmunds, 1999; Wang et al., 2012). The heterogeneity of oil sands reservoirs has a significant effect on SAGD process (Shin and Choe, 2009). Many oil sands reservoirs are heterogeneous, containing high permeability zones and generally at least one high water saturation zone. It is unlikely that there would be a uniform steam chamber in a heterogeneous oil sands reservoir. Gotawala and Gates (2010) studied several heterogeneous oil sands reservoirs and concluded that these reservoir heterogeneities cause unequal steam chamber growth, resulting in some low mobility regions not being affected by steam injection.

Before the normal SAGD production stage, a SAGD start-up process should be conducted to build up inter-well communication by implementing steam circulation for both injection well and production well (Parmar et al., 2009). Normally, duration time for the SAGD start-up process is about 3 to 6 months. Once the desired temperature profile has been observed between the well pair, it can be switched to the normal SAGD production stage (Vincent et al., 2004).

During SAGD production time, a steam trap control method should be used to prevent live steam production from the steam chamber by maintaining a liquid pool above the producer as shown in Figure 1.2.3, in order to reduce steam loss and cSOR (Doan et al., 1999). One control strategy would be subcool control method, which keeps a temperature difference between steam been injected and fluid been produced. Gotawala and Gates (2012) mentioned that it is important to control the temperature difference in a moderate level, since if this temperature difference is small, then the liquid pool above the injector is shallow and the ability of liquid pool to prevent live steam production is limited. However, when the temperature difference is large, the injector may be submerged by the liquid pool, and the gravity drainage would be interrupted. In simulation models, the steam trap control method can be simulated by constraining the producer with maximum steam rate (Gates and Chakrabarty, 2008).

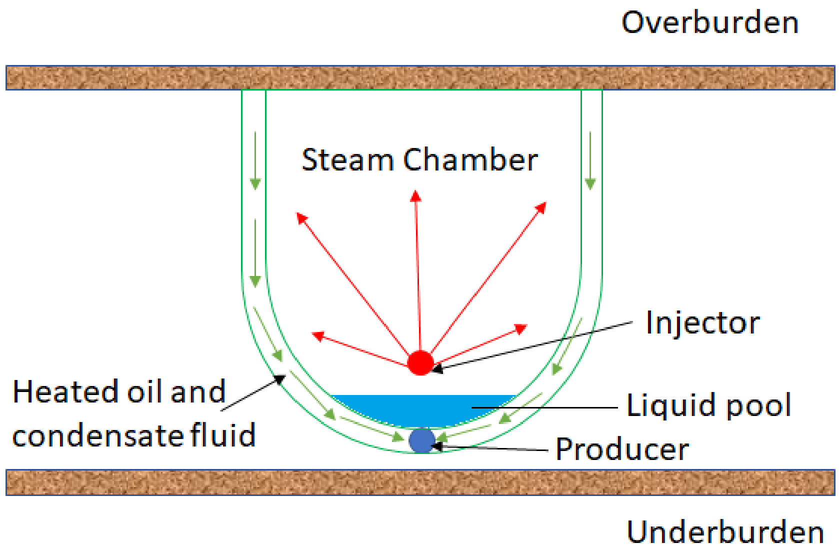

Figure 1.2.3. Schematic of SAGD steam chamber with a steam trap control.

The main cost of the SAGD process is the consumption of extensive steam injected into the reservoir. The volume of steam required to produce one unit of oil can be measured by cumulative Steam-to-Oil ratio, which is commonly abbreviated as cSOR. The cSOR varies from 2 to 10 m^3/ m^3 (Butler, 1998). The lower the cSOR, the less steam used to produce oil. According to Edmunds and Chhina (2001), the economics of the SAGD process are more sensitive to cSOR than the oil production rate, which means cSOR is an important indicator of whether or not the SAGD process is economical.

1.3 Dilation Start-up Process

A dilation start-up process has been proposed to achieve more uniform thermal conformance along SAGD well pairs (Yuan et al., 2011; Yuan and McFarlane, 2009). Using a short-period of high-pressure fluid injection, the dilation start-up creates high porosity zones between the well pair that vertically connects the SAGD well pair and laterally becomes uniform along the well length (Zhang et al., 2016). The dilation start-up process is applied before SAGD start-up, and it aims to allow more convective heat transfer through the dilation zone (microcracks) to the inter-well area, compared to conventional SAGD start-up. Finally, the dilation start-up process can shorten the steam circulation (preheating) time and lead to less steam consumption before converting to the normal production stage.

The dilation start-up process was applied in the Xinjiang oilfield beginning in 2013 and expanded to include all SAGD wells in 2015. The field results demonstrated the dilation start-up process could reduce 70-80% of steam circulation time. In addition, increased oil production rate and reduced cSOR were the main parameters to illustrate the success of using the dilation start-up process. (Zhang et al., 2016)

Yuan et al. (2013) implemented the dilation start-up process in Karamay, which worked successfully on the one demonstration well. After three weeks of steam circulation, 80 to 90% of the inter-well area was measured to have high temperature profiles, which showed the dilation start-up process could assist thermal conformance between the well pair and along the well length.

1.4 Problem Statement

The difficulty with using the dilation start-up process is that the dilation fluid tends to escape through the high mobility zones, making it challenging to dilate the low permeability zones. Liu et al. (2010) indicated that water channeling is a big issue for waterflooding and chemical flooding process. An early breakthrough of injected water and chemicals can be found in high permeability channels/zones. Therefore, it is essential to temporarily block high permeability zones and push the dilation fluid to flow into the low permeability zones, in order to enhance the dilation start-up process in a heterogeneous oil sands reservoir.

1.5 Conformance Control Methods for Conventional Oil Reservoirs

Various conformance control methods to reduce fluid flow in high permeability zones have been widely studied by researchers. For conventional oil reservoirs, the dominant technology that has been used for water shutoff is the injection of plugging agents such as cements (Borling et al., 1994), polymer combined with cross-linker (Liu et al., 2017; El-Karsani et al., 2014), resin (Kabir 2001), or other gel-like agents (Bai and Zhang, 2011; Imqam and Bai, 2015; Sang et al., 2014). As Moradi (2010) mentioned, selection of the proper gel for the preparation of a plugging agent is a complicated process because it is influenced by temperature, the hardness level of water, and salinity as well as lithology, and the cost of such treatment should also be carefully considered. The use of cement can give rise to potential formation damage (Kabir 2001), and it is not able to elongate the gelation time as expected (El-Karsani et al., 2014). Dai et al. (2010) illustrated that some polymers used for water shutoff are not suitable for large volume treatment, and most of the injected polymers accumulate near the wellbore, which would not support deep propagation. These uncertainties and disadvantages make conformance control methods used for conventional oil reservoirs not easily applied to oil sands reservoirs. Especially when applying the dilation start-up process in oil sands reservoirs, the injected conformance control substance should not permanently block the high permeability channel/zone but needs to have sufficient strength to prevent dilation fluid from fingering through high permeability channels/zones. However, an oil-in-water (O/W) emulsion has been proposed as a promising method to reduce fluid flow in high permeability zones during the dilation start-up process, based on its several advantages and successful implementation in lab work and field tests.

1.6 O/W Emulsion as a Conformance Control Method

1.6.1 Mechanism of O/W Emulsion Blockage

An O/W emulsion can easily be prepared from oils, alkalis, and surfactants. Alkali and surfactant are first added into water and then mixed with oil to generate O/W emulsion (Sagitani, 1981). In-situ O/W emulsion can be formed by the synergy between alkali and surfactant when the IFT is reduced between oil and water during alkaline-surfactant flooding (Liu et al., 2006). The pore throats blocked by the oil droplets contained in the O/W emulsion can be treated as the mechanism for O/W emulsion to reduce fluid flow. The blockage mechanism can be explained based on the size comparison between oil droplets contained in O/W emulsion and pore throat. As shown in Figure 1.6.1, the oil droplet in emulsion deformed to pass through the pore throat, which gives resistance to the fluid flow when the oil droplet size is larger than the pore throat. This phenomenon is also called "Jamin" effect (Jamin, 1860; McAuliffe, 1973a).

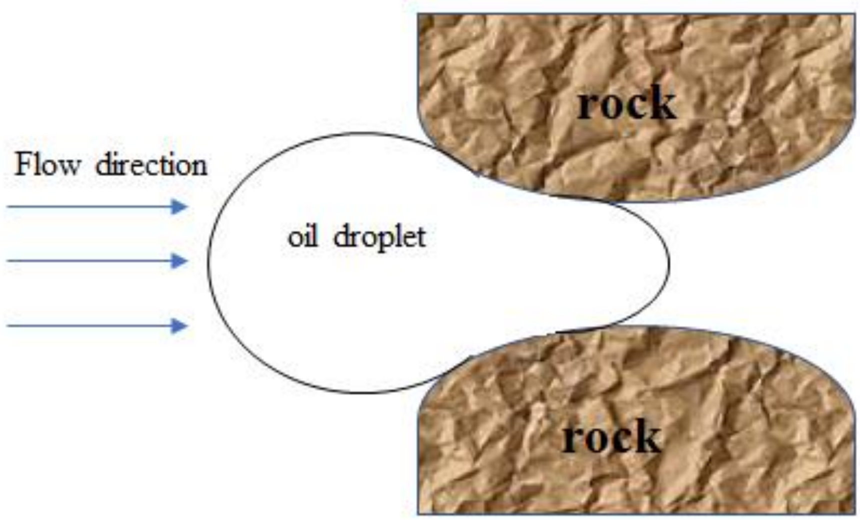

Figure 1.6.1 Oil droplet flows through pore throat.

Soo and Radke (1984) proposed that oil droplet, which size is smaller than the pore throat, can also have plugging ability. The diameter of pore throat is decreased when the smaller oil droplets starts to crowding and captured by the wall of pore throat, as shown in Figure 1.6.2. A decrease in diameter of pore throat can cause flow path reduction. Therefore, the fluid flow is reduced.

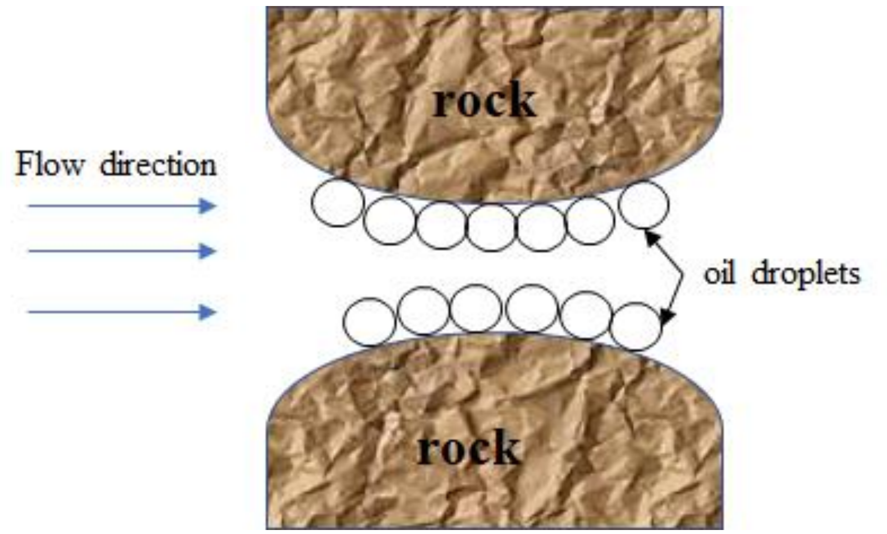

Figure 1.6.2. Oil droplets captured by the wall of pore throat.

1.6.2 Lab and Field Tests of Using O/W Emulsion

Romero et al. (1996) demonstrated that an O/W emulsion can be easily transported to the oilfield and injected into the formation because its viscosity is comparable to that of water. Injection of an O/W emulsion can block high permeability zones and improve oil recovery due to trapped emulsions (Dong et al., 2012; Wang and Dong, 2010). McAuliffe (1973a) also concluded that the injection of a prepared O/W emulsion was able to have a deep penetration distance and to decrease flow in high permeability porous media, and thereby improving fluid distribution. It has been shown that the technology of oil-in-water (O/W) emulsions deployed in sandpacks can improve sweep efficiency and increase the effectiveness of oil recovery (Mandal et al. 2010).

Jennings et al. (1974) did coreflood tests on heavy oils, and the experimental results showed that the water channels could be blocked by the injection of in-situ O/W emulsion, thereby diverting the flow to improve the total sweep efficiency. The O/W emulsion is not a permanent plugging agent since it can be removed by de-emulsification, which leads to less damage to the formation. Experimental results show the O/W emulsion is a good plugging agent to block high permeability core/sandpack, and it also been proved that using O/W emulsion flooding in field tests can improve sweep efficiency and increase oil recovery.

According to McAuliffe (1973b), a field test was conducted in section 5K of the MidWay-Sunset Oilfield near Taft, California. The sands in the formation are the Top oil sands and the Kinsey oil sands. Waterflooding was started in September 1962, and the water cut was found to increase from approximately 25% in 1962 to approximately 92% in 1965. The O/W emulsion was injected into three wells in April 1967. An increase in oil production and a decrease in water cut can be observed after the emulsion injection. A favorable change in flood patterns was also observed after emulsion injection. Sweep efficiency was also improved by obtaining more produced formation water after emulsion injection, and an increased salinity can be observed in the produced water. According to Zhou et al. (2019), the in-situ O/W emulsion helped to decrease the water cut from 96.9% to 80.7% for the Xing-V well in the Daqing Oilfield, China. The water cut decreased from 100% to 50.7%, and increased oil recovery of more than 20% for the Xing-II well in the Daqing Oilfield was also observed.

1.6.3 Key Parameters Affecting Plugging Ability of O/W Emulsion

Yu et al. (2017) conducted experiments to investigate the effects of IFT and emulsion droplets size on permeability reduction. The results showed that a greater IFT caused greater permeability reduction because the capillary resistance force created by the emulsion when it passing through the pore throats was proportional to IFT. In the other word, it is difficult for the subsequent water to push an emulsion with higher IFT flow through pore throats. Therefore, greater permeability reduction occurred. The results also indicated that larger emulsion droplets were more easily trapped in the pore constrictions, which could cause larger resistance force to the fluid flow. Thus, an emulsion with a larger droplet size has strong plugging ability that leads to greater permeability reduction.

Yu et al. (2018a) conducted permeability reduction tests in single sandpack, and the purpose of these tests was to determine the permeability reduction caused by plugging strengths of O/W emulsions by observing the pressure drop curves at different properties, such as oil quality, sandpack permeability, injection flow rate, and emulsion slug size. Oil quality is also called emulsion quality represents the concentration of an O/W emulsion. As shown in Figure 1.6.3, the emulsion with an oil quality of 10 wt% contains more oil droplets than with an oil quality of 5 wt%. The injection process for this permeability reduction test included an O/W emulsion injection stage, and the extended water injection stage. The results for each emulsion property are described as follows:

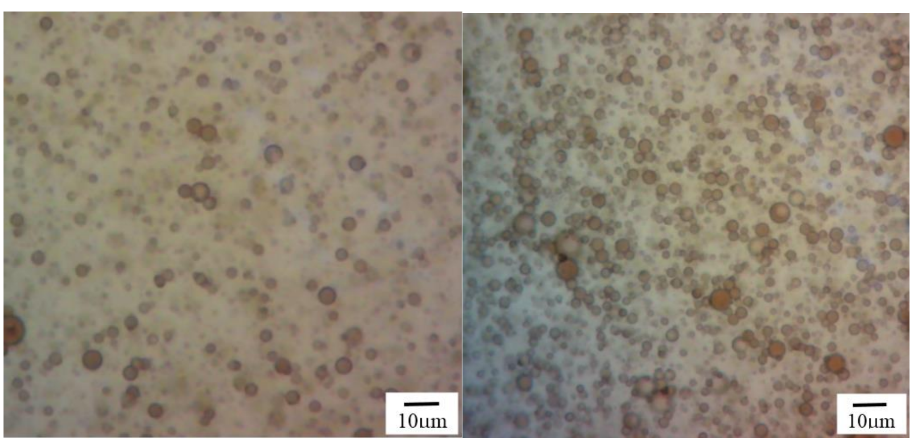

(a) (b)

Figure 1.6.3. Microscopic pictures of emulsions with different oil qualities:
(a) 5 wt%, (b) 10 wt%

For oil quality, the highest permeability reduction of sandpack was 99.95 % when using emulsion with an oil quality of 10 wt%, and the permeability reduction decreased to 99.47% when using emulsion with an oil quality of 2.5 wt%. Even after the sandpack was flooded by 2 PV of extended water, the permeability reduction was still around 99.92% and 98.99%, respectively. This indicated that the plugging ability of emulsion increased as oil quality increased and a good plugging performance of emulsion in the subsequent water flooding process was also observed.

For emulsion slug size, the largest permeability reduction was observed around 99.97% at the largest emulsion slug size, and it decreased to 99.34% at the smallest emulsion slug size. The permeability reduction remained effective even after the emulsion was flooded by 2PV of extended water. The results also mentioned that the largest pressure drop for injection of larger emulsion slug size started to decline due to the breakthrough of emulsion front. And for the injection of smaller emulsion slug size, a decrease in the largest pressure drop caused by the breakthrough of displacing water from the emulsion zone in the sandpack.

For sandpack permeability, as sandpack permeability increased, the largest permeability reduction and highest pressure drop decreased. High permeability sandpack contains pore throats with larger diameters than in low permeability sandpack, that makes oil droplets in the O/W emulsion difficult to trapped in the pore constriction, and leads to a decrease in plugging strength. Therefore, a decrease in permeability reduction caused by the O/W emulsion was observed as sandpack permeability increased.

For injection flow rate, a slight change in permeability reduction was observed at different injection flow rates during different injection stages. The largest permeability reduction decreased as the injection flow rates increased. The largest permeability reduction at the lowest flow rate was 99.87%, and it at the highest flow rate was 99.85%. After 2PV of extended water injection, the permeability reduction decreased to 99.79% for the emulsion with lowest injection flow rate and it decreased to 99.70% for the emulsion with highest injection flow rate.

Yu et al. (2018b) conducted conformance control tests in parallel-sandpack models to investigate the effect of IFT on conformance control performance of O/W emulsions by observing the fractional flow curves of the high permeability sandpack and the low permeability sandpack during the emulsion injection stage and extended waterflooding stage. When an ideal fractional flow (50:50) can be reached, a good conformance control in the parallel-sandpack was achieved. It was found that injection of an O/W emulsion with moderate IFT can achieve good conformance control performance because the emulsion with moderate IFT not only have sufficient plugging strength to block the high permeability sandpack, but also have favorable deformability and flexibility to move deeply into the parallel-sandpacks. The result also illustrated that larger emulsion slug size could improve conformance control performance at moderate IFT. An improved oil phase viscosity and IFT can assist the plugging ability when injecting O/W emulsion into a severely heterogeneous sandpacks (greater permeability ratio). Ding et al. (2019) also indicated that a carefully designed O/W emulsion with moderate IFT, oil phase viscosity, and droplet size can plug the high permeability sandpack effectively and penetrate deeply int both the high permeability sandpack and the low permeability sandpack, thus achieving good conformance control performance.

1.7 Objectives

The objectives of this thesis are as follows:

(1) To build a simulation model using the STARS module in the Computer Modelling Group (CMG, 2015) simulator to simulate the permeability reduction test in the single sandpack experiments conducted by Yu et al. (2018a) and to match the pressure drop curves from the experimental results.

(2) The history-matched simulation model can then also be used to investigate the effect of the combination of IFT, emulsion oil quality, emulsion slug size, and oil phase viscosity on conformance control performance by first matching the experimental results conducted by Yu et al. (2010b), and then a sensitivity tests are conducted to find optimal combination of different emulsion properties to achieve good conformance control performance.

(3) A conceptual field-scale model is proposed to investigate the effects of an O/W emulsion treatment on improving the dilation start-up process to achieve better SAGD conformance control by observing steam chamber growth, cumulative oil production, and cSOR reduction.

1.8 Thesis Outline

This thesis consists of four chapters, as follows:

Chapter One: In this chapter, the mechanism and main parameters of the SAGD process are described. The dilation start-up process is introduced, and the difficulty of using this process because of reservoir heterogeneity is also described in detail. The main technology used for water shutoff for conventional oil reservoirs and its uncertainty in application as a conformance control method in oil sands reservoirs is stated. The O/W emulsion is proposed to be a promising plugging agent that can assist the dilation start-up process.

Chapter Two: This chapter summarizes the experimental details conducted by Yu et al. (2018a) and Yu et al. (2018b).

Chapter Three: In this chapter, First, a mechanism of establishing the simulation model is introduced. The retention factor and capture coefficient are two parameters used in the simulation model. The simulation model matches the experimental results of permeability reduction in a single sandpack. Second, the optimal combination of emulsion quality, slug size, IFT, and oil phase viscosity can be found to achieve good conformance control for parallel-sandpack tests. A sensitivity test using O/W emulsion with a high oil phase viscosity is simulated to find a critical combination of emulsion properties, in order to obtain good conformance control. Last, conceptual field-scale models are established to demonstrate the results of applying an O/W emulsion treatment before the dilation start-up process by observing steam chamber growth, cSOR, and cumulative oil production.

Chapter Four: This chapter summarizes the main conclusions and introduces recommendations for future study.

Chapter 2. Experiments Summary

2.1 Emulsion Permeability Reduction Tests in single Sandpack Model (Yu et al., 2018a)

According to Yu et al. (2018a), O/W emulsions were injected into the sandpack with a diameter of 2.5 cm and a length of 30 cm at different oil qualities, sandpack permeabilities, emulsion slug sizes and flow rates. The purpose of these experiments was to investigate the permeability reduction during the O/W emulsion injection stage and subsequent water injection stage. In this experiment, a 0.1 wt% concentration of surfactant (Span 60 and Tween 80) combined with 0.025 wt% NaOH were used to make a heavy crude oil with viscosity of 1200 mPa.s at 60℃ emulsify in water by using mulser (T25, IKA, Germany) at a specific stirring speed for a specific stirring time. The O/W emulsions were characterized by their stabilities, droplet sizes and rheological properties. The stability of O/W emulsions was tested by observing the creaming ratio. The creaming ratio can be obtaining by using height of the creamed emulsion divided by the whole emulsion system. The droplet size distribution of emulsions was measured by a laser particle size distribution analyzer (Bettersize 2000, Dandong better, China). The bulk viscosity of O/W emulsion at different shear rate, and the relationship between shear stress and shear rate were measured to demonstrate the rheological properties of O/W emulsions.

The experimental apparatus used for this permeability reduction tests consisted of a displacement pump (Teledyne ISCO, USA) used to inject water and O/W emulsions holding in the cylinders into the prepared sandpack (uniform permeability). A pressure transducer was connected at the inlet of sandpack to measure the pressure drops at different injection stages. A graduated measuring cylinder was connected at the outlet of sandpack which can collect the injected fluid. The flow resistance and permeability reduction for the O/W emulsion with different properties at different injection stages are listed from Table 2.1 to Table 2.4.

Table 2.1. Flow resistance and permeability reduction for O/W emulsions with different oil qualities.

Oil quality, wt%	Flow resistance at the largest pressure drop	Flow resistance at the residual pressure drop (2PV of extended water injection)	Largest permeability reduction, %	Residual permeability reduction, %
2.5	189.8	99.3	99.47	98.99
5.0	759.3	464.3	99.87	99.78
7.5	1684.6	751.3	99.94	99.87
10	2111.7	1298.2	99.95	99.92

Table 2.2. Flow resistance and permeability reduction for O/W emulsions with different sandpack permeabilities.

Permeability, mD	Flow resistance at the largest pressure drop	Flow resistance at the residual pressure drop (2PV of extended water injection)	Largest permeability reduction, %	Residual permeability reduction, %
700	940.7	520	99.89	99.81
980	759.3	464.3	99.87	99.78
1630	334.8	162.5	99.70	99.38
2450	127	90.2	99.21	98.89

Table 2.3. Flow resistance and permeability reduction for O/W emulsions with different injection flow rates.

Flow rate, mL/min	Flow resistance at the largest pressure drop	Flow resistance at the residual pressure drop (2PV of extended water injection)	Largest permeability reduction, %	Residual permeability reduction, %
0.1	786.3	473.7	99.87	99.79
0.2	775.5	569.5	99.87	99.79
0.3	759.3	464.3	99.87	99.78
0.5	660.7	334	99.85	99.70

Table 2.4. Flow resistance and permeability reduction for O/W emulsions with different emulsion slug sizes.

Slug size, PV	Flow resistance at the largest pressure drop	Flow resistance at the residual pressure drop (2PV of extended water injection)	Largest permeability reduction, %	Residual permeability reduction, %
0.3	152.3	473.7	99.34	99.00
0.5	759.3	464.3	99.87	99.78
0.7	1609.2	906	99.94	99.89
1.0	3087.4	2010.7	99.97	99.95

Figure 2.1.1 shows a linear relationship between flow resistance created by O/W emulsion and oil quality. The flow resistance increases as the oil quality increases because the O/W emulsion with higher oil quality can create higher plugging strength. The oil quality of O/W emulsion is an important factor to explain the permeability reduction caused by the blockage of emulsion droplets.

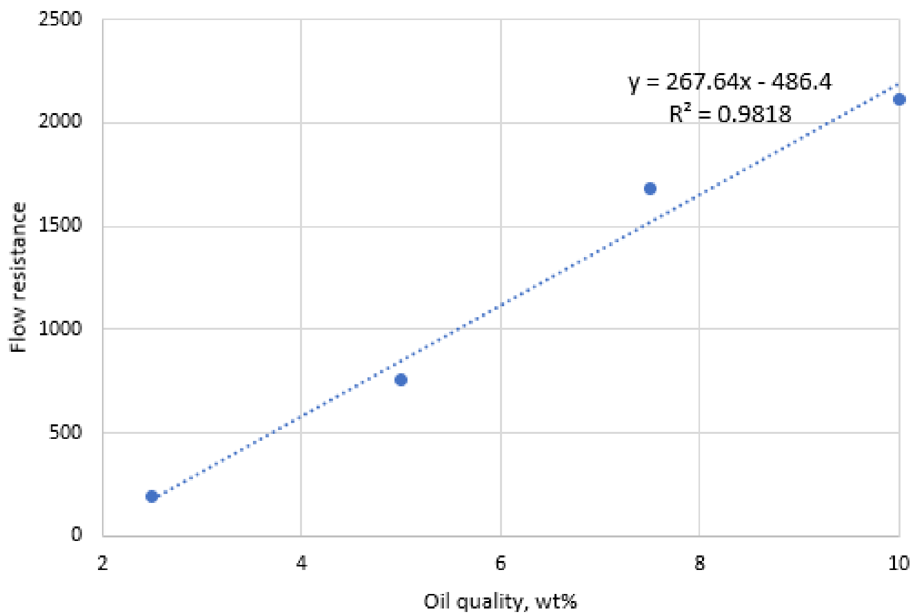

Figure 2.1.1. The relationship between flow resistance and oil quality.

Figure 2.1.2 shows an exponential relationship between flow resistance created by O/W emulsion and sandpack permeability. The flow resistance decreases as the sandpack permeability increases because the O/W emulsion can easily pass through the sandpack with a higher permeability. It indicates that the emulsion property such as oil quality or slug size needs to be adjusted to a higher value if the high permeability sandpack is desired to be blocked.

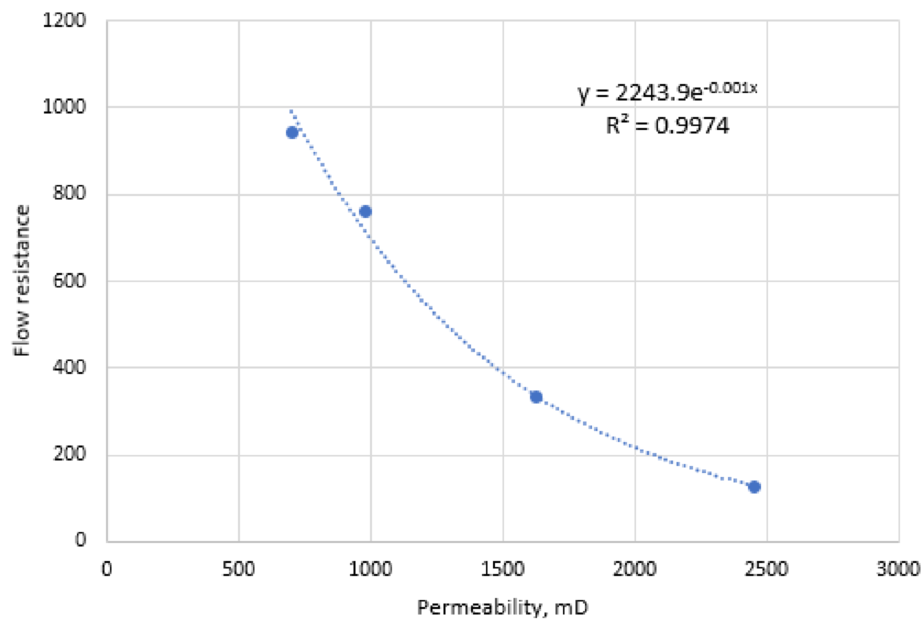

Figure 2.1.2. The relationship between flow resistance and sandpack permeability.

Figure 2.1.3 shows a linear relationship between flow resistance and injection flow rate. The slope of this curve is quite smooth, which means the flow rate has little impact on the change of flow resistance.

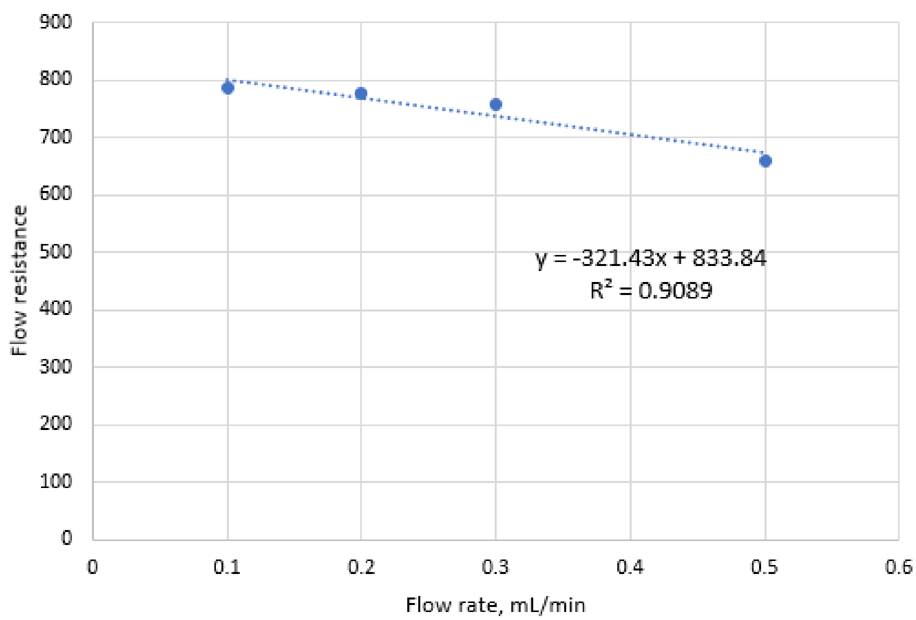

Figure 2.1.3. The relationship between flow resistance and flow rate.

Figure 2.1.4 shows a linear relationship between flow resistance and slug size of emulsion injection. Injecting O/W emulsion with a larger slug size can create higher plugging strength to block the sandpack compared with injecting emulsion with a shorter slug size. The change of emulsion slug size can be used to block the sandpack with different permeabilities.

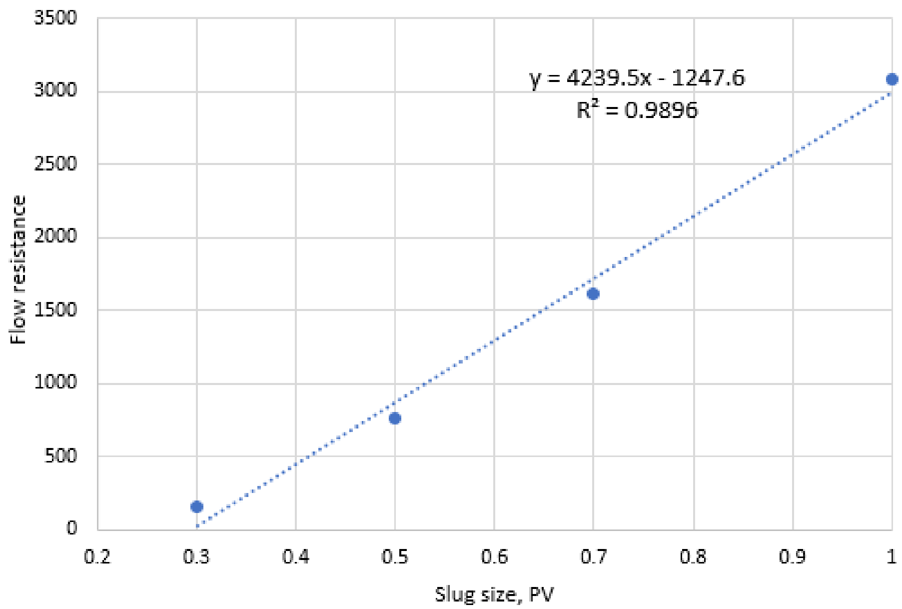

Figure 2.1.4. The relationship between flow resistance and slug size.

2.2 Emulsion Conformance Control Tests in Parallel-sandpack Models (Yu et al., 2018b)

Yu et al. (2018b) conducted conformance control tests in parallel-sandpack models. The high permeability sandpack (sandpack 1) and low permeability sandpack (sandpack 2) used in this experiment had the same diameter and length, which was 2.5 cm and 30 cm, respectively. The experiments were conducted to investigate the effect of IFT, slug size of emulsion, permeability ratio of sandpacks, and oil phase viscosity on the performance of conformance control by measuring pressure drops and fractional flow curves. In this experiment, Sand (Jiangsu Haian Petroleum Chemical Factory, China) with 40-60 mesh was used to make high permeability sandpacks, and sand (Jiangsu Haian Petroleum Chemical Factory, China) with 100-120 mesh was used to make low permeability sandpacks. The sandpacks were saturated with water via imbibition method. 0.5 wt% of Span40 combined with 0.5 wt% of EL-80, 1 wt% of Triton X-100, 0.5 wt% of Triton X-100, and 0.5 wt% of Span40 combined with 0.5 wt% of Tween80 were used as emulsifiers to form an emulsion with an IFT of 0.04 mN/m, 0.15 mN/m, 0.92 mN/m, and 5.2 mN/m, respectively. The apparatus installed for this experiment was kept the same as the apparatus conducted in the permeability reduction tests, but connected another sandpack with different permeability and its corresponding graduated mearing cylinder into the whole setup system. The pressure drops at each injection stage were measured using a pressure transducer. The fractional flow changes were measured by the effluents collected from the two sandpacks. The established parallel-sandpack simulation model will be simulated to match these pressure drops curves, and the results will be discussed in the next Chapter. The results of fractional flow curves from this conformance control tests will be demonstrated in the next Chapter.

Chapter 3. Results and Discussion

3.1 Simulation for Permeability Reduction Tests in Single Sandpack

Yu et al. (2018a) generated O/W emulsions with different oil qualities (2.5 wt%, 5.0 wt%, 7.5 wt%, and 10 wt%), an IFT of 0.44 mN/m and an average droplet size of 3.0 μm. They conducted single sandpack tests to investigate how oil quality, sandpack permeability, slug size of emulsion, and injection rate affect plugging strengths. Observation of pressure drop profiles during O/W emulsion injection and extended water injection were recorded. According to Yu et al. (2017), the plugging ability of an O/W emulsion primarily depends on retention of emulsion droplets in the porous media rather than on the bulk viscosity of the emulsion. Similarly, Soo and Radke (1984, 1986) illustrated the permeability reduction caused by the retention and capture of emulsion droplets in their examined cores. Accordingly, the filtration model is accepted as the most appropriate model for simulating the flow of diluted emulsions; the model considers emulsion droplets trapped by rock in porous media, which cause irreversible permeability reduction. According to Demikhova et al. (2016), the filtration model was successfully used to match the experimental emulsion effluent profiles and enhanced oil recovery profiles. The simulation model developed in this study was established based on the mechanisms of the filtration model as follows:

(1) Entrapment of emulsion droplets is represented by retention;

(2) Emulsion buck viscosity is constant;

(3) Flow diversion depends on resistance caused by captured emulsion droplets;

(4) Phases are incompressible.

Two main parameters used in the simulation model and developed based on the mechanism of the filtration model are retention factor (RF) and capture coefficient. Retention factor describes resistance to emulsion flow caused by plugged droplets in the porous media. Capture coefficient is another critical parameter in determining the number of emulsion droplets that are trapped at pore throats in the porous media. The maximum capture coefficient (at highest oil quality) can be determined based on the fact that 60% of emulsion droplets can be flushed out from the sandpack; that value is 5.55×10^{-6}. In the experiment, the O/W emulsion behaves as a Newtonian fluid, since shear stress shows a linear relationship with respect to shear rate at different oil qualities (i.e., the bulk viscosity of emulsion remained stable at increasing shear rate). Therefore, no matter how the injection flow rates changed, the bulk viscosity of emulsion was set to 1.4 mPa.s, based on the experimental result for the simulation model. In this study, the number of grid blocks and the size of each block were determined by conducting sensitivity analysis of grid block size when injecting 5 wt% of emulsion with 0.5 PV slug size into a 980 mD sandpack. As shown in Figure 3.1.1, the pressure drop curves overlapped with each other when using 100 and 150 grid blocks, and the experimental result was also matched, which means the simulation results would not be affected by the size of grid blocks when using 100 grid blocks. Therefore, a 100 x 1 x 1 O/W emulsion flood model (one-dimensional) was built using CMG STARS (CMG, 2015), and each block was 0.3 cm long. The length of the simulation model was 30 cm. The cross sectional-area and pore volume of this model were 4.9 cm^2 and 60 cm^3, respectively. The purpose of this simulation study was to determine retention factor and capture coefficient by matching the highest blocking pressure and residual pressure (after 2 PV water injection) from experimental results with different scenarios, such as different concentrations of O/W emulsion (oil quality), slug sizes of injected emulsion, permeabilities, and injection flow rates.

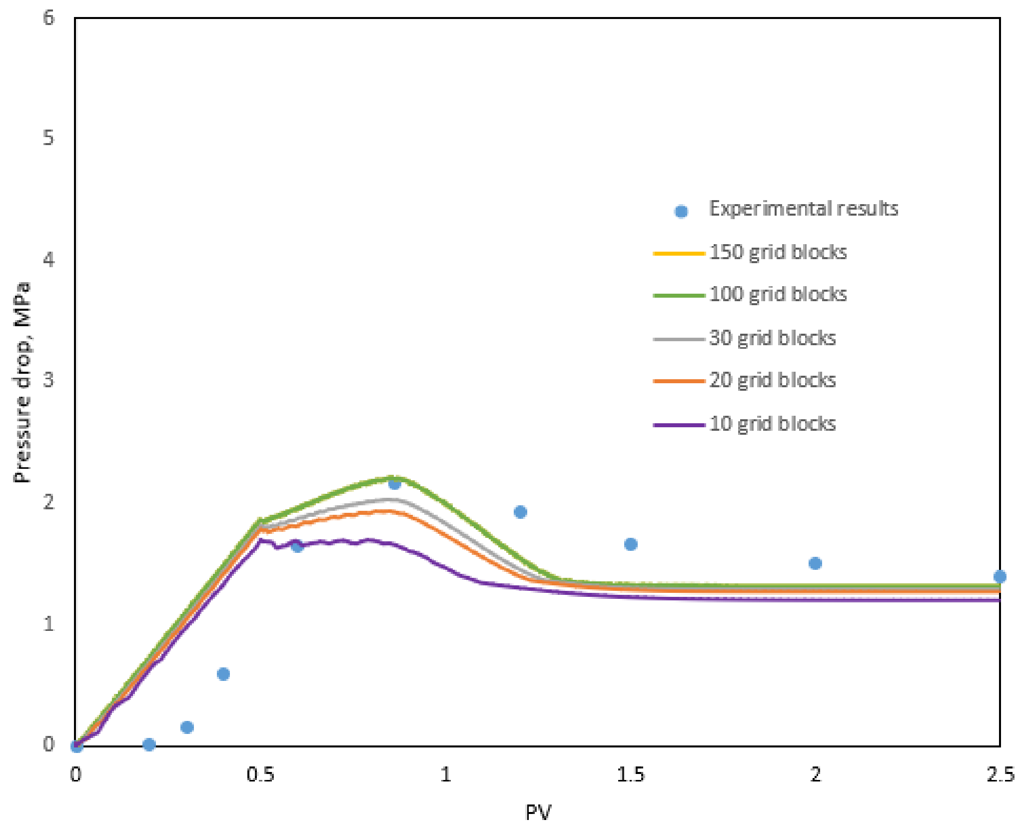

Figure 3.1.1. Sensitivity analysis on grid blocks for the simulation model.

The single sandpack simulation model was first conducted to match the pressure drops for injection of a 0.5 PV emulsion with different oil qualities into a 980 mD sandpack. The retention factor at each oil quality was calculated using the highest pressure drop for each emulsion during the extended waterflooding stage divided by the pressure drop at the initial emulsion flooding stage, and was calculated using the following equation:

$$CAP_{block} = \frac{RF_{block}}{RF_{max}} * CAP_{max} \qquad (1)$$

where CAP_{block} is the capture coefficient at each oil quality, RF_{block} is the retention factor at each oil quality, RF_{max} is the maximum retention factor obtained at the highest oil quality, and CAP_{max} is the maximum capture coefficient, which is 5.55×10^{-6} as mentioned before. Input of the capture coefficient into the simulation model automatically resulted in calculation of the value of RFs at each value of oil quality entered. Once the highest pressure drop was matched, the residual capture coefficient was determined to match the pressure drops after 2 PV of extended water injection. This value can be obtained using the following equation:

$$CAP_{residual} = \frac{RF_{2PV}}{RF_{max}} * CAP_{max} \qquad (2)$$

where $CAP_{residual}$ is the capture coefficient after 2 PV of waterflooding at each oil quality, and RF_{2PV} is the retention factor after 2 PV of waterflooding at each oil quality, which can be obtained from experiments. All parameters mentioned above for matching pressure drops are listed in Table 3.1.

Table 3.1. Parameters for matching variations of pressure drops at different oil qualities

Oil quality, wt%	RF	CAP_{block}	RF_{2PV}	$CAP_{residual}$
2.5	181	5.21×10^{-7}	91	2.62×10^{-7}
5.0	758	2.18×10^{-6}	421	1.21×10^{-6}
7.5	1682	4.84×10^{-6}	768	2.21×10^{-6}
10	1929	5.55×10^{-6}	1123	3.23×10^{-6}

Figure 3.1.2 shows the simulation and experimental results for variations of pressure drops for emulsion injection with four oil qualities into a sandpack with a permeability of 980 mD at a flow rate of 0.3 mL/min. The solid lines in this figure demonstrate simulation results. The experimental results were collected from experiments (Yu et al., 2018a) and plotted as symbols. Pressures increase during the emulsion injection stage, especially for the emulsion with highest oil quality (10 wt%), which attains the highest pressure drop. This can be explained by the “Jamin” effect (Jamin, 1860). Since the pore throats are blocked by the trapped emulsion droplets, an increase in pressure is needed for emulsion droplets to move further. For emulsion with higher oil

quality, it contains more emulsion droplets and these droplets tend to create larger resistance force to the fluid flow, which requires higher pressure gradient to make it to pass through the pore throats. It is also observed that the pressure drops still increase in the early stage of the following water injection process, indicating deeper movement of emulsion droplets in the sandpack. However, once the emulsion front breaks through and flows out from the sandpack, the pressure drops decrease gradually. The highest permeability reduction of about 99.95% occurred with the highest oil quality emulsion (10 wt%). After 2 PV of waterflooding, permeability reduction decreases to 99.92%, which shows that the emulsion with 10 wt% oil quality still maintains outstanding plugging strength during the waterflooding stage. It can be observed that the pressure drops increased faster for the simulation result than it for the experimental result during the emulsion injection stage, this is caused by an experimental error when preparing the sandpack. The loose sand with a higher permeability occupied at the inlet area of the prepared sandpack, however the permeability value for the simulation model is uniform. Therefore, the pressure drops for the experimental result increased much slower than it for the simulation result when injecting the emulsion at the same injection rate.

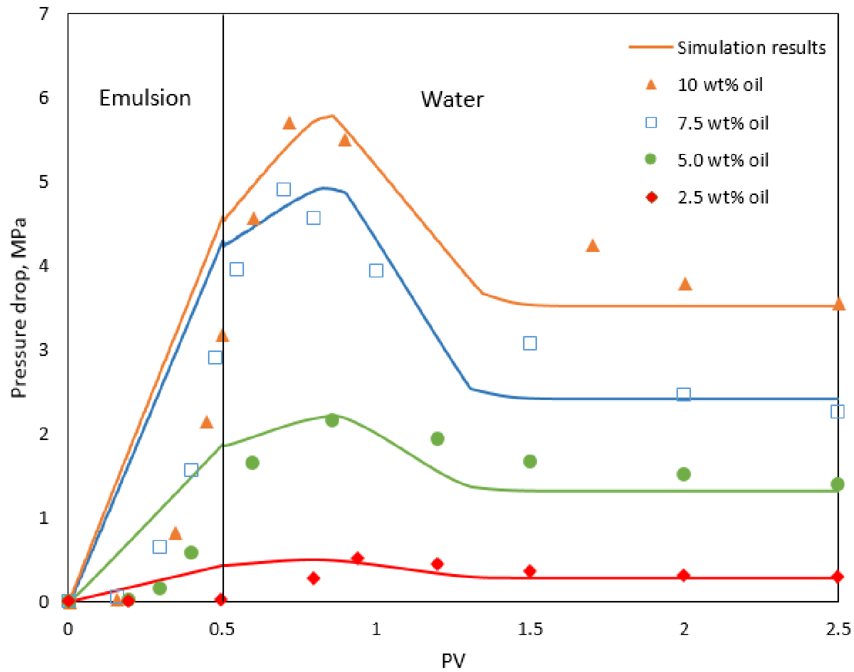

Figure 3.1.2. Variation of pressure drops of emulsions with different oil qualities.

Figure 3.1.3 shows the emulsion concentration profiles at the outlet of the simulation model during the emulsion injection stage and the subsequent water injection stage, which indicates the changes of emulsion concentration before and after the emulsion breakthrough occurred. Before the emulsion breakthrough occurred, no emulsion content can be observed at the outlet of the model. An increase in the emulsion content can be observed after the emulsion breakthrough occurred, and it starts to drop and to become zero once it has reached to its peak value.

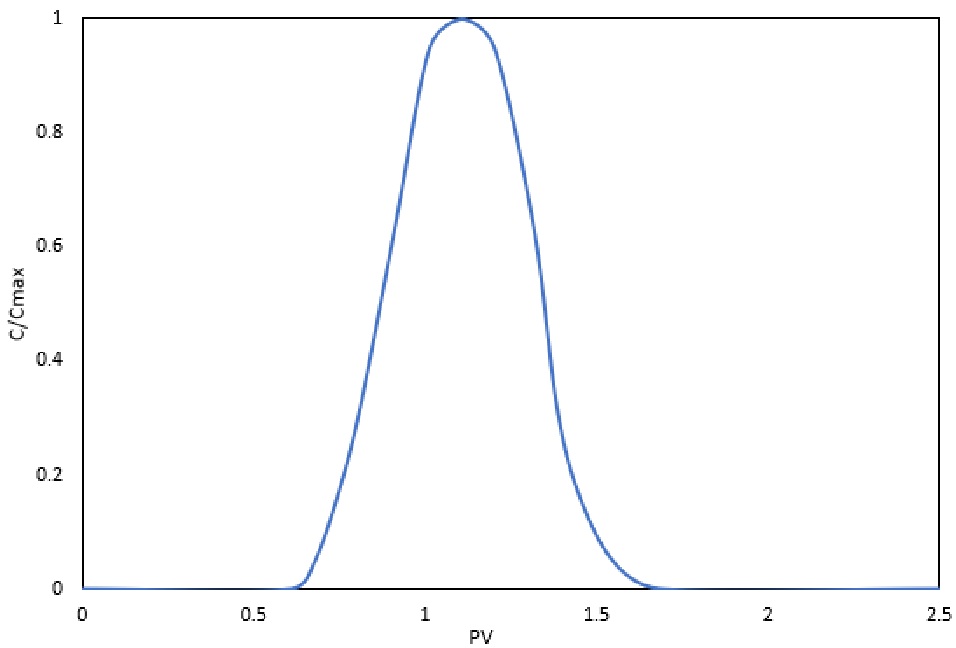

Figure 3.1.3. The changes of emulsion concentration at the outlet of the simulation model.

Figure 3.1.4 demonstrates simulation and experimental results for variations of pressure drops with emulsion injection for sandpacks with four permeabilities at an injection flow rate of 0.3 mL/min with 0.5 PV of emulsion slug size and oil quality of 5.0 wt%. In this figure, injection pressure drop reached its highest value of 3.8 MPa when emulsion was injected into the sandpack with the lowest permeability of 700 mD. Of course, the diameters of the pore throats were much larger in the higher permeability sandpack than in the lower permeability sandpack, which makes emulsion droplets more likely to be trapped in low permeability porous media. The trapped emulsion droplets restrict the injecting fluid from penetrating deep into the sandpack. Therefore, higher pressure is required to push the O/W emulsion further along in a low permeability sandpack. Table 3.2 shows that retention factor increases as permeability of a sandpack decreases due to resistance to fluid flow when O/W emulsion is injected into lower permeability sandpacks. However, note that the residual capture coefficient remains the same for all examined permeabilities.

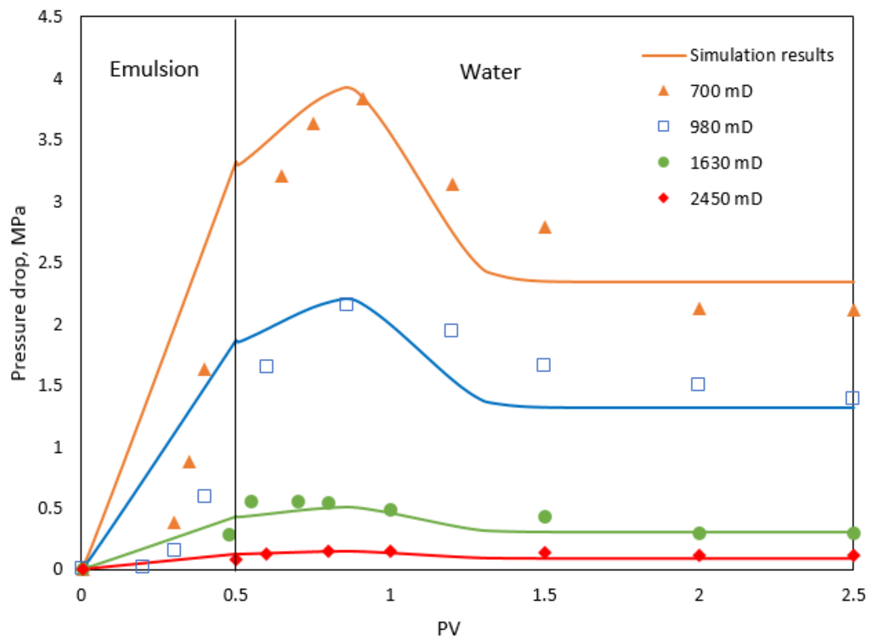

Figure 3.1.4. Variation of pressure drops of O/W emulsions with different permeabilities.

Table 3.2. Parameters for matching variation of pressure drops at different permeabilities

Permeability, mD	RF	$CAP_{residual}$
700	2450	1.21×10^{-6}
980	1929	
1630	730	
2450	300	

Figure 3.1.5 demonstrates simulation and experimental results for variations of pressure drops for emulsion injection with four slug sizes at a flow rate of 0.3 mL/min with oil quality of 5.0 wt% into a sandpack with permeability of 980 mD. The pressure drop increased as emulsion slug size increased. When 1.0 PV of O/W emulsion was injected into the sandpack, it was expected that the front of the emulsion slug had already reached the outlet of the sandpack. Emulsion breakthrough had in fact occurred, corresponding to pressure reduction at the onset of the extended

water injection stage. However, when less than 1 PV of emulsion was injected, at the onset of the following extended waterflood, the injected water would push the emulsion slug further along the sandpack, meaning that the resistance effect could proceed deeper into the sandpack. As a result, a pressure increase, before its final reduction, could be observed once extended water injection was initiated.

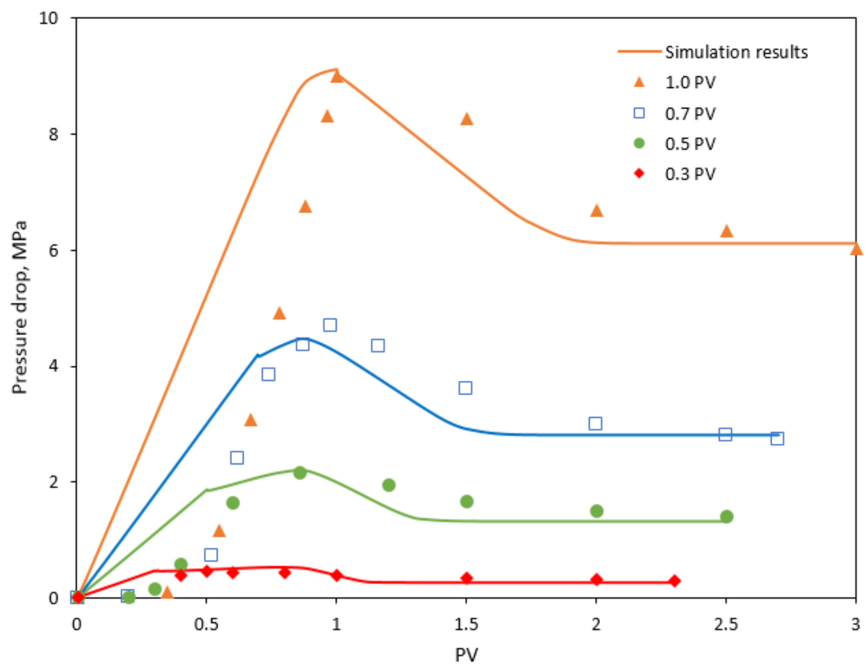

Figure 3.1.5. Variation of pressure drops of emulsions with different slug sizes.

Table 3.3 illustrates the values of retention factor and residual capture coefficient obtained from matching simulation results with experimental results. Note that larger slug sizes of emulsion injection result in greater retention factors and residual capture coefficients.

Table 3.3. Parameters for matching variation of pressure drops at different slug sizes

Slug size, PV	RF	$CAP_{residual}$
0.3	800	5.5×10^{-7}
0.5	1929	1.2×10^{-6}
0.7	3100	1.8×10^{-6}
1.0	5200	2.2×10^{-6}

Figure 3.1.6 shows simulation and experimental results for variations of pressure drops with emulsion injection at four injection rates with 0.5 PV of emulsion slug size and oil quality of 5.0 wt% into a sandpack with a permeability of 980 mD. When emulsion was injected at higher flow rates, greater pressure drops were needed to push the emulsion droplets move through the pore throats. Table 3.4 illustrates that the values of retention factor and residual capture coefficient are the same for matching pressure drops at different injection flow rates.

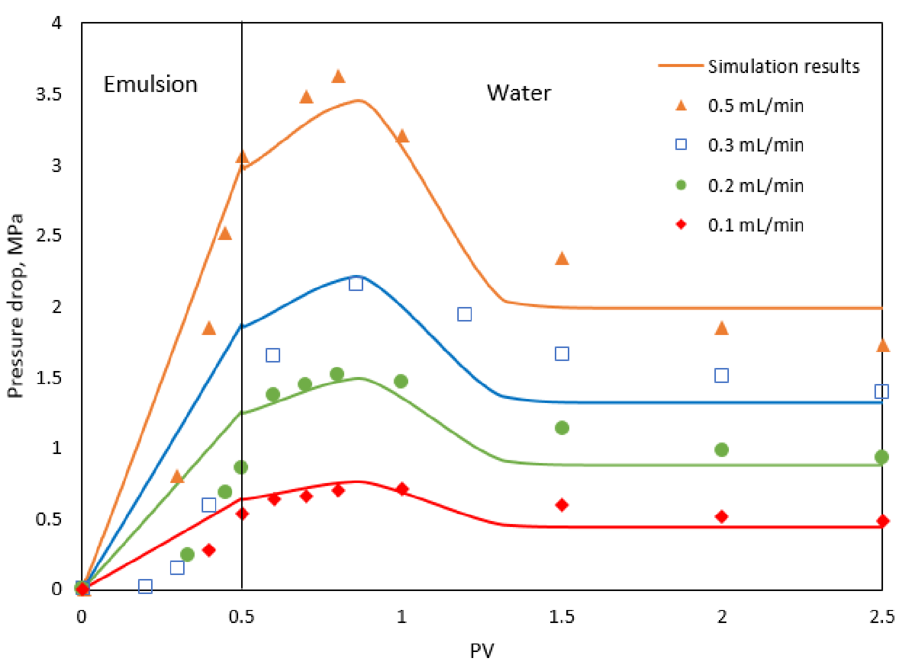

Figure 3.1.6. Variation of pressure drops of O/W emulsions with different injection flow rates.

Table 3.4. Parameters for matching variation of pressure drops at different flow rates

Flow rate, mL/min	RF	$CAP_{residual}$
0.1	1929	1.21×10^{-6}
0.2		
0.3		
0.5		

The correlations of main parameters between different emulsion properties were obtained by matching the experimental results. When changing the emulsion properties, the values of two main parameters can be correlated. Matching the results of single sandpack tests was an important step to allow the feasibility of sensitivity tests conducted on the simulation models of parallel-sandpack.

3.2 Simulation for Conformance Control Tests in Parallel-sandpack Models

A simulation model was established with the objectives of matching the experimental results of conformance control tests in parallel-sandpacks, and subsequently investigating the effects of the combination of IFT, emulsion quality, slug size of emulsion injection, and oil phase viscosity on the performance of conformance control.

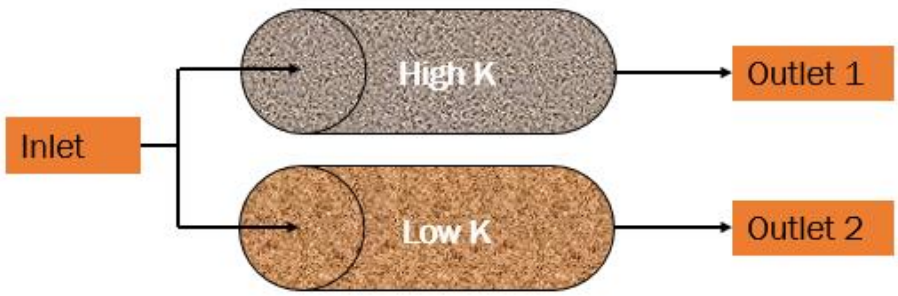

Figure 3.2.1. Illustration of parallel-sandpack model.

Figure 3.2.1 depicts the schematic of the parallel-sandpack flow tests by Yu et al. (2018b). Each sandpack of the model was 30 cm in length, with a cross-sectional area of 4.9 cm^2 and pore volume of 60 cm^3. There was no connectivity between two sandpacks. One injection line connected both sandpacks, and the two production lines were for the two separate productions from the sandpacks. Both sandpacks were saturated with water before emulsion injection. The simulation model was first used to match the experimental results which illustrated the variation of pressure drops of O/W emulsion injection with different IFTs into sandpacks with permeabilities of 820 mD and 2770 mD (so the permeability ratio is about 3.4:1). The injection process for the parallel-sandpack test included an initial waterflooding stage, an emulsion injection stage, and an extended water injection stage. The changes of fractional flows of parallel-sandpacks were also matched for injected emulsions with IFTs of 0.04 mN/m, 0.15 mN/m, and 5.2 mN/m. The propagation fronts of the sandpack 1 and sandpack 2 were plotted by the simulator to illustrate the effect of emulsion penetration distance on the performance of conformance control. The retention factor and residual capture coefficient for each sandpack used in the simulation model can be calculated by the following steps and equations:

(1) Plug different permeabilities into the following equations to obtain RF for each sandpack (the correlation between RF and permeability were obtained from Table 3.2):

$$RF_{high\ k} = 5966.7 * \exp\left(-0.0012 * K_{high\ K}\right) \qquad (3)$$

$$RF_{low\ k} = 5966.7 * \exp(-0.0012 * K_{low\ K}) \qquad (4)$$

(2) Use the following equations to correlate the calculated RF for the high permeability and low permeability sandpacks from the previous step, based on the slug size of emulsion penetrated into each sandpack:

$$RF_{new\ high\ k} = \frac{6285.7 * L_{high\ k} - 1171.4}{6285.7 * L_b - 1171.4} * RF_{high\ k} \qquad (5)$$

$$RF_{new\ low\ k} = \frac{6285.7 * L_{low\ k} - 1171.4}{6285.7 * L_b - 1171.4} * RF_{low\ k} \qquad (6)$$

where $RF_{new\ high\ k}$ is the final retention factor for the high permeability sandpack after correlation of slug size, and $L_{high\ k}$ is the slug size of emulsion moved into the high permeability sandpack, and $RF_{high\ k}$ is the retention factor for the high permeability sandpack as calculated from Equation 3. L_b is the base slug size, which is 0.5PV, and the value of RF at L_b is 1929. Similar definitions can be used for $RF_{new\ low\ k}$, $L_{low\ k}$, and $RF_{low\ k}$.

(3) Determine the $CAP_{residual}$ for each sandpack by the following equations:

$$CAP_{residual\ high\ k} * 10^6 = 1.40 * \ln\left(L_{high\ k}\right) + 2.23 \qquad (7)$$

$$CAP_{residual\ low\ k} * 10^6 = 1.40 * \ln(L_{low\ k}) + 2.23 \qquad (8)$$

where $CAP_{residual\ high\ k}$ is the residual capture coefficient for the high permeability sandpack, $L_{high\ k}$ has the same definition as mentioned in the previous step, and $CAP_{residual\ low\ k}$ is the residual capture coefficient for the low permeability sandpack. $L_{low\ k}$ has the same definition as specified in the previous step.

Figure 3.2.2 shows experimental and simulation results of pressure drops at different injection stages for 0.5 PV emulsion injection with four IFTs and oil quality of 15 wt%. The experimental results were collected (Yu et al., 2018) and plotted as symbols. The solid lines show the simulation results. In this figure, the pressure drop for O/W emulsion injection with an IFT of 5.2 mN/m was largest during the extended water injection stage due to its large capillary resistance to fluid flow. However, emulsions with higher IFTs do not have good deformability, and this explains why pressure drops for the IFTs of 0.92 mN/m and 5.2 mN/m decreased rapidly once they reached peak values. For emulsions with a moderate IFT of 0.15 mN/m and a low IFT of 0.04 mN/m, the pressure drops gradually decreased because the emulsion droplets are flexible enough to deform and are able to penetrate deeply into the sandpack.

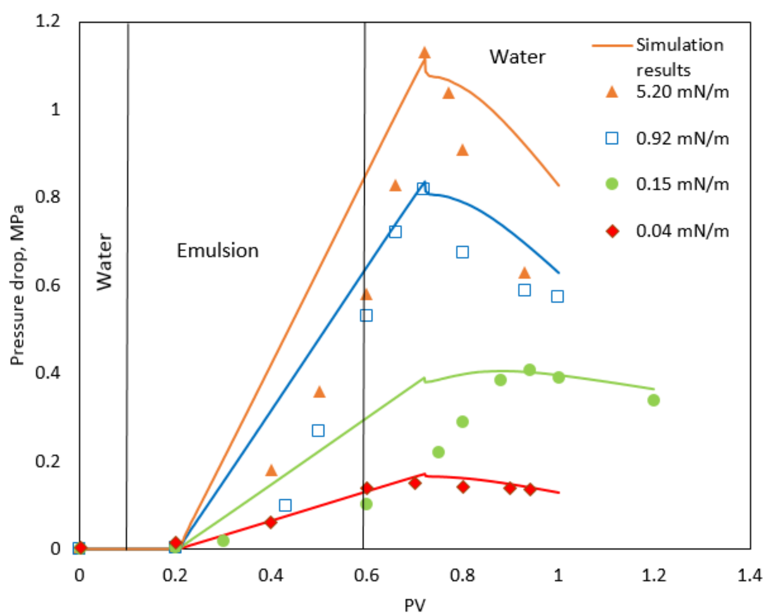

Figure 3.2.2. Pressure drops of O/W emulsion with different IFTs.

The performance of conformance control cannot be fully illustrated by observing only pressure drop curves. Thus, fractional flows for high permeability sandpack (sandpack 1) and low permeability sandpack (sandpack 2) were plotted to investigate the conformance control ability. Figure 3.2.3 shows the fractional flow experimental (left) and simulation (right) results for O/W emulsion injection with different IFTs. The fractional flow of the sandpack 1 is much higher than the sandpack 2 during the extended waterflooding stage for an emulsion with IFTs of 0.04 mN/m and 5.2 mN/m, indicating poor conformance control ability. For the emulsion with a moderate IFT of 0.15 mN/m, the fractional flow ratio decreased from 77:23 during initial water injection to 65:35 during emulsion injection, and it remained the same during extended waterflooding stages, which means the plugging strength of emulsion still existed. Flow diversion occurred at the end of extended waterflooding and demonstrated better conformance control ability. Figure 3.2.4 and Figure 3.2.5 show the propagation front of the injected emulsion in the parallel-sandpack which can provide a better understanding of flow pattern changes.

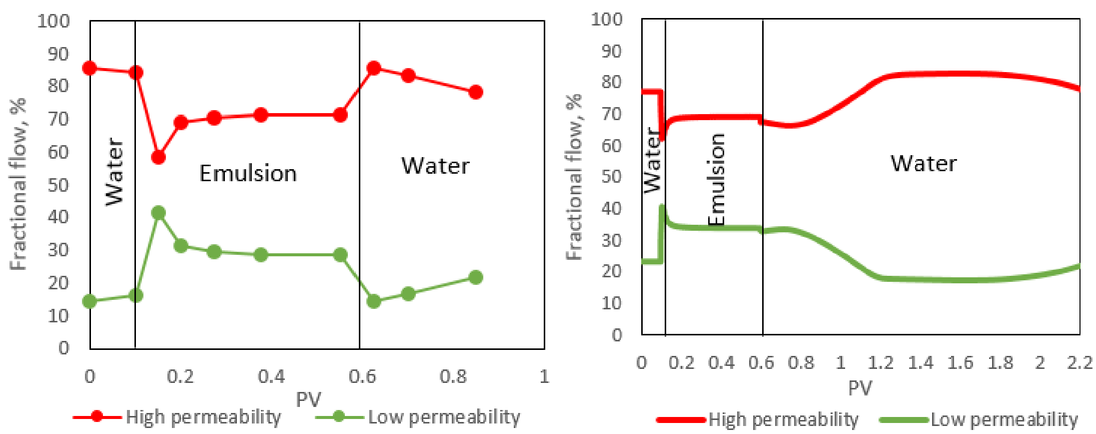

(a)

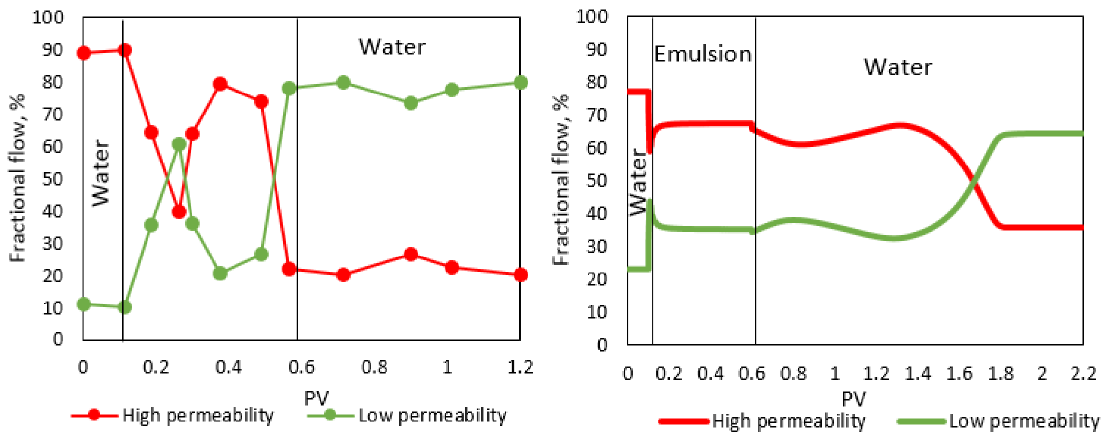

(b)

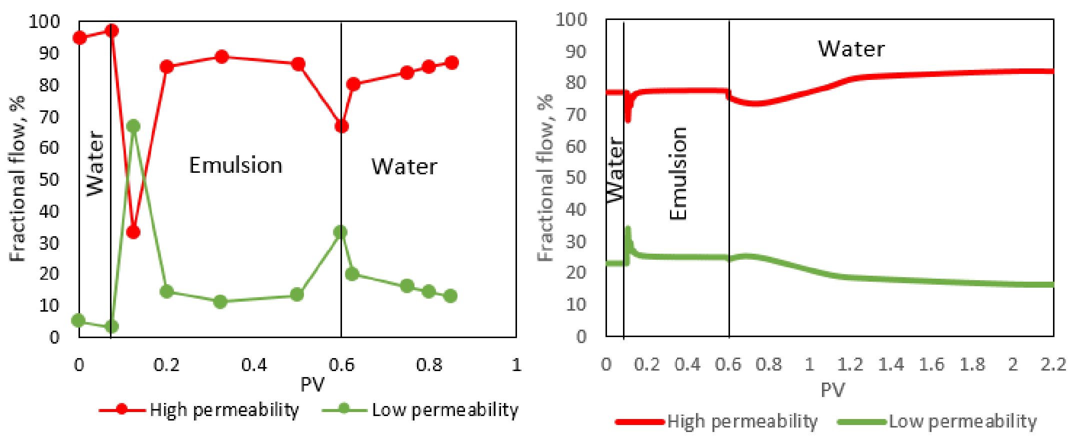

(c)

Figure 3.2.3. Fractional flows at different IFTs of experimental results (left) and simulation results (right): (a) 0.04mN/m (b) 0.15mN/m (c) 5.2mN/m.

Remembering that retention factor represents flow resistance, Figure 3.2.4 (a) shows that only a small amount of emulsion enters the sandpack 2 because, for an emulsion with an IFT of 5.2 mN/m, it is difficult to push emulsion droplets through the pore throats due to their low deformability. Thus, the emulsion droplets tend to accumulate near the inlet of the sandpack 2, and that accumulated emulsion created a large resistance to fluid flow. Figure 3.2.4 (b) illustrates that the retention factor is much higher in the sandpack 2 than in the sandpack 1 after about 1 PV of extended waterflooding. Thus, more fluid tends to enter the sandpack 1, resulting in limited conformance control ability. Consistently, the fractional flow curves show no flow diversion during the following extended water injection stage because the sandpack 2 is sufficiently blocked by the trapped emulsion droplets, as Figure 3.2.4 (c) indicates.

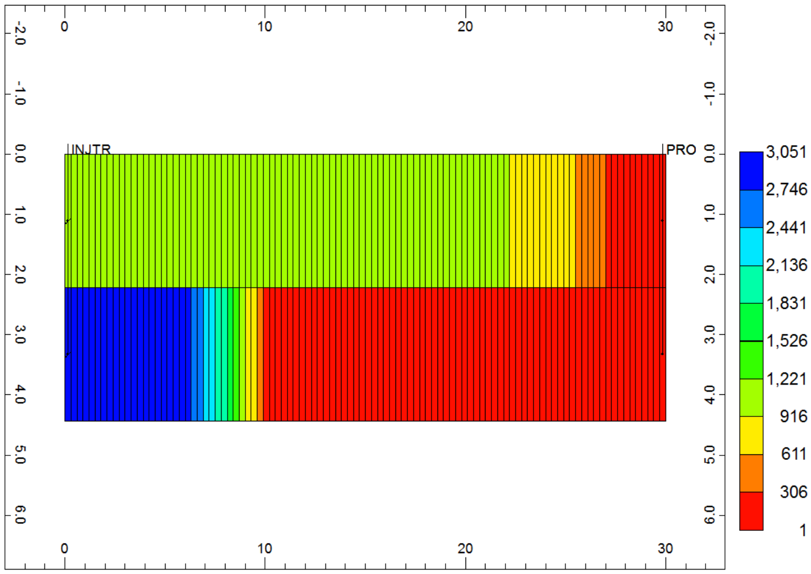

(a)

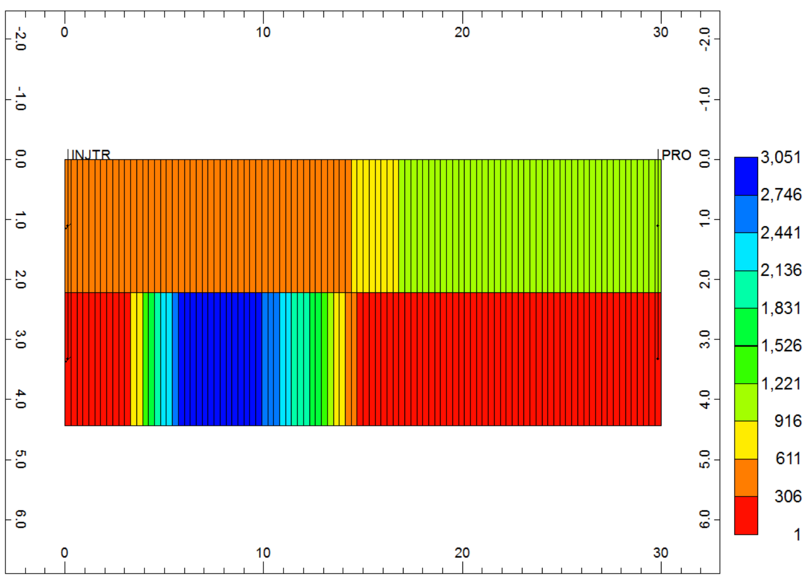

(b)

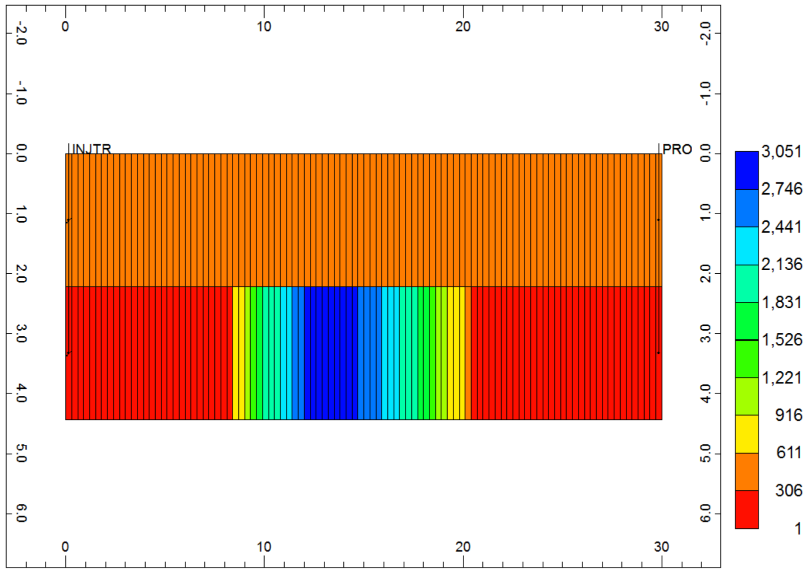

(c)

Figure 3.2.4. Retention factor profiles for emulsion with an IFT of 5.2 mN/m at different stages: (a) 0.596 PV (b) 0.875 PV (c) 1.5 PV.

Figure 3.2.5 (a) demonstrates that retention factor in the sandpack 1 is slightly larger than in the sandpack 2 for an emulsion with an IFT of 0.15 mN/m. This indicates that a moderate IFT emulsion has readily deformable emulsion droplets that can thereby pass through the pore throats and move further along in both sandpacks. Once the flow resistance in the sandpack 1 is higher than in the sandpack 2, as shown in Figure 3.2.5 (b) and Figure 3.2.5 (c), promoting more injected fluid to enter into the low permeability sandpack, flow diversion occurs during the extended water injection stage to show a good performance of conformance control.

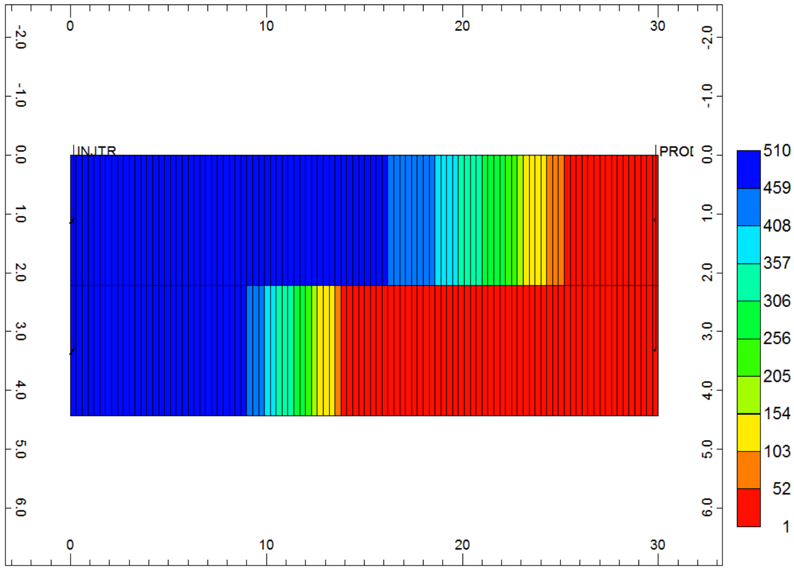

INJTR
PROI
510
459
408
357
306
256
205
154
103
52
1

(a)

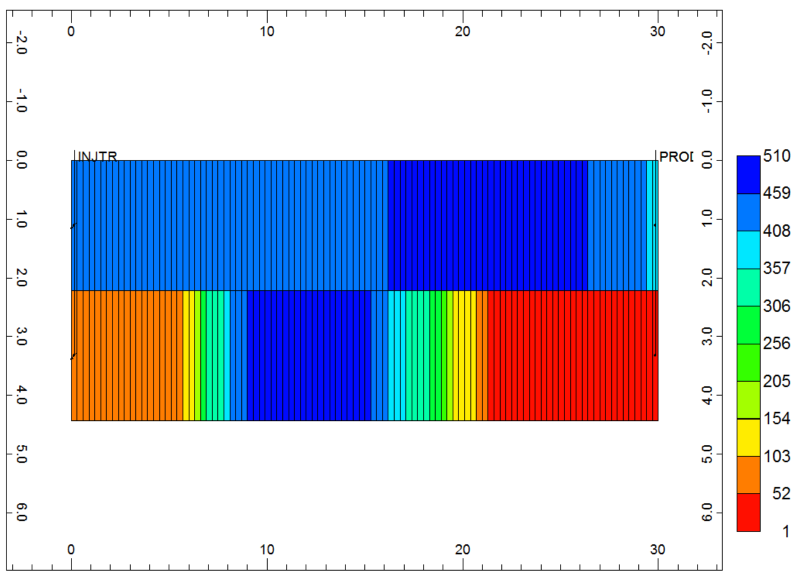

INJTR
PROI
510
459
408
357
306
256
205
154
103
52
1

(b)

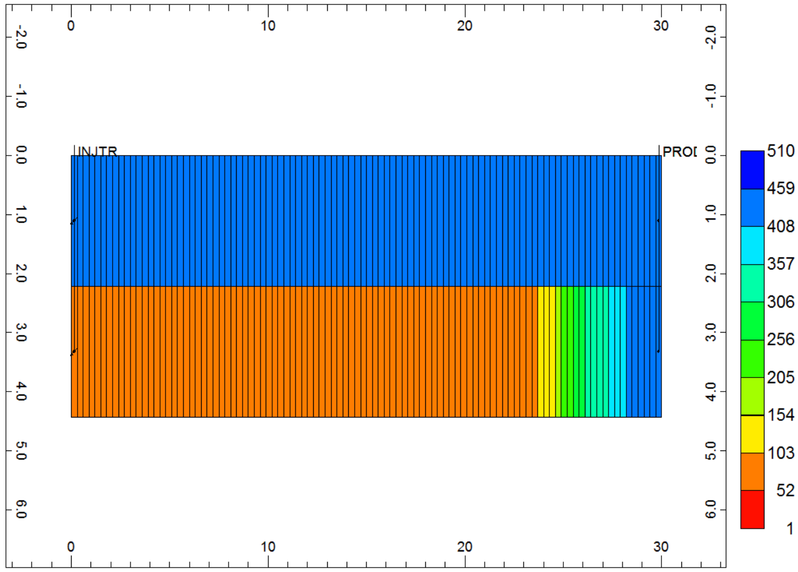

(c)

Figure 3.2.5. Retention factor profiles for emulsion with an IFT of 0.15 mN/m at different stages: (a) 0.596 PV (b) 0.875 PV (c) 1.5 PV.

Figures 3.2.6 and 3.2.7 show the change of fractional flow at different emulsion slug sizes in the experimental and simulation results. According to simulation results, fractional flow at the initial waterflooding stage is 77:23; it decreases to 65:35 during 0.5 PV of emulsion injection, and to 56:44 during 0.8 PV of emulsion injection, demonstrating that better conformance control performance can be achieved by increasing the emulsion slug size. For a larger emulsion slug size, more emulsion droplets flow into the high permeability zone and are trapped at pore throats, which can restrict fluid flow due to increased capillary resistance force. Thus, with a larger emulsion slug size, more fluid flow can be diverted to the low permeability sandpack, improving overall sweep efficiency.

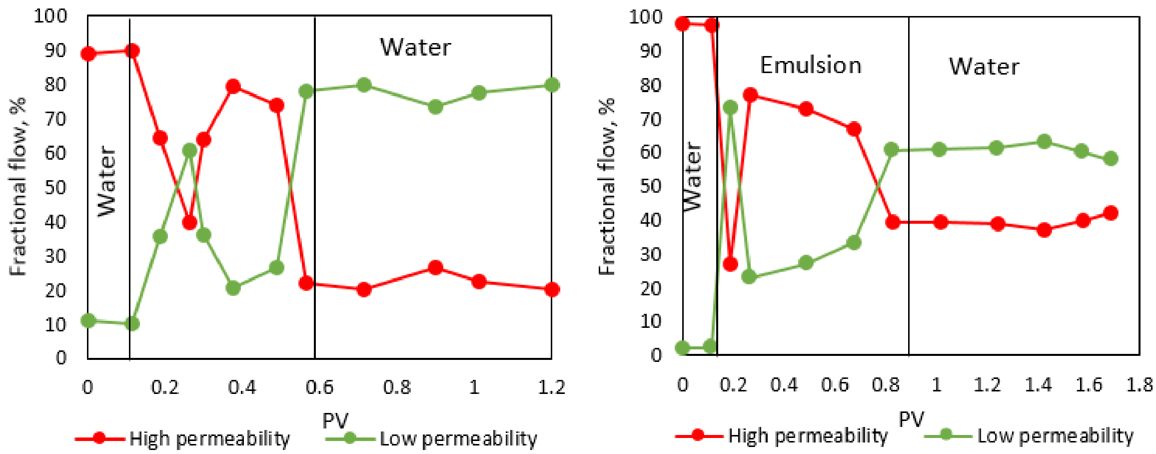

(a) (b)

Figure 3.2.6. Experimental results of fractional flows at different emulsion slug sizes: (a) 0.5 PV (b) 0.8 PV.

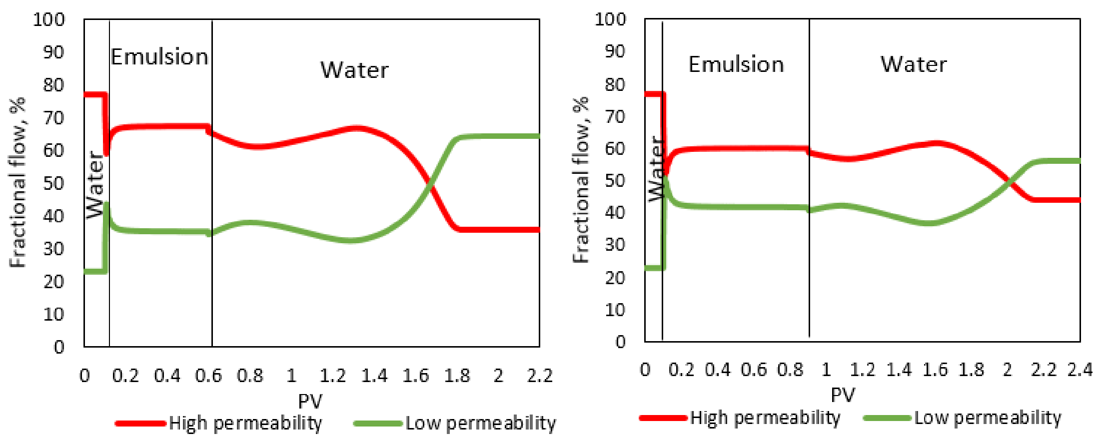

(a) (b)

Figure 3.2.7. Simulation results of fractional flows at different emulsion slug sizes: (a) 0.5 PV (b) 0.8 PV.

In addition, as demonstrated in Figure 3.2.8, the simulation results well match the experimental results and indicate that the pressure drops increase as emulsion slug sizes increase.

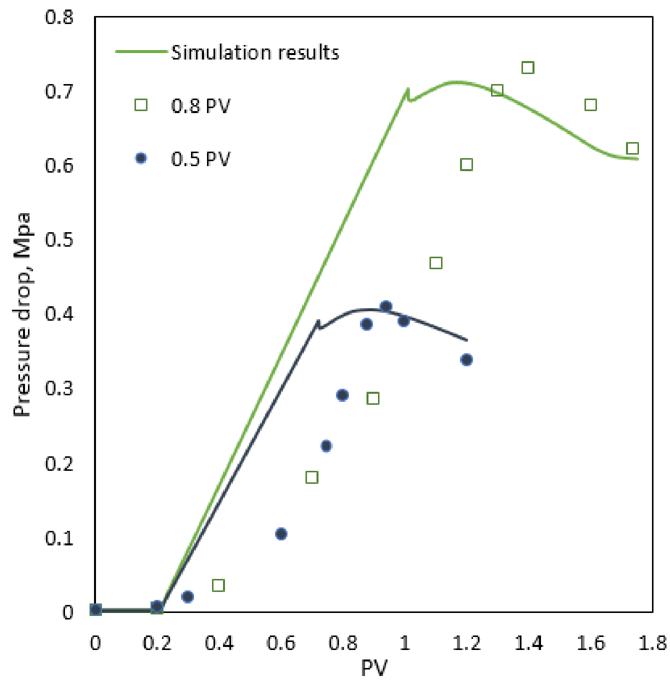

Figure 3.2.8. Pressure drops for emulsion slug sizes of 0.5 PV and 0.8 PV.

When injecting O/W emulsion into a weakly heterogenous parallel-sandpack with a permeability ratio of about 2:1 (1810 mD:920 mD), the IFT and oil quality can be adjusted using the simulation model to achieve similar conformance control performance. By way of example, Figure 3.2.9 shows that good conformance control can be obtained in both Case (a) (experimental) and Case (b) (simulated), as the fractional flow ratio reaches 50:50 at the extended waterflooding stage. Because the heterogeneity of the sandpack is not severe, slightly decreasing oil quality and increasing IFT can make the emulsion in Case (b) achieve a similar flow pattern as in Case (a). Figure 3.2.10 demonstrates that the pressure drops for Case (a) and Case (b) are almost the same, meaning that the plugging strength caused by the blockage effect of these two emulsions is essentially the same.

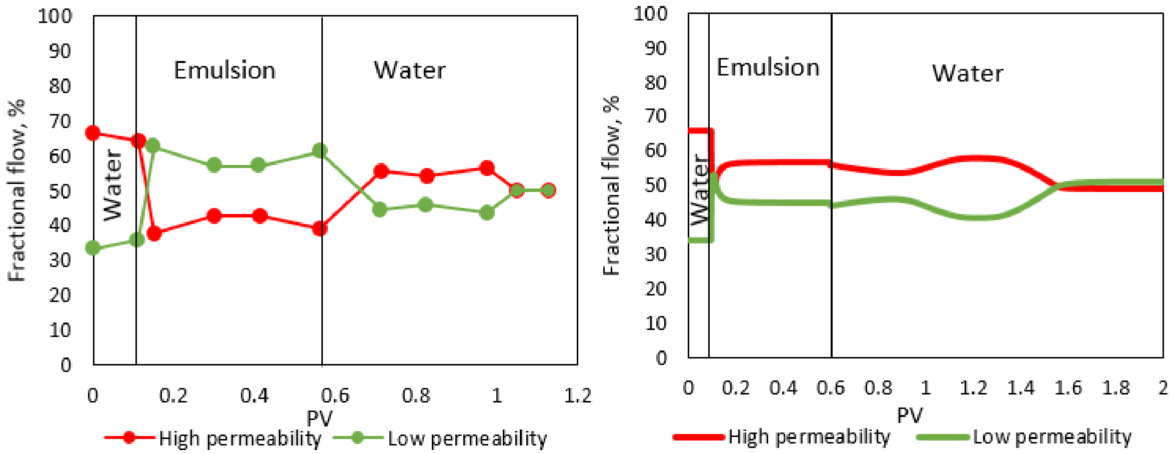

(a) (b)

Figure 3.2.9. Fractional flow of different combinations of IFT and oil quality: (a) 15 wt% and IFT=0.15 mN/m; (b) 10 wt% and IFT=0.44 mN/m.

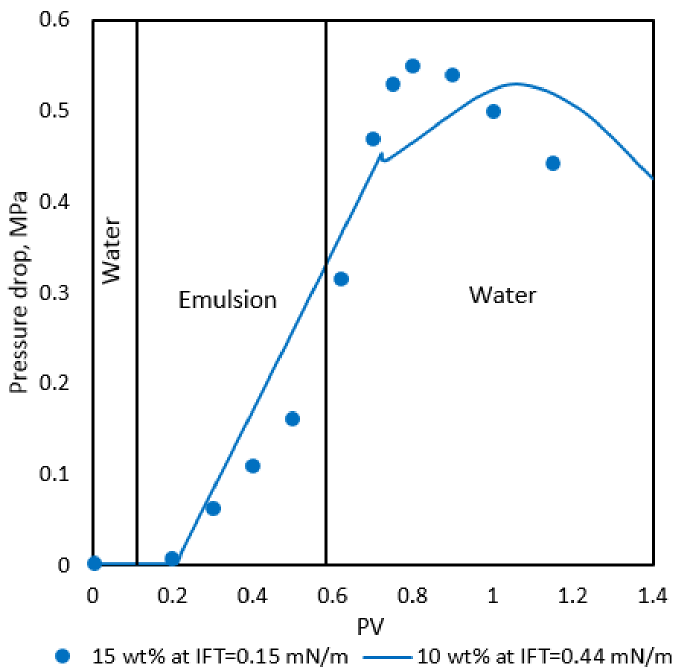

Figure 3.2.10. Pressure drops of different combinations of IFT and oil quality.

In the previous experiments and simulations, the sandpack was initially saturated with water, but the following modeling is for a sandpack that has been initially saturated with 40% water and 60% immobile oil. This change resulted in an increased pressure drop, as the existing oil (immobile oil) in the sandpack increased flow resistance when injected with O/W emulsion. A parametric simulation study was conducted to find the optimal combination of oil quality and slug size that can achieve good comformance control performance. The assumption made for this simulation model is that the free oil in the sandpack is immobile and therefore cannot be flushed out. Figure 3.2.11 below shows the flow pattern when injecting 0.5 PV emulsion slug with emulsion quality of 2.5 wt% and IFT of 0.44 mN/m. The flow pattern is slightly different compared with the flow pattern in Figure 3.2.9 (b), but still shows good conformance control performance. It was found that decreasing the oil quality of emulsion could enhance the injectivity of emulsion. The pressure drops approached 2.6 Mpa, which is five times higher than that of the comparable sandpack test with 100% water saturation as shown in Figure 3.2.10.

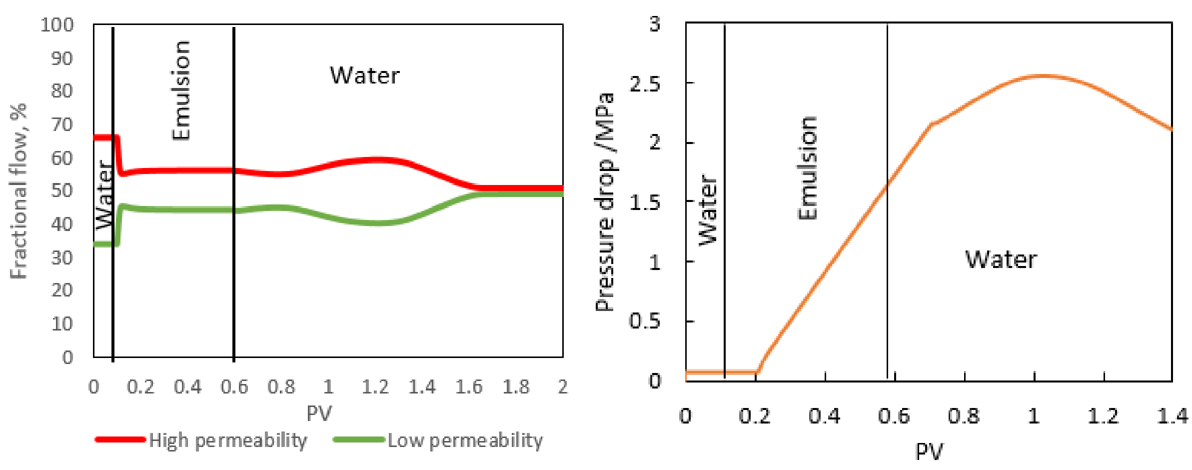

Figure 3.2.11. Fractional flows (left) and pressure drops (right) of emulsion injection in the sandpack with a permeability ratio of 2:1 and with 40% initial water saturation.

It was found that injection of an O/W emulsion with a low oil phase viscosity into a severely heterogenous parallel-sandpack with a permeability ratio of about 4.6:1 (3520 mD:770 mD) had limited conformance control performance (Yu et al., 2018b). Therefore, for a severely heterogenouos model, an O/W emulsion with higher plugging strength is desired, which can be achieved by increasing oil phase viscosity and/or IFT. An experiment was conducted (Yu et al., 2018b) using the emulsion with an increased oil phase viscosity of 1200 mPa.s at 60℃ and an increased IFT of 0.24 mN/m showed good performance of conformance control when other emulsion properties were kept the same as before (0.5 PV of emulsion injection with quality of 15 wt%). As shown in Figure 3.2.12, the fractional flow ratio decreased during the emulsion injection stage, and flow diversion can be observed during the following extended waterflooding stage. Figure 3.2.13 shows the pressure drops during the different injection stages. The highest pressure drop approached 500 KPa, which is higher than when using a low viscosity oil-in-water emulsion.

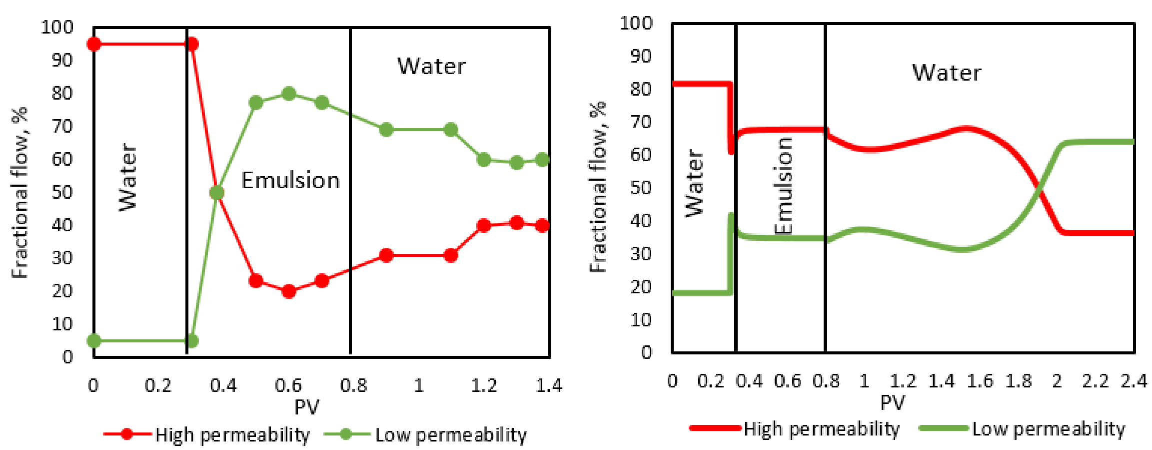

(a) (b)

Figure 3.2.12. Fractional flows of higher viscous oil-in-water emulsion injection: (a) Experimental results (b) simulation results.

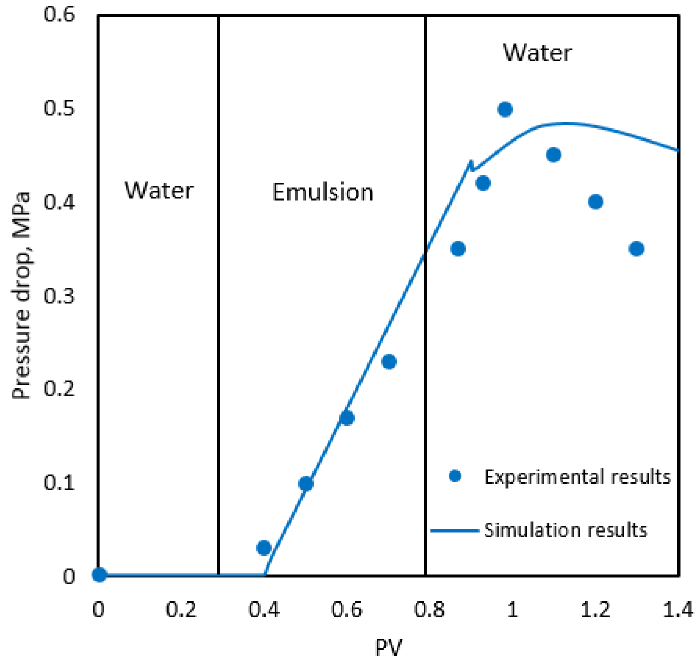

Figure 3.2.13. Pressure drops of higher viscous oil-in-water emulsion injection.

The previous parallel-sandpack simulation result showed that when injecting 0.5 PV of an O/W emulsion (low oil phase viscosity) with emulsion quality of 10wt% and IFT of 0.44 mN/m into the heterogeneous parallel-sandpack with a permeability ratio of about 2:1 (1810 mD:920 mD), good conformance control performance can be achieved, as shown in Figure 3.2.9 (b). What will be the results if an O/W emulsion with a high oil phase viscosity at the same emulsion slug size, emulsion quality, and IFT is injected into the sandpacks with the same permeability ratio. As shown in Figure 3.2.14, the diversion of fractional flow curves can be observed during the extended waterflooding stage, which means the O/W emulsion can block the high permeability sandpack and divert more water to flow into the low permeability sandpack. However, the fractional flow for the low permeability sandpack at the extended waterflooding stage is much higher than for the high permeability sandpack at the initial waterflooding stage which means the injected O/W emulsion creates too much flow resistance in the high permeability sandpack. Obtaining good conformance control performance is not as likely if the high permeability sandpack is permanently blocked by the O/W emulsion. In order to determine when the fractional flow ratio will reach 50:50 at the extended waterflooding stage, more simulation models of O/W emulsion injection at different emulsion quality and slug size need to be conducted.

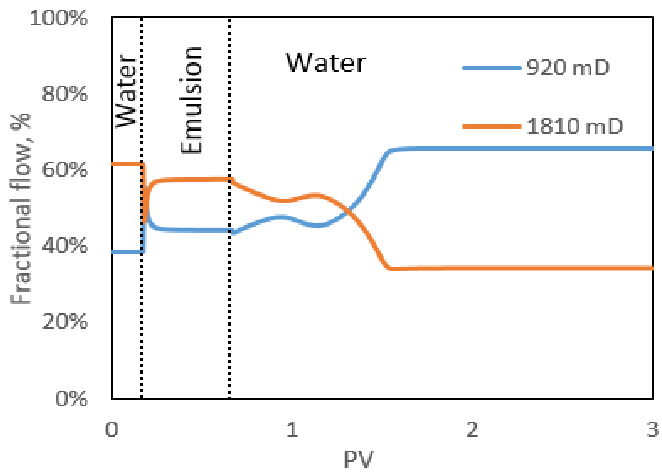

Figure 3.2.14. Fractional flows of O/W emulsion with a high oil phase viscosity injection in the sandpack with a permeability ratio of 2:1-emulsion quality of 10wt%.

Because good conformance control performance can not be obtained when injecting an O/W emulsion (high oil phase viscosity) with emulsion quality of 10wt%, the emulsion quality will be decreased to 5wt% to see the changes in fractional flow curves. Figure 3.2.15 shows better conformance control performance compared with the result shown in Figure 3.2.14, as the fractional flow ratio tends to approach 50:50 at the extended waterflooding stage. However, flow diversion occurred and the fractional flow for the low permeability sandpack is higher than for the high permeability sandpack, which means the emulsion quality still needs to be adjusted to a smaller value.

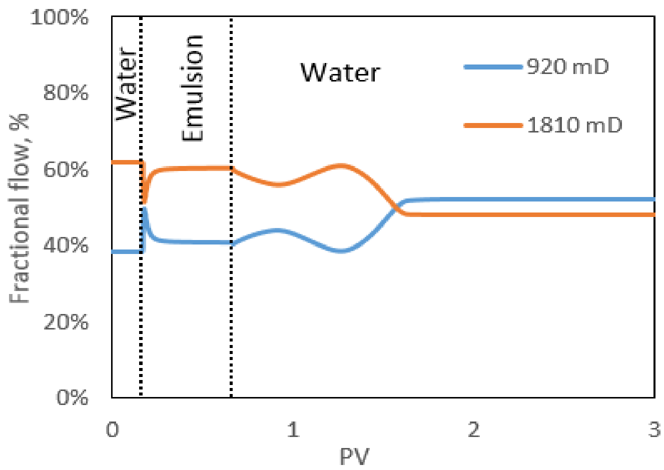

Figure 3.2.15. Fractional flows of O/W emulsion with a high oil phase viscosity injection in the sandpack with a permeability ratio of 2:1-emulsion quality of 5wt%.

Figure 3.2.16 shows the fractional flow curves when adjusting the emulsion quality to 2.5wt%. No flow diversion occurred at the extended waterflooding stage, which indicates the injected emulsion does not have enough plugging strength to block the high permeability zone. The fractional flow for the low permeability sandpack at the extended waterflooding stage is lower than at the initial water injection stage, which indicates that the emulsion remaining in the low permeability sandpack prevents water flowing into it at the extended waterflooding stage. The result demonstrates that the emulsion quality of 2.5wt% for emulsion injection is too small to have an effect on conformance control. Therefore, the fractional flow ratio can reach 50:50 when injecting an O/W emulsion with emulsion quality between 2.5wt% and 5wt%. After conducting several simulation models, 4wt% was found to an appropriate emulsion quality to perform good conformance control, as shown in Figure 3.2.17.

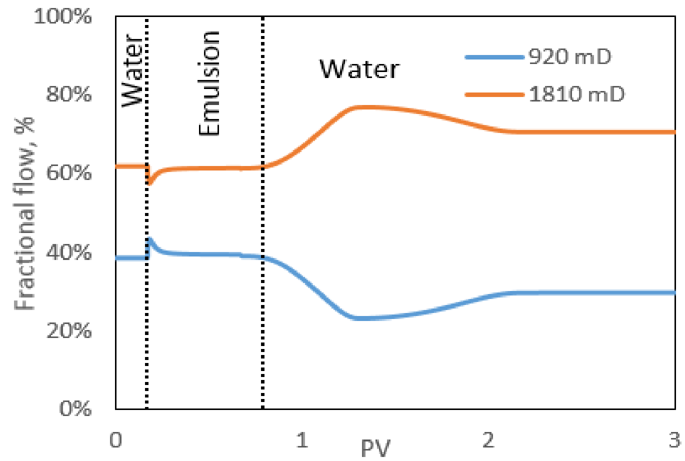

Figure 3.2.16. Fractional flows of O/W emulsion with a high oil phase viscosity injection in the sandpack with a permeability ratio of 2:1-emulsion quality of 2.5wt%.

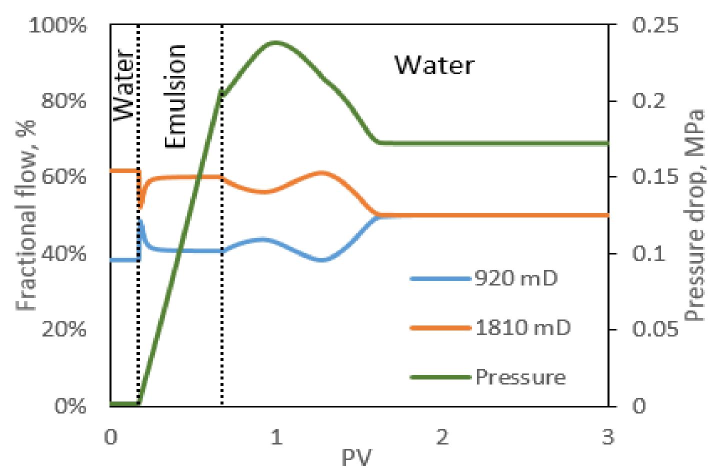

Figure 3.2.17. Fractional flows and pressure drops of O/W emulsion with a high oil phase viscosity injection in the sandpack with a permeability ratio of 2:1-emulsion quality of 4wt%

In Figure 3.2.17, the fractional flow ratio reaches 50:50 at the subsequent waterflooding stage, which indicates promising conformance control performance can be obtained. The highest pressure drop approached around 230 kPa. Figure 3.2.18 shows the changes in pressure drops for emulsion injection with different emulsion qualities. In this figure, the highest pressure drop for 10wt% of emulsion injection reached around 1000 kPa, and this value is higher than for injection of emulsion with a low oil phase viscosity which is 520 kPa, as shown in Figure 3.2.13. This highest pressure drop comparison indicates that the injection of emulsion with a high oil phase viscosity can create higher plugging strength, and it needs more pressure to push the blocked emulsion out of the sandpack during the extended waterflooding stage.

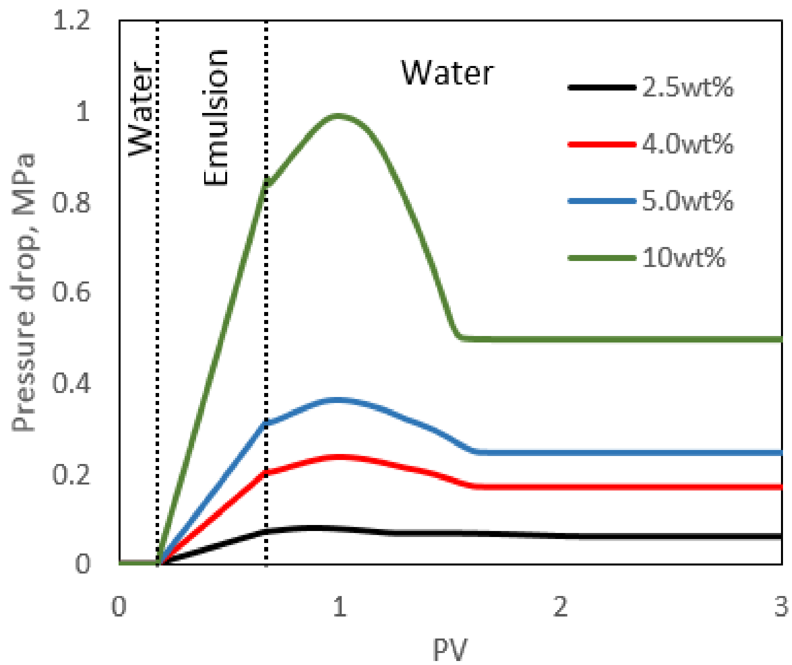

Figure 3.2.18. Variation of pressure drops of emulsions (high oil phase viscosity) with different emulsion qualities.

As shown in Figure 3.2.19, when decreasing the emulsion slug size from 0.5 PV to 0.3 PV, fractional flow for the low permeability sandpack increased more rapidly at the extended waterflooding stage and, finally, the fractional ratio reached 50:50, which means the captured emulsion droplets in the low permeability sandpack can be easily flushed out and the plugging strength created in the high permeability sandpack is strong enough to stop injected water from flowing through the high permeability sandpack. However, no flow diversion occurred when injecting emulsion slug size of 0.2 PV into the parallel-sandpack, observed in Figure 3.2.20. Therefore, the injection of O/W (high oil phase viscosity) with 4wt% of emulsion quality and 0.3

PV of emulsion slug size can be treated as a critical combination to achieve good conformance control performance.

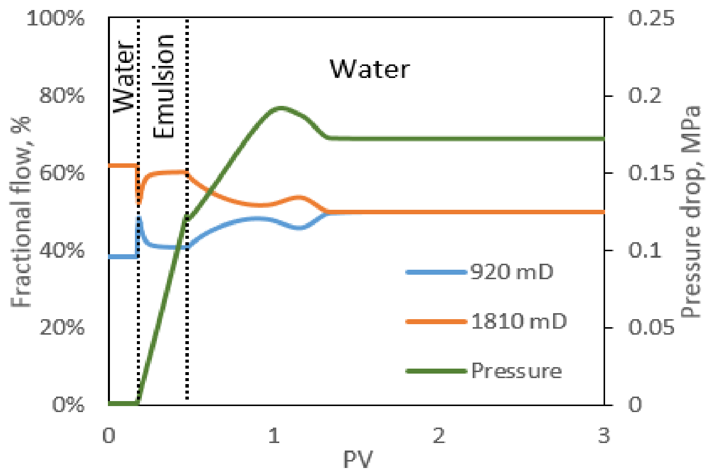

Figure 3.2.19. Fractional flows and pressure drops of O/W emulsion with a high oil phase viscosity injection in the sandpack with a permeability ratio of 2:1- emulsion quality of 4wt% and emulsion slug size of 0.3PV.

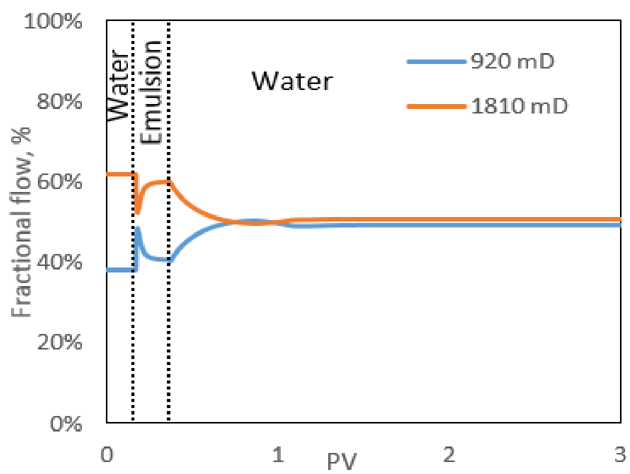

Figure 3.2.20. Fractional flows and pressure drops of O/W emulsion with a high oil phase viscosity injection in the sandpack with a permeability ratio of 2:1- emulsion quality of 4wt% and emulsion slug size of 0.2PV.

3.3 Field Scale Simulation Models

The field scale simulation was performed with a three-dimensional heterogeneous model containing 30,000 grid blocks. This 3D model is a half size model because it is symmetrical on each side of the well pair, so only one side of the model needs to be simulated. The model dimension is 50 m in width with 50 grid blocks, 1000 m in length (along the horizontal wells) with 20 grid blocks, and 30 m in height with 30 grid blocks. The heterogeneity of the simulation model can be created by adding high permeability zones between the injection well and the production well (case 1) and by placing the same size of high permeability zones right above the injection well (case 2). This section, investigates the effects of reservoir heterogeneity on steam chamber development, cumulative oil production, and cSOR for case 1 and case 2. Figure 3.3.1 (a) and (b) show the reservoir model in I-K direction and J-K direction for case 1, respectively. Figure 3.3.2 (a) and (b) show the reservoir model in I-K direction and J-K direction for case 2, respectively. In these figures, the blue area represents a permeability of 1000 mD, and the red area represents a high permeability zone of 3000 mD with 100m in length, 3 m in width, and 6 m in thickness. One injector and one producer as a well pair are perforated along the J direction and are operated for a duration of five years. The injector and producer are parallel to each other, and the vertical distance between them is 5 m.

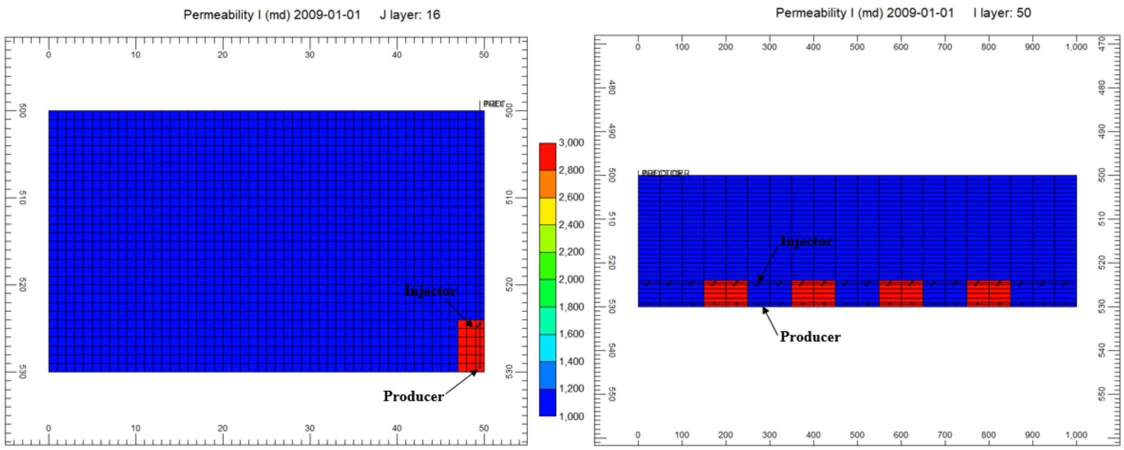

(a) (b)

Figure 3.3.1. Reservoir model for case 1: (a) I-K direction (b) J-K direction.

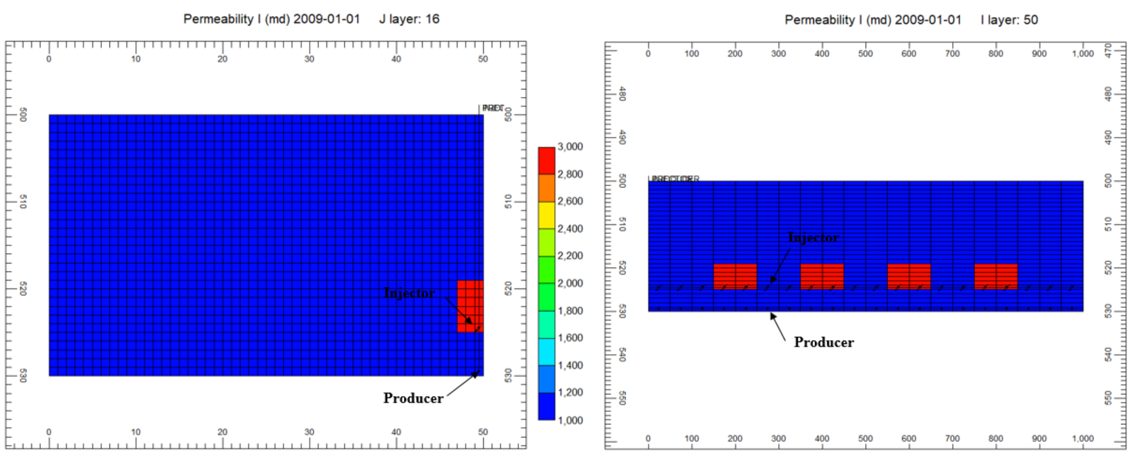

(a) (b)

Figure 3.3.2. Reservoir model for case 2: (a) I-K direction (b) J-K direction.

Reservoir properties and input parameters used in the simulation model are listed in Table 3.5. The O/W emulsion can be treated as an aqueous phase with extremely low bulk viscosity and it can also be mixed with injected water. Therefore, only one pair of the water-oil relative permeability curve and liquid-gas relative permeability curve is used in the field scale simualtion models as shown in Figure 3.3.3 and Figure 3.3.4 (Nasr et al., 2000).

Table 3.5. Reservoir properties and input parameters for SAGD simulation

Reservoir properties and input parameters			
Parameters	**Value**	**Parameters**	**Value**
Grid top, m	500	High permeability I and J, mD	3000
Layer thickness, m	1	High permeability K, mD	2400
Porosity, fraction	0.33	Initial temperature, °C	12
Permeability I and J, mD	1000	Initial pressure, kPa	3000
Permeability K, mD	800	Reference depth, m	500
Bitumen viscosity at 10 °C, cp	5.24×10^{6}	Initial water saturation, %	20
Initial oil saturation, %	80	Porosity Reference Pressure, kPa	3100
Formation Compressibility, 1/kPa	1.0×10^{-6}	Volumetric Heat Capacity, $J/(m^3 \cdot °C)$	2.3×10^{6}
Thermal Conductivity of Reservoir Rock, J/(m*day*°C)	2.7×10^{5}	Thermal Conductivity of Water Phase, J/(m*day*°C)	5.4×10^{4}
Thermal Conductivity of Oil Phase, J/(m*day*°C)	1.2×10^{4}	Thermal Conductivity of Gas Phase, J/(m*day*°C)	4.0×10^{3}
Overburden Volumetric Heat Capacity, $J/(m^3 \cdot °C)$	2.3×10^{6}	Overburden Thermal Conductivity, J/(m*day*°C)	1.5×10^{5}
Underburden Volumetric Heat Capacity, $J/(m^3 \cdot °C)$	2.3×10^{6}	Underburden Thermal Conductivity, J/(m*day*°C)	1.5×10^{5}

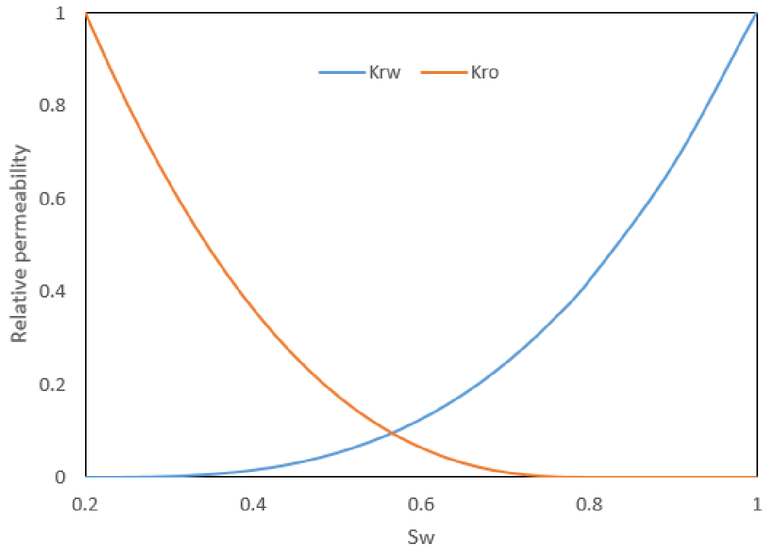

Figure 3.3.3. Water-oil relative permeability curves.

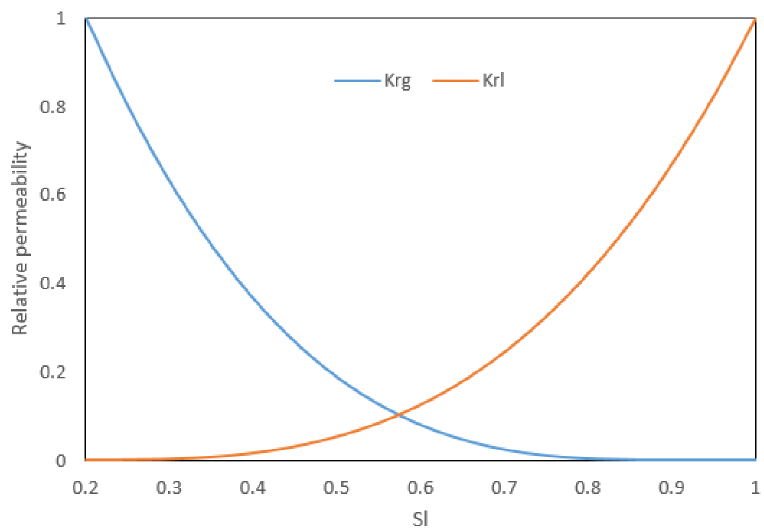

Figure 3.3.4. Liquid-gas relative permeability curves.

A dilation start-up process was applied to build up inter-well communication along the well length before steam injection and to shorten the preheating period, which leads to developing a more uniform/robust steam chamber, thereby reducing the cumulative SOR. However, due to the appearance of heterogeneity in the reservoir, it was necessary to investigate how this heterogeneity could affect the efficiency of the dilation start-up process and to demonstrate the advantages of using O/W emulsion treatment. Therefore, two models for each case were established to separately compare steam chamber growth, cumulative oil production, and cumulative SOR, one employing only a traditional dilation start-up process, and the other utilizing an O/W emulsion treatment before a dilation start-up process.

The analytical dilation recompaction model in CMG STARS module was used to simulate the dilation start-up process, which works for an unconsolidated oil sands reservoir. The porosity and permeability for this model can be altered by a change in pressure only. Figure 3.3.5 shows the schematic of dilation-recompaction model. The corresponding input parameters used in this model are listed in Table 3.6.

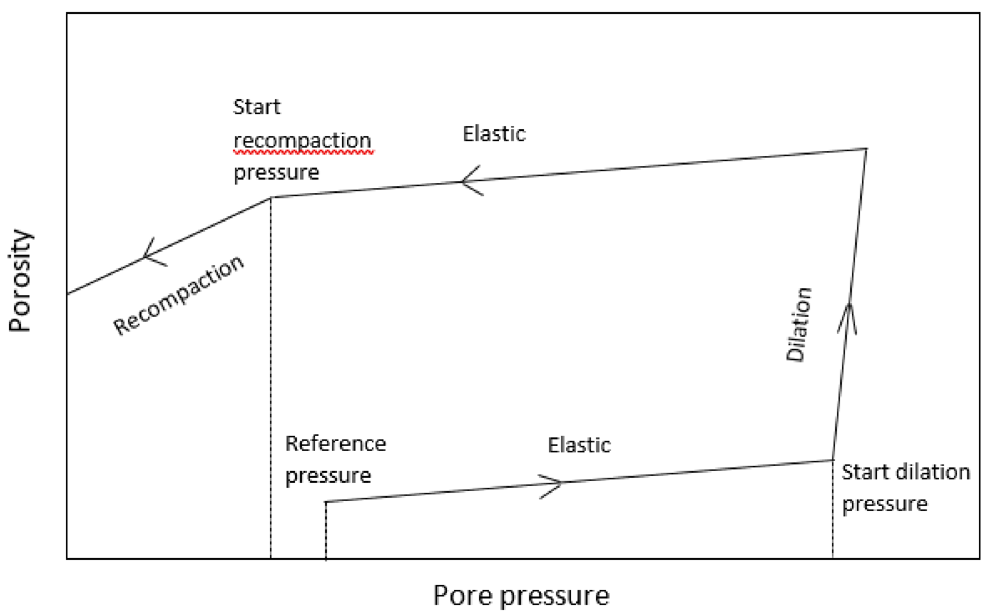

Figure 3.3.5. The dilation-recompaction model in STARS.

Table 3.6. Input parameters for dilation start-up simulation

Parameters	Value	Parameters	Value
Reference pressure, kPa	3100	Dilation Rock Compressibility, 1/kPa	2.0×10^{-4}
Residual dilation fraction	0.77	Start dilation pressure, kPa	3900
Start recompaction pressure, kPa	3000	Maximum allowed proportional increase in porosity	1.2
Permeability Mutiplier in I, J and K	3		

For this dilation start-up model, the dilation process will be initiated when injection pressure exceeds 3900 kPa. The porosity can be increased to its maximum value of 0.396, and the change in permeability is based on porosity change. The value of dilation rock compressibility determines the speed of an increase in porosity. The rock starts recompaction at a pressure of 3000 kPa, and this value can be obtained from the product of residual dilation fraction and start dilation pressure.

A traditional dilation start-up process operates with an injection of high pressure hot dilation fluid (60℃) into the formation at 5000 kPa and an injection rate of 300 m^3/day for half a month. A dilation start-up process with emulsion treatment added a half month of a 2.5 wt% O/W emulsion injection with injection temperature of 60℃ and injection pressure of 3500kPa prior to the traditional dilation start-up process. The producer for these two models is shut-in during the emulsion injection stage and dilation stage. After dilation, both models were set up with one month of preheating period and with identical well constraints for injection and production wells. The well constraint applied to the injection well was 4,000 kPa (maximum bottom-hole pressure), with a steam temperature of 250.3℃ and steam quality of 0.8. The injection well was constrained by a maximum surface water rate of 600 m^3/day in cold water equivalent (CWE). The production well was constrained by a maximum liquid rate of 1200 m^3/day, and a maximum steam rate of 10 m^3/day to prevent the production of live steam. The reservoir models were preheated, both injector and producer, for one month before oil was extracted. Duration of the normal SAGD production process is five years.

3.3.1 Results for Case 1 Simulation Model

Due to the heterogeneity of the reservoir, the steam chamber growth was uneven when only applying dilation start-up process, which can be observed in Figure 3.3.6 below. In this figure, the high permeability zones located between the well pair shows the height of the steam chamber in the high permeability zones grows faster than for the low permeability zones, because the injected steam tends to pass through the high permeability zones. The uneven steam chamber can affect cumulative oil production and cSOR.

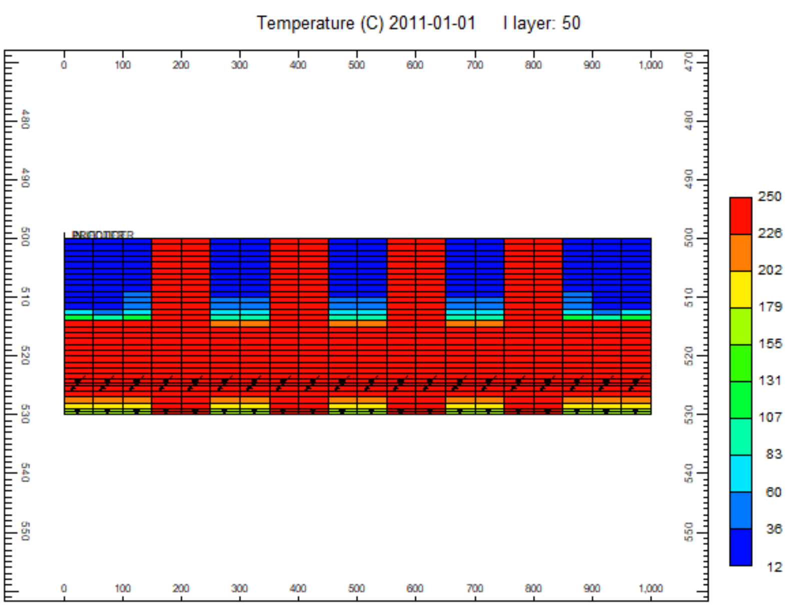

Figure 3.3.6. Temperature profile in J-K direction at one year and ten months of production time for case 1- without O/W emulsion treatment.

Uniform steam chamber growth can be observed in Figure 3.3.7, compared with Figure 3.3.6. This phenomenon shows that the combination of emulsion treatment with traditional dilation start-up process can improve steam chamber growth. In order to observe the boundary and size of steam chamber development, the temperature profiles for case 1 model in I-K direction were plotted as needed.

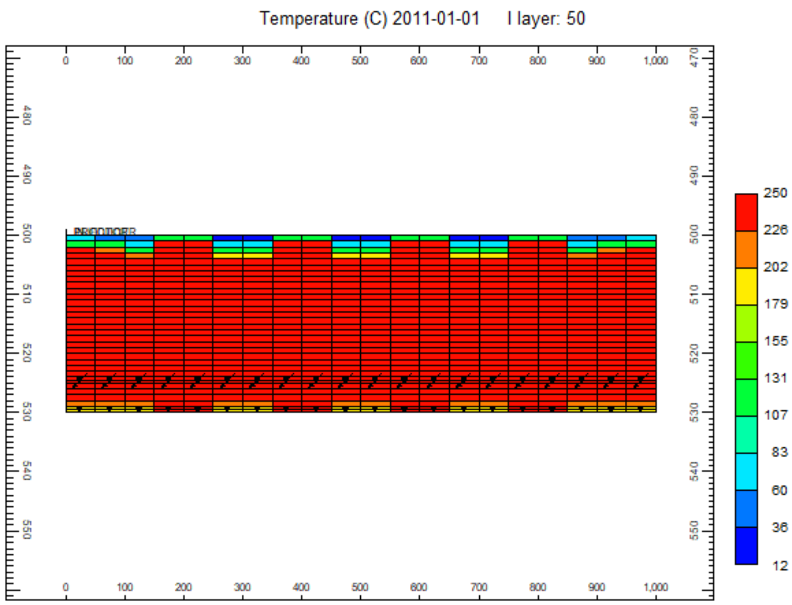

Figure 3.3.7. Temperature profile in J-K direction at one year and ten months of production time for case 1- with O/W emulsion treatment.

Figure 3.3.8 (a) shows that, compared with the traditional start-up process without emulsion treatment depicted in Figure 3.3.8 (b), the start-up process with emulsion treatment has a more uniform temperature profile between the injector and producer, which means that inter-well communication has been successfully achieved at ten months of SAGD production time. After one year and ten months and four years and ten months of SAGD production time, better development of the steam chamber for the model with emulsion treatment can be observed in Figure 3.3.9 (a) and Figure 3.3.10 (a) as the steam chamber are larger than without emulsion treatment, as shown in Figure 3.3.9 (b) and Figure 3.3.10 (b).

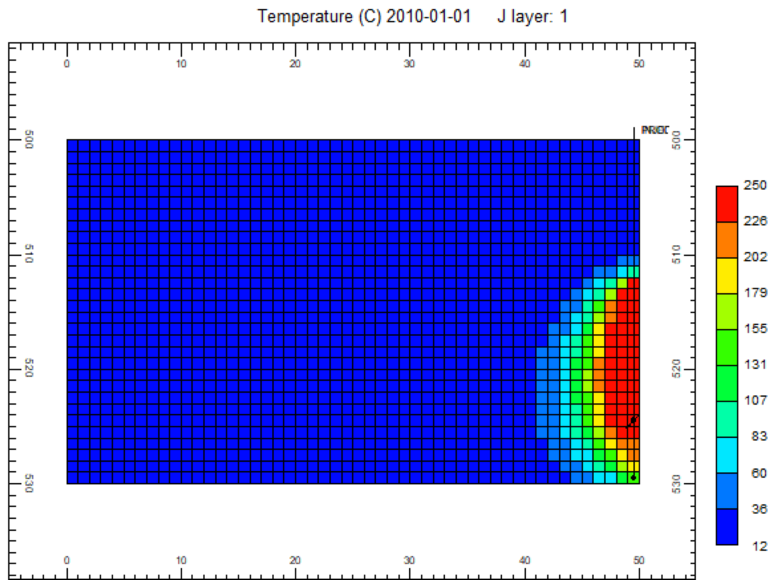

(a)

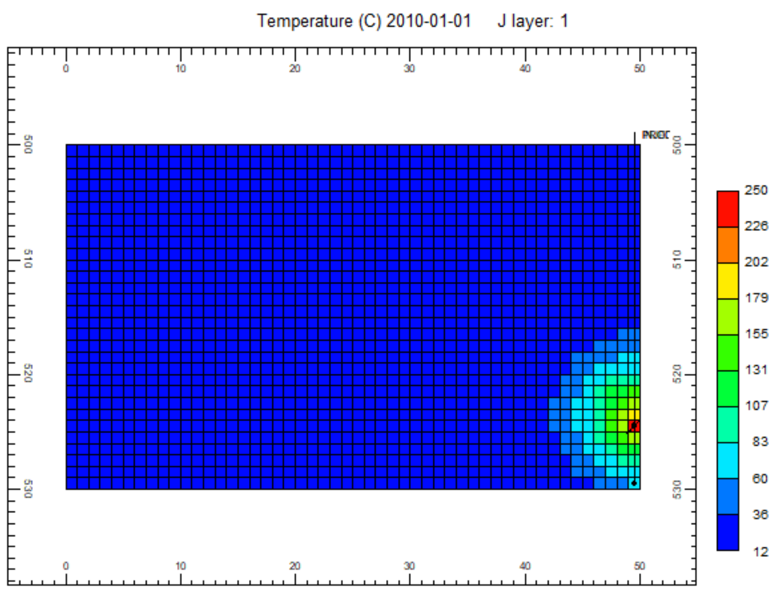

(b)

Figure 3.3.8. Temperature profiles at ten months of production time for case 1: (a) with emulsion treatment (b) without emulsion treatment.

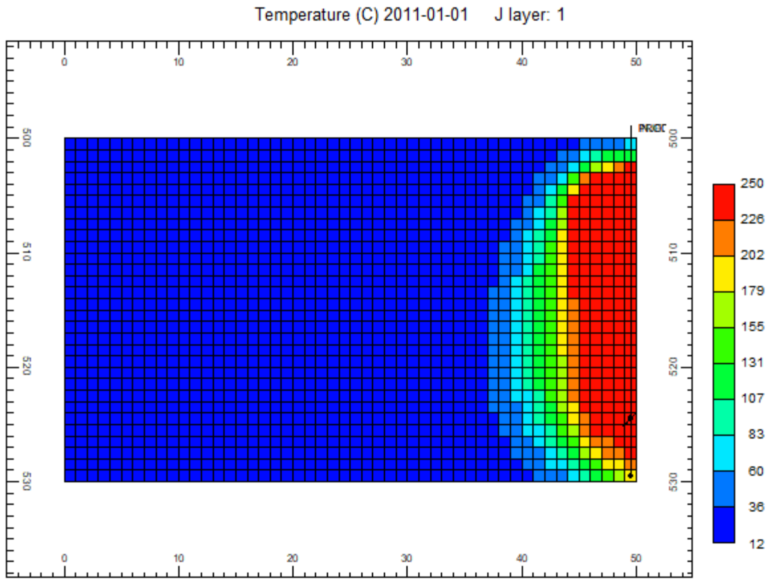

(a)

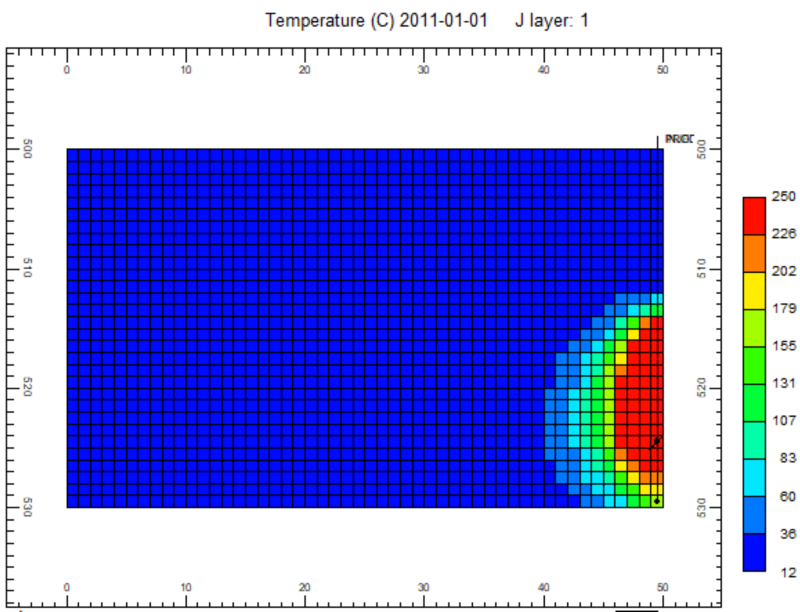

(b)

Figure 3.3.9. Temperature profiles at one year and ten months of production time for case 1: (a) with emulsion treatment (b) without emulsion treatment.

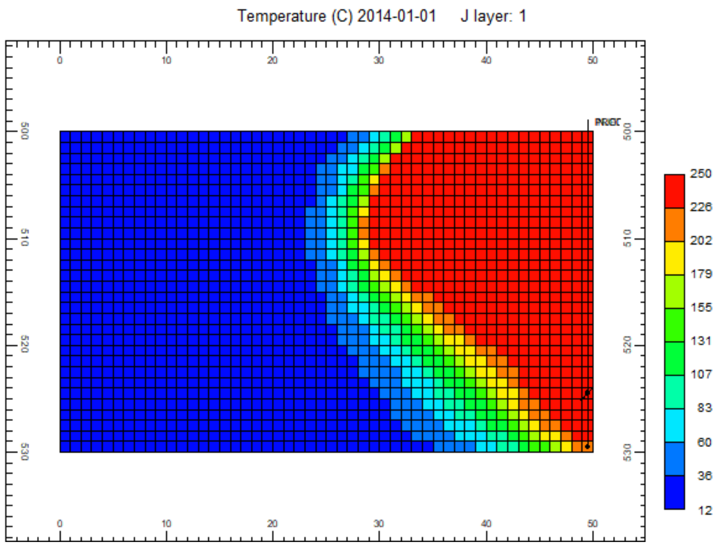

(a)

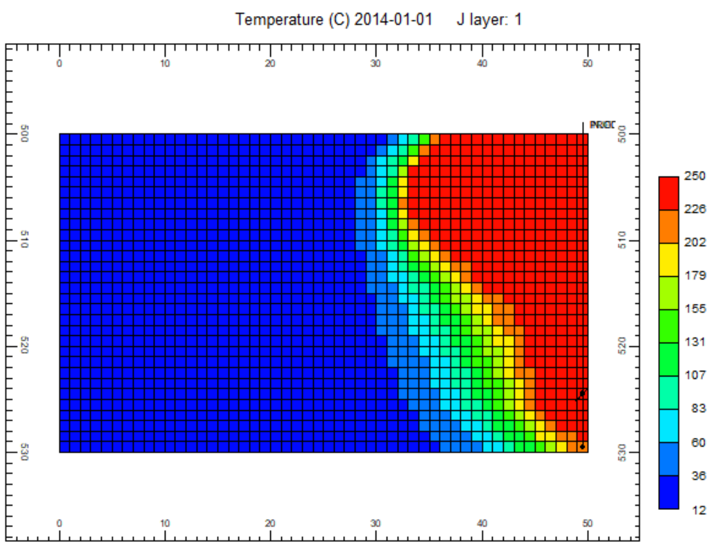

(b)

Figure 3.3.10. Temperature profiles at four years and ten months of production time for case 1: (a) with emulsion treatment (b) without emulsion treatment.

Figure 3.3.11 shows a reduced cumulative SOR (cSOR) with emulsion treatment and, no matter in what stage of the SAGD process, the cSOR for the model with emulsion treatment was always lower than with the traditional dilation start-up process. Better steam chamber growth and reduced CSOR show that the high permeability zones between the injector and the producer (case 1) can be blocked by O/W emulsion and dilation fluid can be diverted to the low permeability zone. Clearly, in the presence of reservoir heterogeneity, O/W emulsion treatment can improve the traditional dilation start-up process. After the high permeability zone is blocked, an increase in fractional flow capability of the low permeability zone will assist steam chamber growth during the preheating and normal SAGD production stages and, finally, will lead to higher cumulative oil production, as shown in Figure 3.3.12. The model with emulsion treatment produced around 79,626 m^3 of oil at the end of the production time which is much higher than the cumulative oil production for the model without emulsion treatment (about 63,355 m^3 of produced oil).

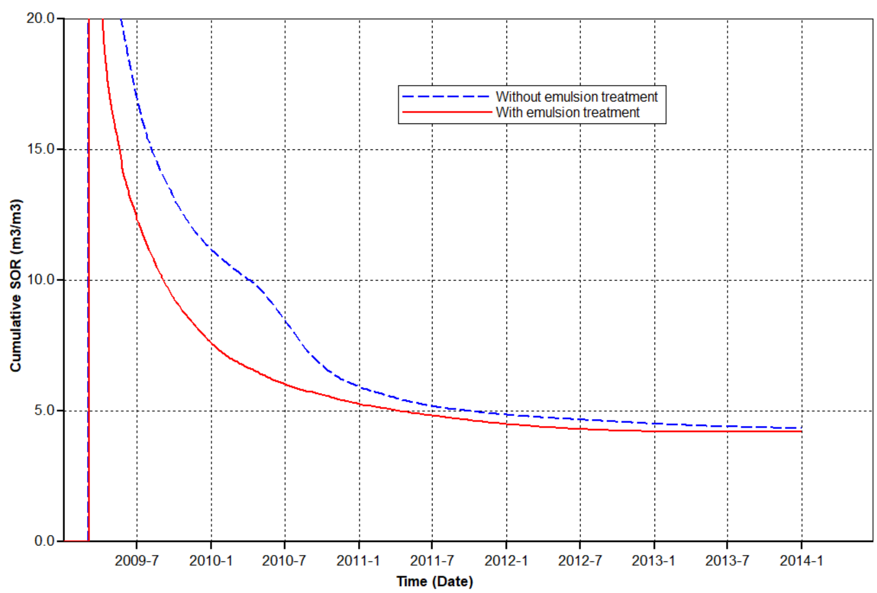

Figure 3.3.11. The cSOR profile for the dilation start-up process with and without emulsion treatment-Case 1.

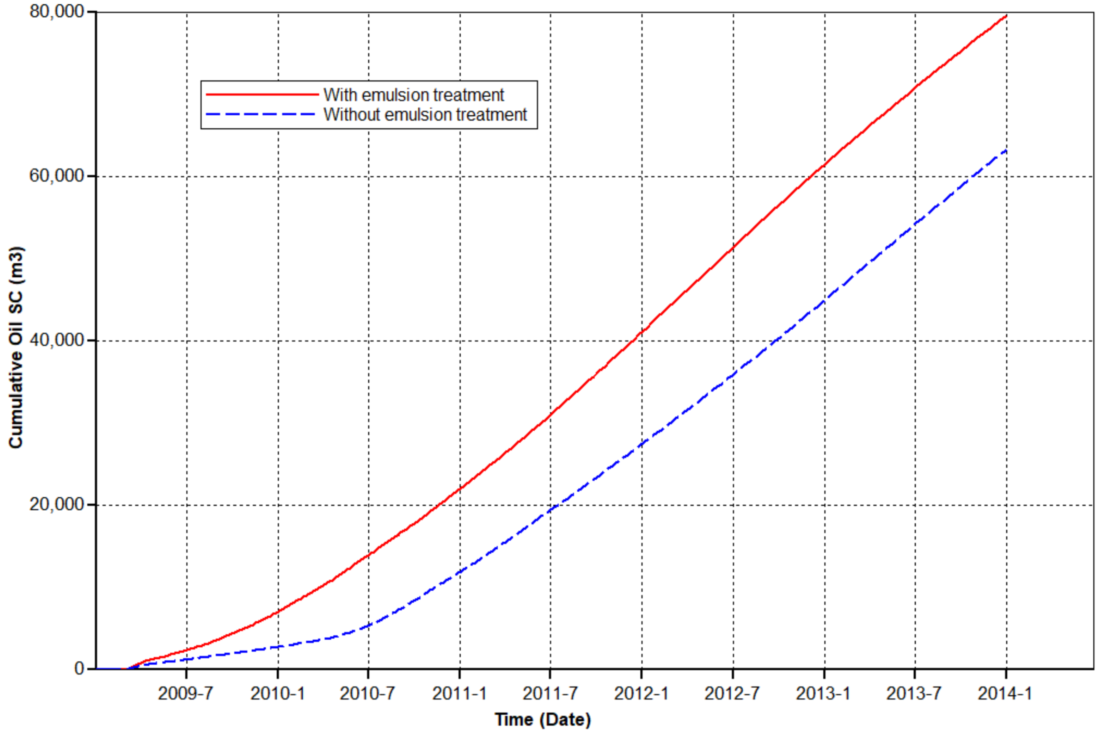

Figure 3.3.12. The cumulative oil production profile for the dilation start-up process with and without emulsion treatment-Case 1.

3.3.2 Results for Case 2 Simulation Model

Figure 3.3.13 shows how high permeability zones located above injectors can affect steam chamber growth. In this figure, the steam tends to flow into the high permeability zones; as we can see, steam chamber growth is uniform for the high permeability zones above injectors. As long as the steam heats the reservoir through the high permeability zones, the low permeability zones under injectors still can not be heated well, which is not good for building up inter-well communication. Therefore, the dilation start-up process can not assist building uniform steam chamber growth when heterogeneity occurs.

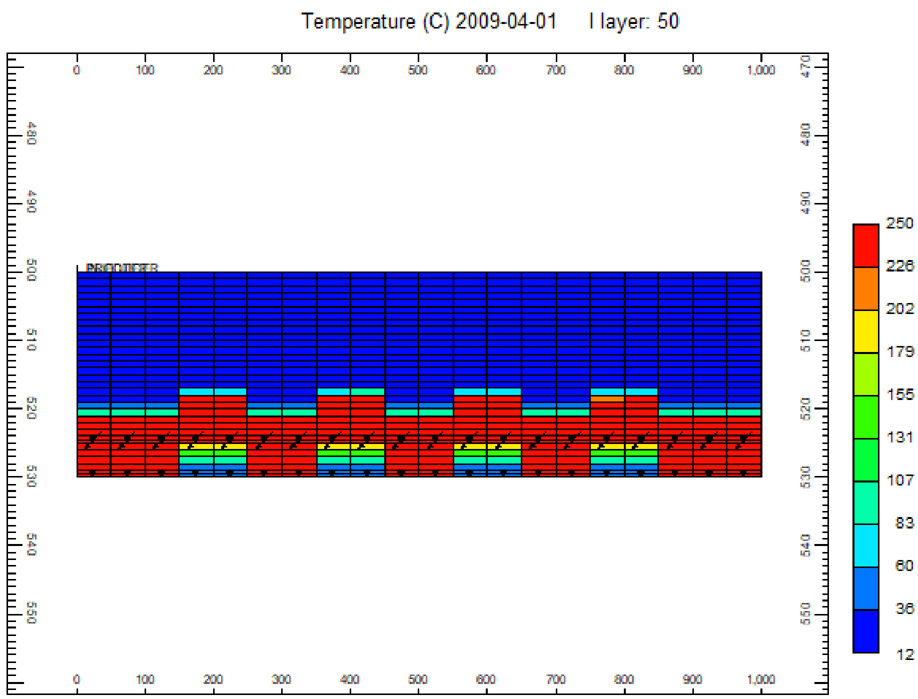

Figure 3.3.13. Temperature profile in J-K direction at one month of production time for case 2-without O/W emulsion treatment.

Figure 3.3.14 demonstrates that, compared with the traditional start-up process without emulsion treatment, illustrated in Figure 3.3.13, the start-up process with emulsion treatment has a more uniform temperature profile between the injector and producer, which means that the emulsion treatment is effective in decreasing the effects of reservoir heterogeneity on steam chamber growth.

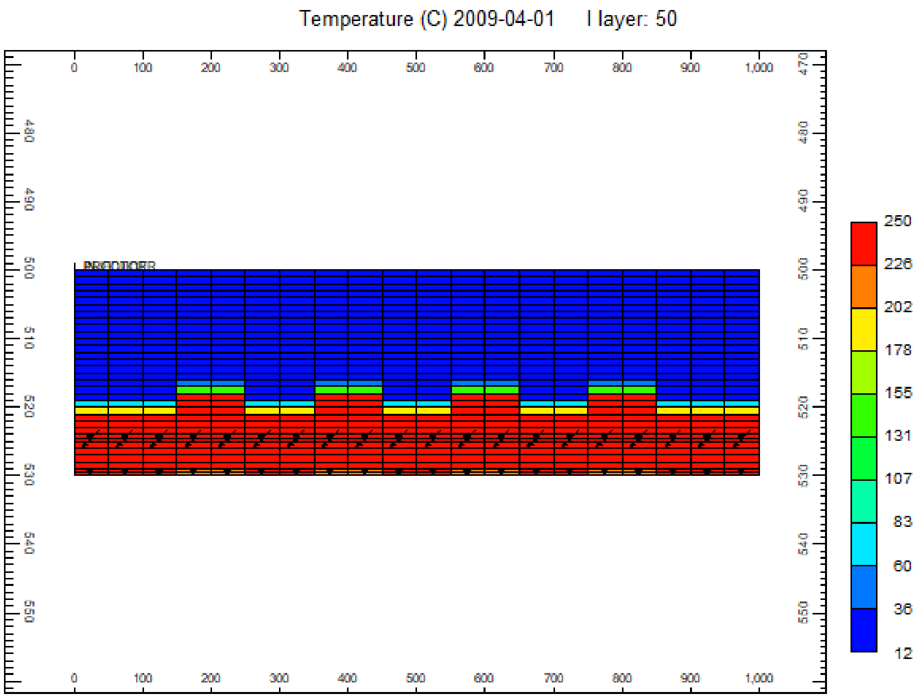

Figure 3.3.14. Temperature profile in J-K direction at one month of production time for case 2-with O/W emulsion treatment.

Figure 3.3.15 shows the temperature profile in J-K direction at one year of production time without O/W emulsion treatment. In this figure, steam chamber growth for the whole reservoir model is not uniform. Since inter-well communication can not be built up during the start-up process, the oil becomes more difficult produce from the zones which are unheated. However, O/W emulsion treatment can assist the dilation start-up process in building good communication between the injection well and the production well. More uniform steam chamber growth can be observed in Figure 3.3.16.

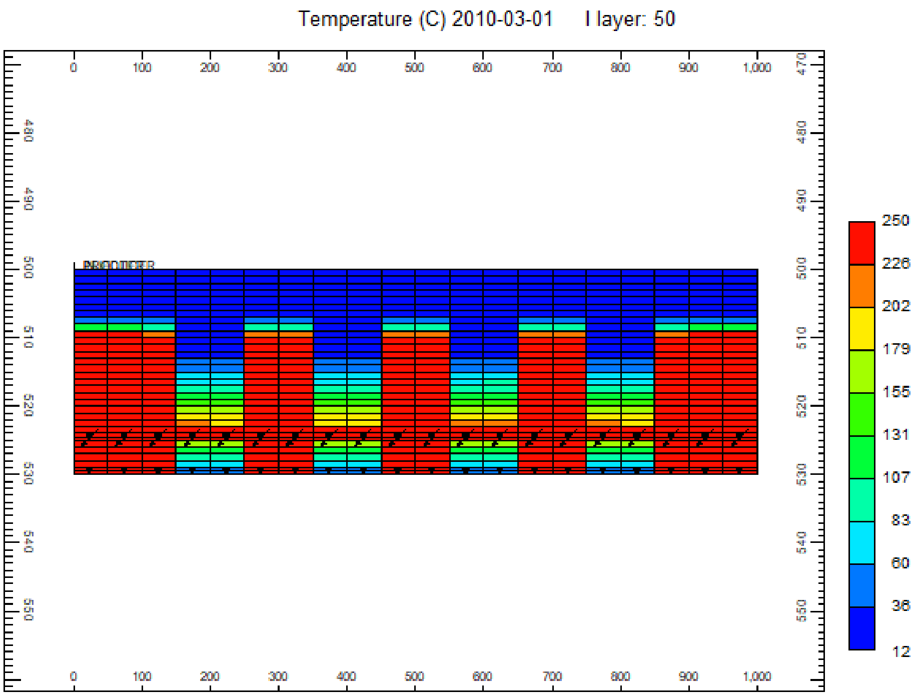

Figure 3.3.15. Temperature profile in J-K direction at one year of production time for case 2-without O/W emulsion treatment.

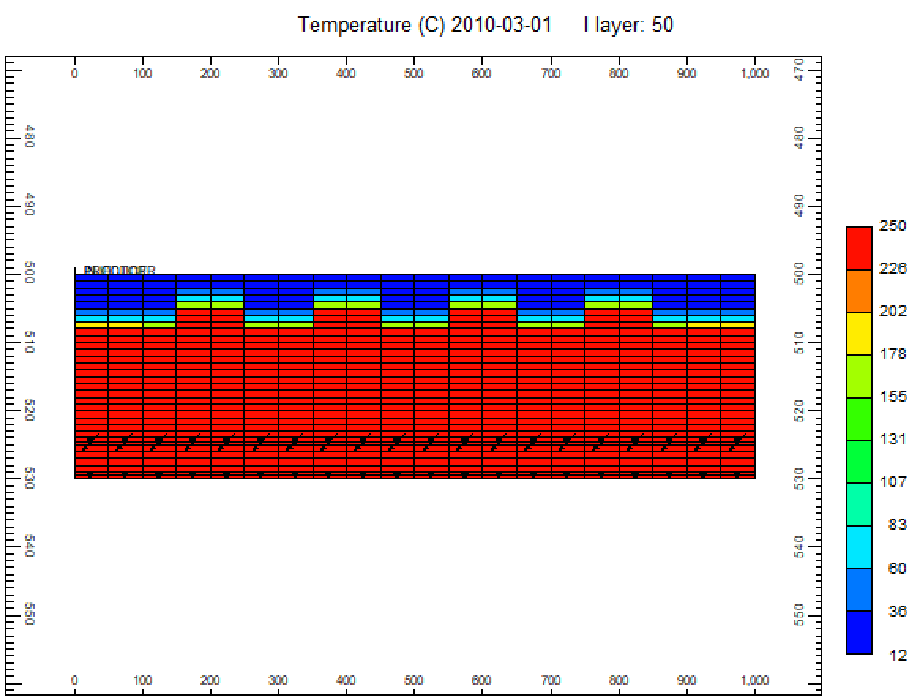

Figure 3.3.16. Temperature profile in J-K direction at one year of production time for case 2-with O/W emulsion treatment.

Figure 3.3.17 (a) demonstrates that, compared with the traditional start-up process without emulsion treatment depicted in Figure 3.3.17 (b), a more uniform temperature profile between the injector and producer can be achieved via the start-up process with O/W emulsion treatment, which means that inter-well communication has been successfully built up at one month of SAGD production time. After one year and three months of SAGD production time, better development of the steam chamber and much larger size of the steam chamber for the model with emulsion treatment can be observed in Figure 3.3.18 (a). Figure 3.3.18 (b) shows that inter-well communication is just achieved after one year and three months of production time, which is much slower than for the model with emulsion treatment.

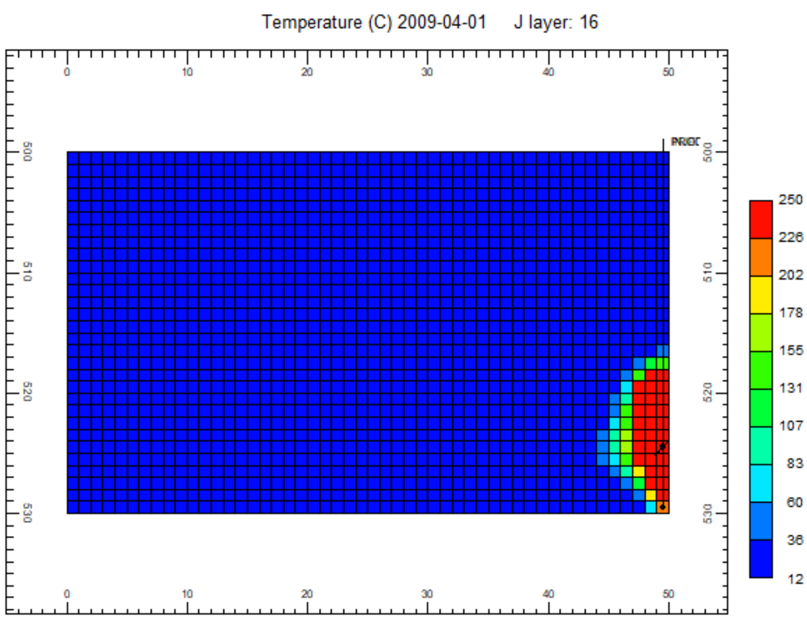

(a)

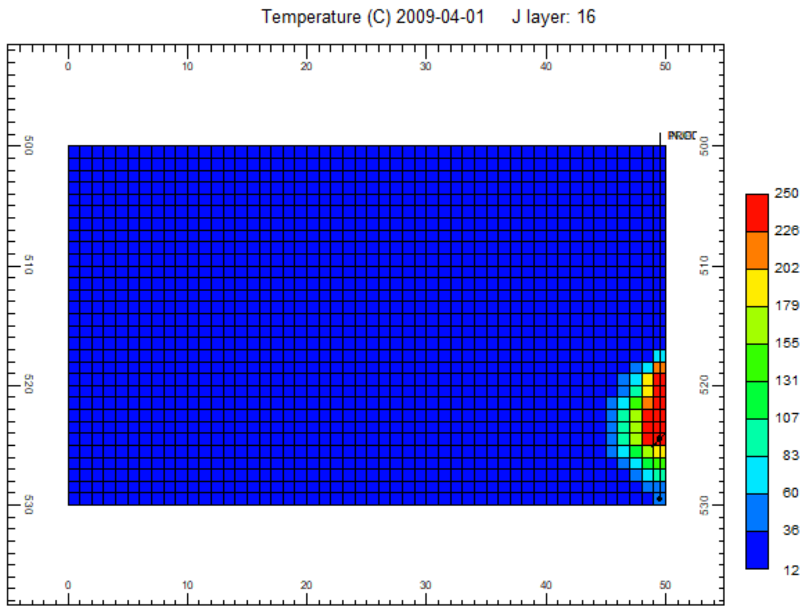

(b)

Figure 3.3.17. Temperature profiles at one month of production time for case 2: (a) with emulsion treatment (b) without emulsion treatment.

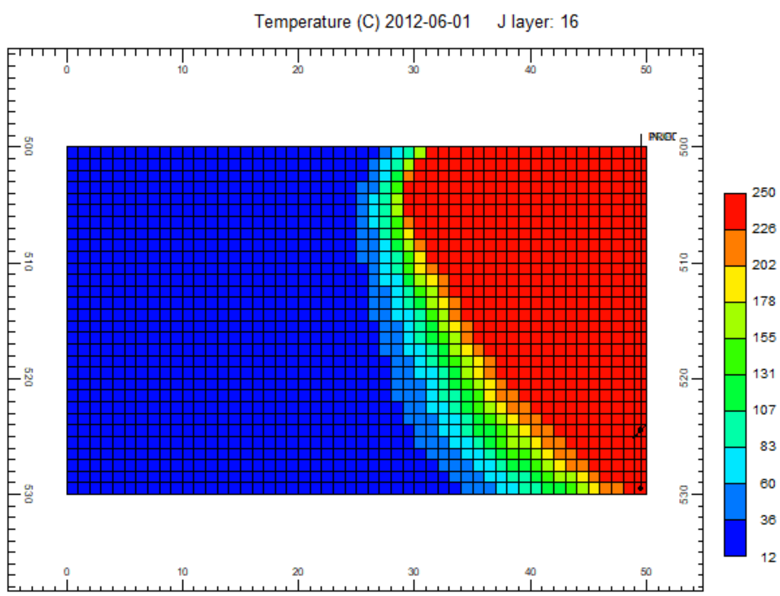

(a)

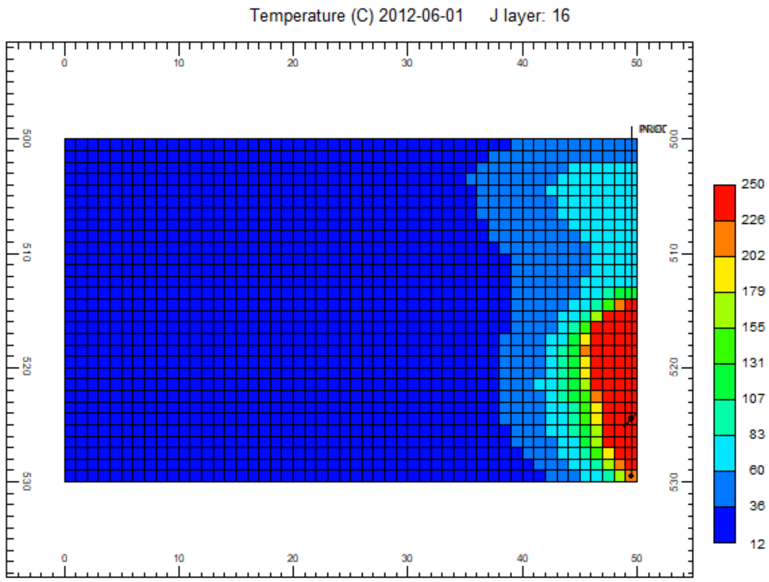

(b)

Figure 3.3.18. Temperature profiles at one year and three months of production time for case 2: (a) with emulsion treatment (b) without emulsion treatment.

The size of the steam chamber at four years and ten months of production time is much larger as shown in Figure 3.3.19 (a) than as shown in Figure 3.3.19 (b), which means the model with emulsion treatment can assist steam chamber growth by building up earlier inter-well communication compared with the model without emulsion treatment. The achievement of earlier inter-well communication can result in an earlier reduction of CSOR and an earlier cumulative oil production, which can be observed in Figure 3.3.20 and Figure 3.3.21.

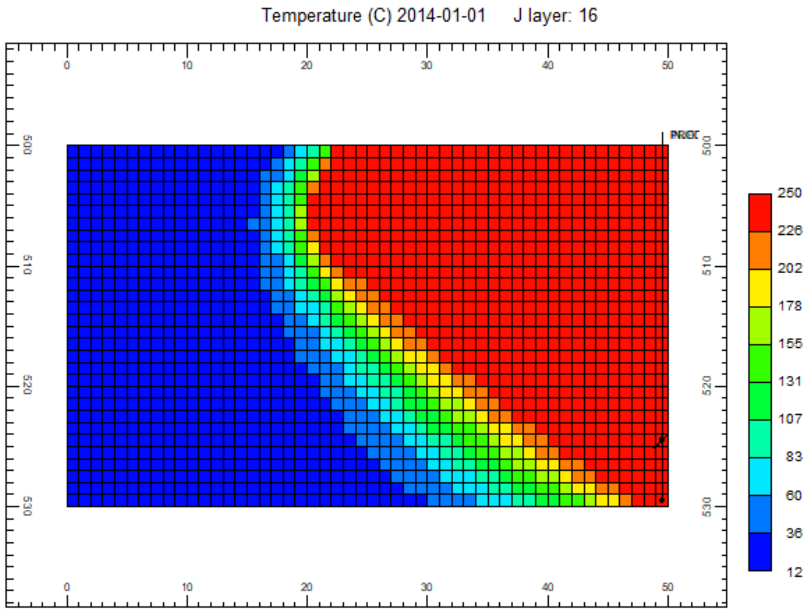

(a)

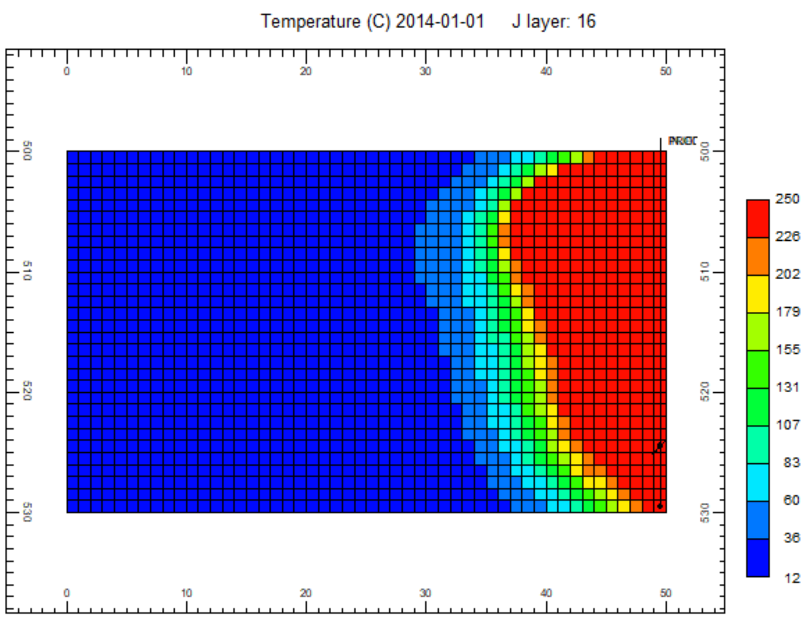

(b)

Figure 3.3.19. Temperature profiles at four years and ten months of production time for case 2: (a) with emulsion treatment (b) without emulsion treatment.

In Figure 3.3.20, the cSOR for the model with emulsion treatments drops earlier than for the model without emulsion treatment, and it remains a lower value during the whole production time. The lower cSOR means the model with emulsion treatment uses less steam to produce oil. The less steam consumed, the better the economics of SAGD production. In Figure 3.3.21, the model with emulsion treatment can start producing oil about seven days earlier than the model without emulsion treatment and, finally, results in more cumulative oil production. The cumulative oil production curve for the model without emulsion treatment has two slopes because the heterogeneity of the reservoir is not overcome at the beginning of production. Once inter-well communication is achieved, the model shows easier production of oil starting in April 2012.

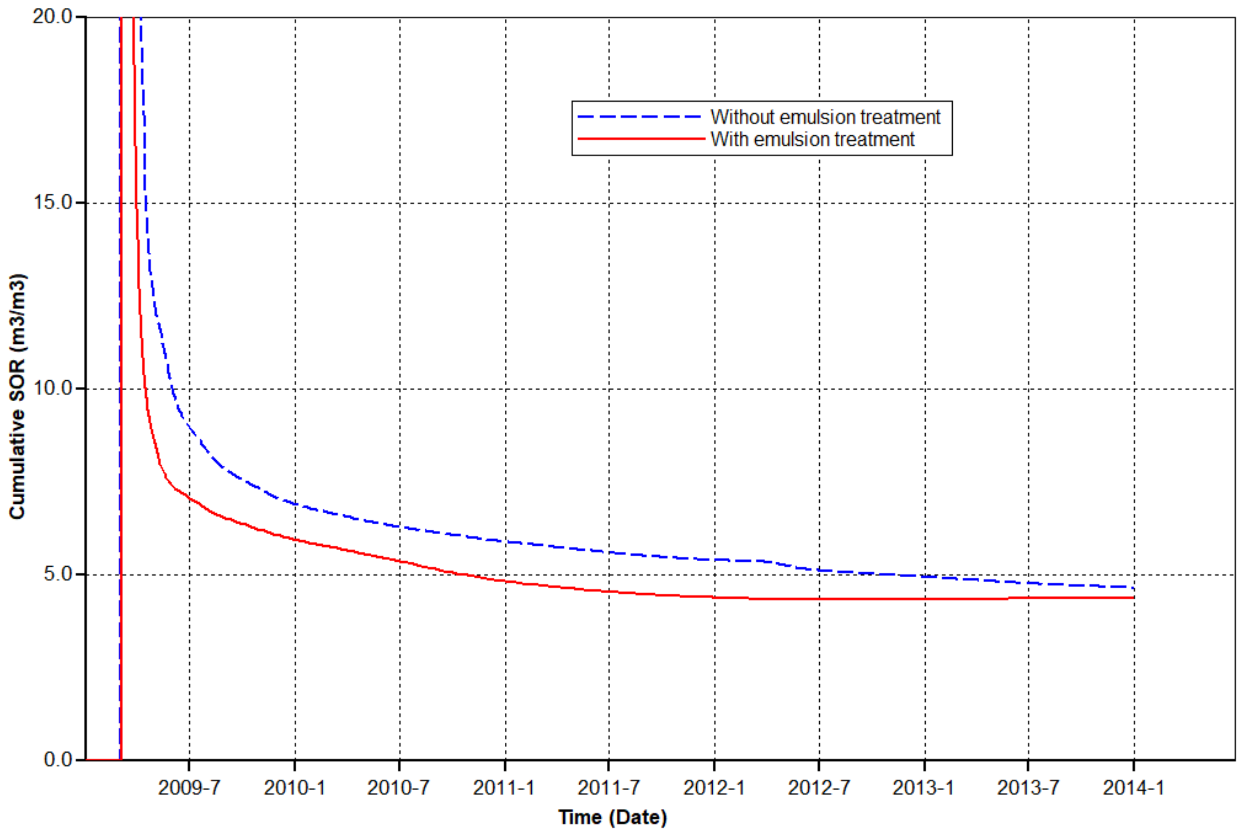

Figure 3.3.20. The cSOR profile for the dilation start-up process with and without emulsion treatment-Case 2.

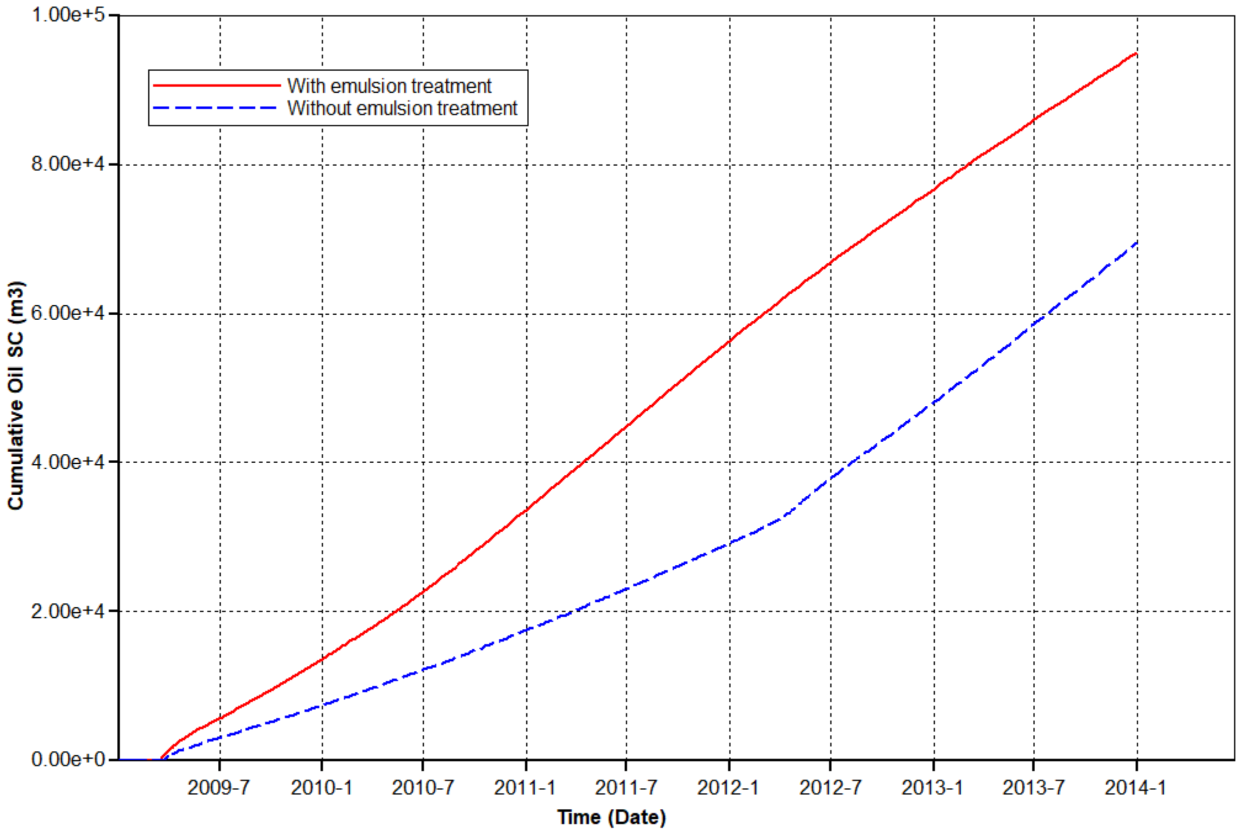

Figure 3.3.21. The cumulative oil production profile for the dilation start-up process with and without emulsion treatment-Case 2.

3.3.3 Sensitivity Tests on Permeability Ratio for Case 1

For the case 1, the high permeability zones are located between the injection well and production well. The permeability ratio of the high permeability zones and the low permeability zones is 3:1. In this section, the permeability ratio will be altered to 4:1 (4000 mD:1000 mD) and 5:1 (5000 mD:1000 mD) in order to investigate the effects of higher permeability ratio on steam chamber growth, cSOR, and cumulative oil production for case 1 simulation model with and without emulsion treatment. As shown in Figure 3.3.22, the heights of steam chamber decrease as the permeability ratio increases. And the temperature profiles between well pair become more non-uniform as the permeability ratio increases. The dilation fluid and injected steam tend to enter high permeability zones, leaving low permeability zones un-dilated and unheated. As permeability for the high permeability zones increased to 5000 mD, more dilation fluid and injected steam escape from these high permeability zones. Therefore, the steam chamber growth becomes more uneven for the model with higher permeability ratio.

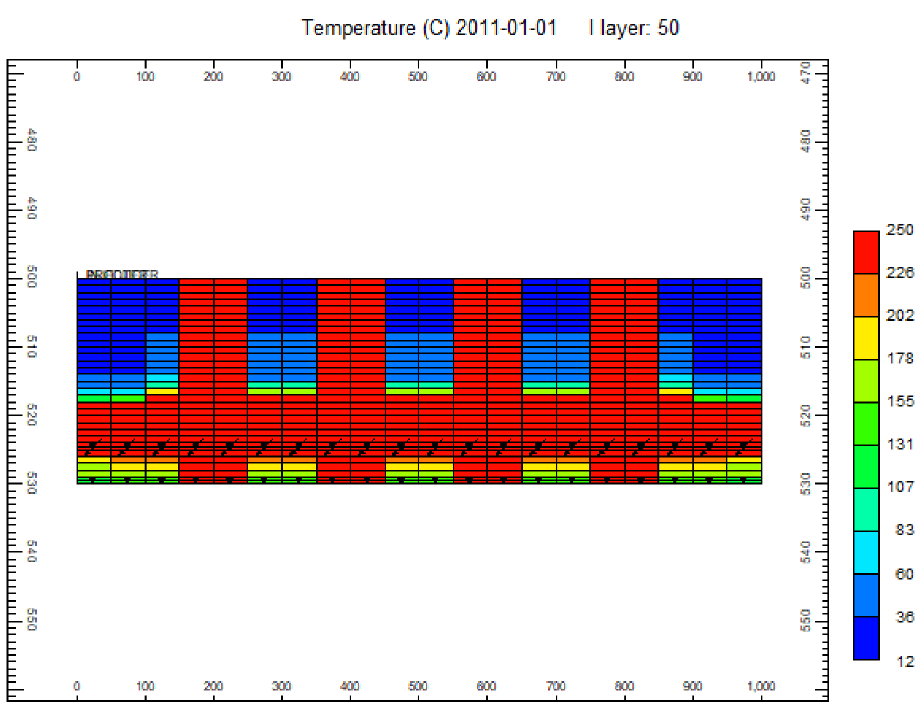

(a)

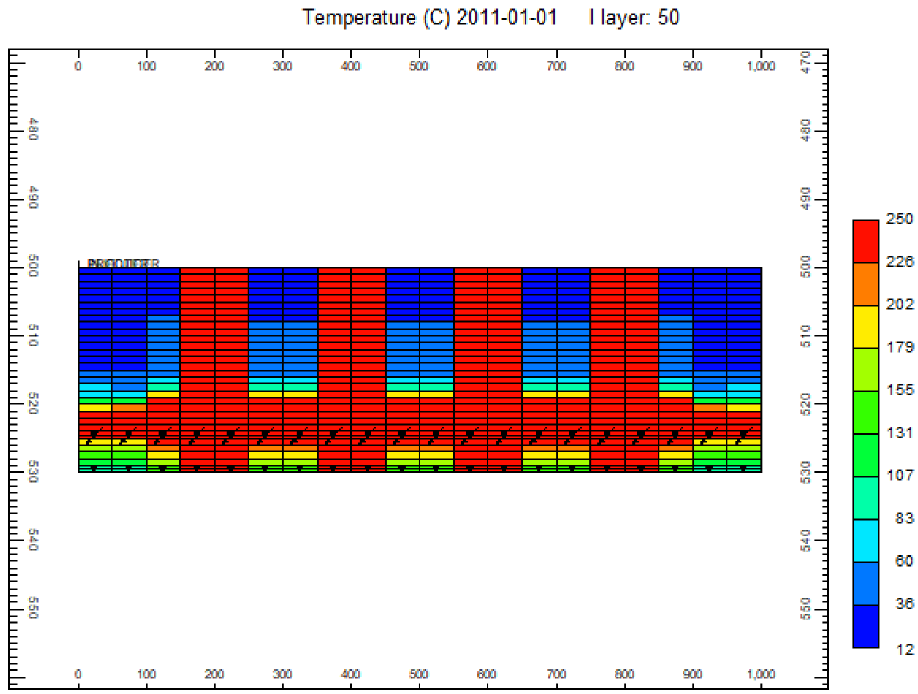

(b)

Figure 3.3.22. Temperature profile in J-K direction at one year and ten months of production time for case 1- without O/W emulsion treatment: (a) permeability ratio of 4:1 (b) permeability ratio of 5:1.

Figure 3.3.23 shows the temperature profiles for the models with emulsion treatment at different permeability ratios. In this figure, an improved steam chamber growth can be observed as the heights of steam chamber increased comparing with Figure 3.3.22. However, the steam chamber growth for the model with a permeability ratio of 5:1 is not promising because the plugging strength created by emulsion droplets is not strong enough to block this high permeability zones (5000 mD) to create more dilation zones between well pair, which indicates that the ability of emulsion to block fluid entering into the high permeability zones is reduced as the permeability ratio increases to 5:1.

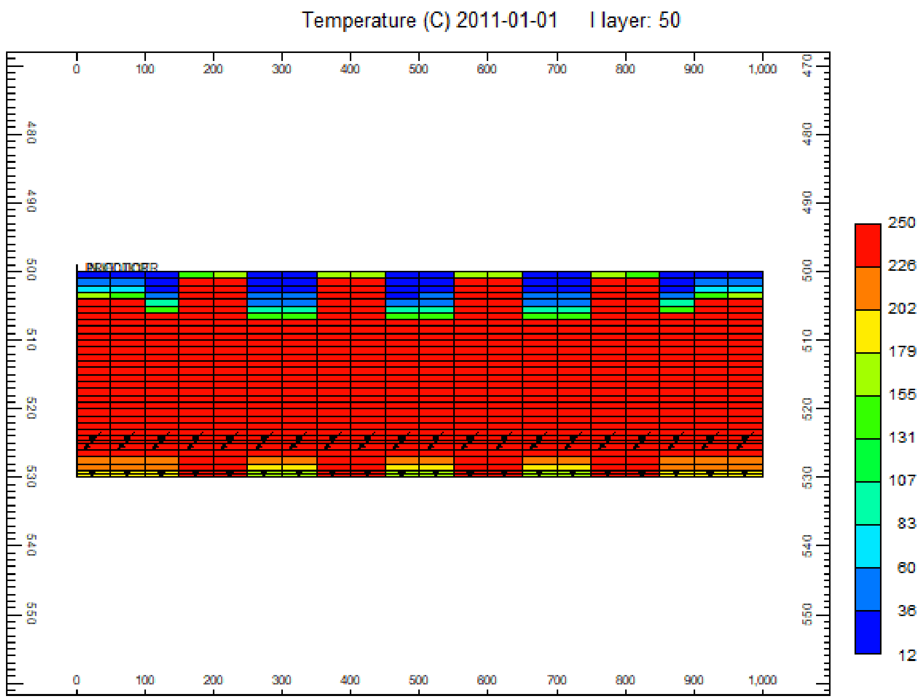

(a)

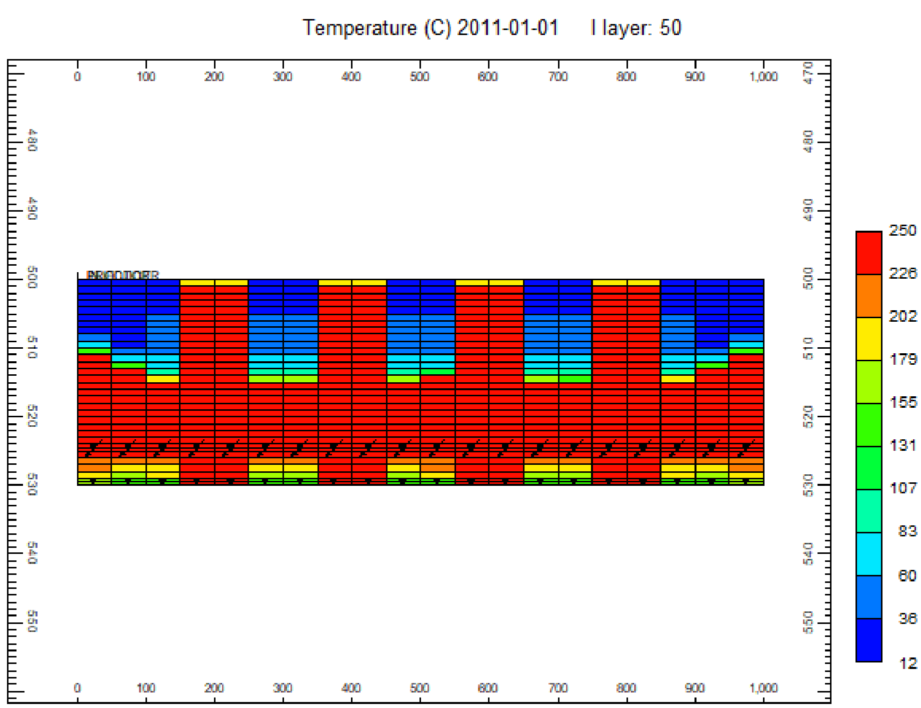

(b)

Figure 3.3.23. Temperature profile in J-K direction at one year and ten months of production time for case 1- with O/W emulsion treatment: (a) permeability ratio of 4:1 (b) permeability ratio of 5:1.

As shown in Figure 3.3.24, the cumulative oil production decreases as the permeability ratio increases. Because the steam chamber developed more uneven for the model with a higher permeability ratio than for the model with a lower permeability ratio, the less amount of oil is produced for more severely heterogeneous model. The earliest cSOR curve drops can be observed for the model with a smallest permeability ratio (3:1) as shown in Figure 3.3.25, since less amount of injected steam is required to produce oil when the reservoir heterogeneity is not severe.

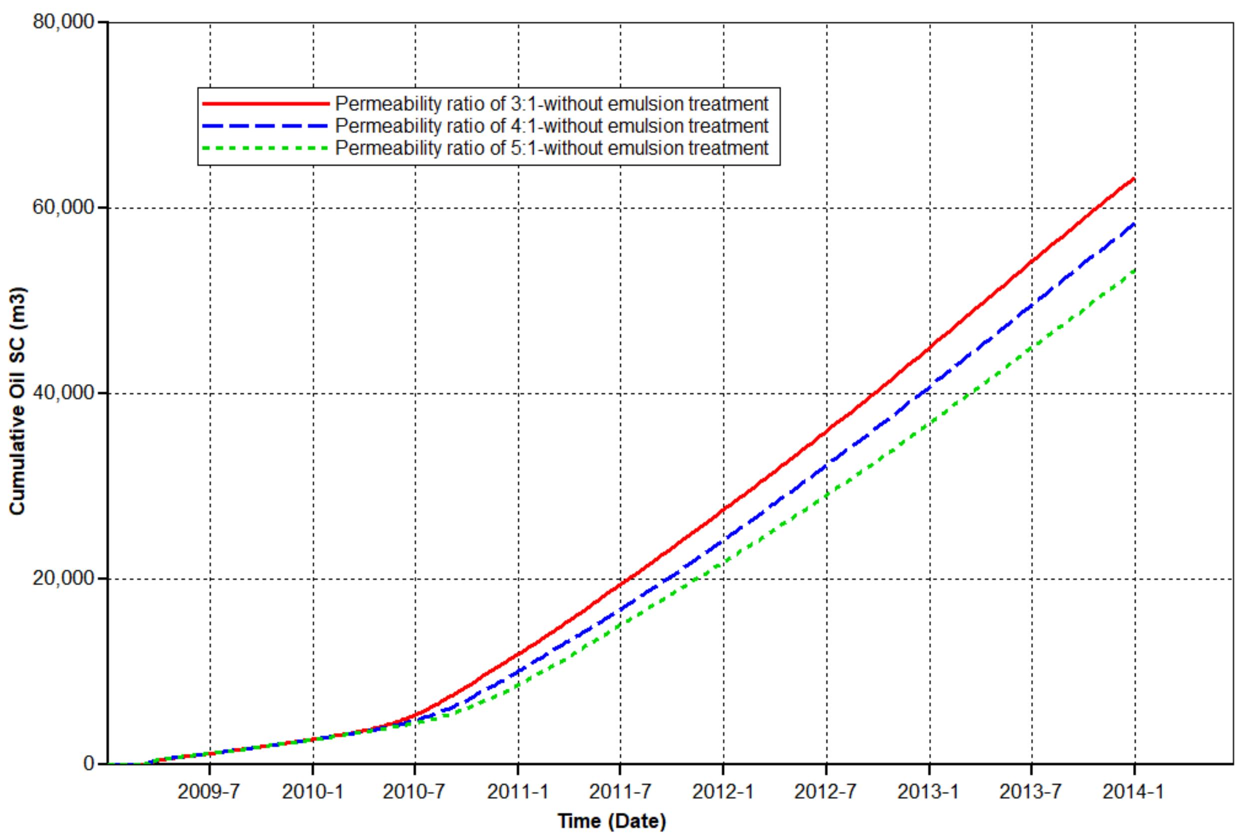

Figure 3.3.24. The cumulative oil production profile at different permeability ratios for case 1 without emulsion treatment.

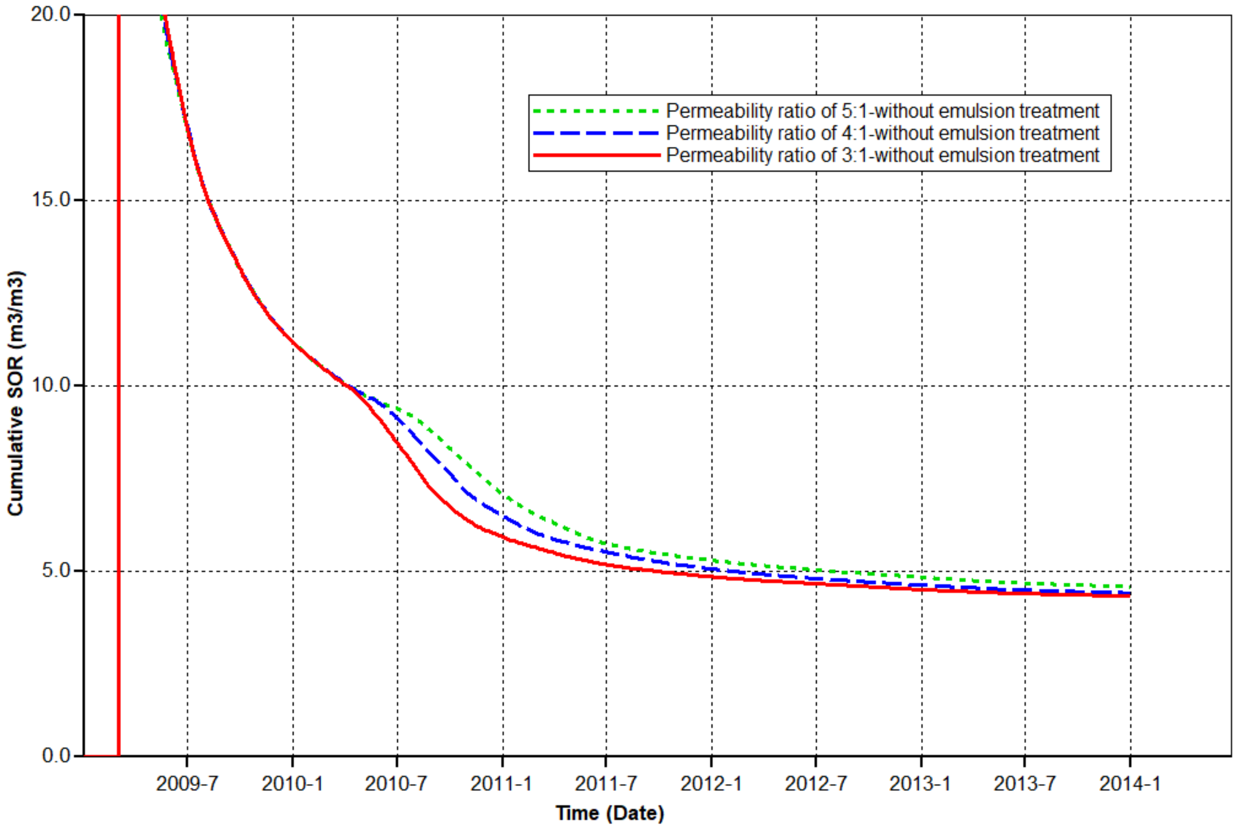

Figure 3.3.25. The cSOR profile at different permeability ratios for case 1 without emulsion treatment.

Figure 3.3.26 shows the cumulative oil production difference between the models with a permeability ratio of 3:1 and with a permeability ratio of 4:1 is small. However, the cumulative oil production difference between the models with a permeability ratio of 3:1 and with a permeability ratio of 5:1 is large, which means the effectiveness of emulsion treatment is reduced due to more severely heterogeneity. Table 3.7 demonstrates the increasing rate in cumulative oil production when using emulsion treatment. The increasing rates for the models with permeability ratio of 3:1 and 4:1 are around 20%. The increasing rate for the model with a permeability ratio of 5:1 is about 13%, which is lower than the models with smaller permeability ratios.

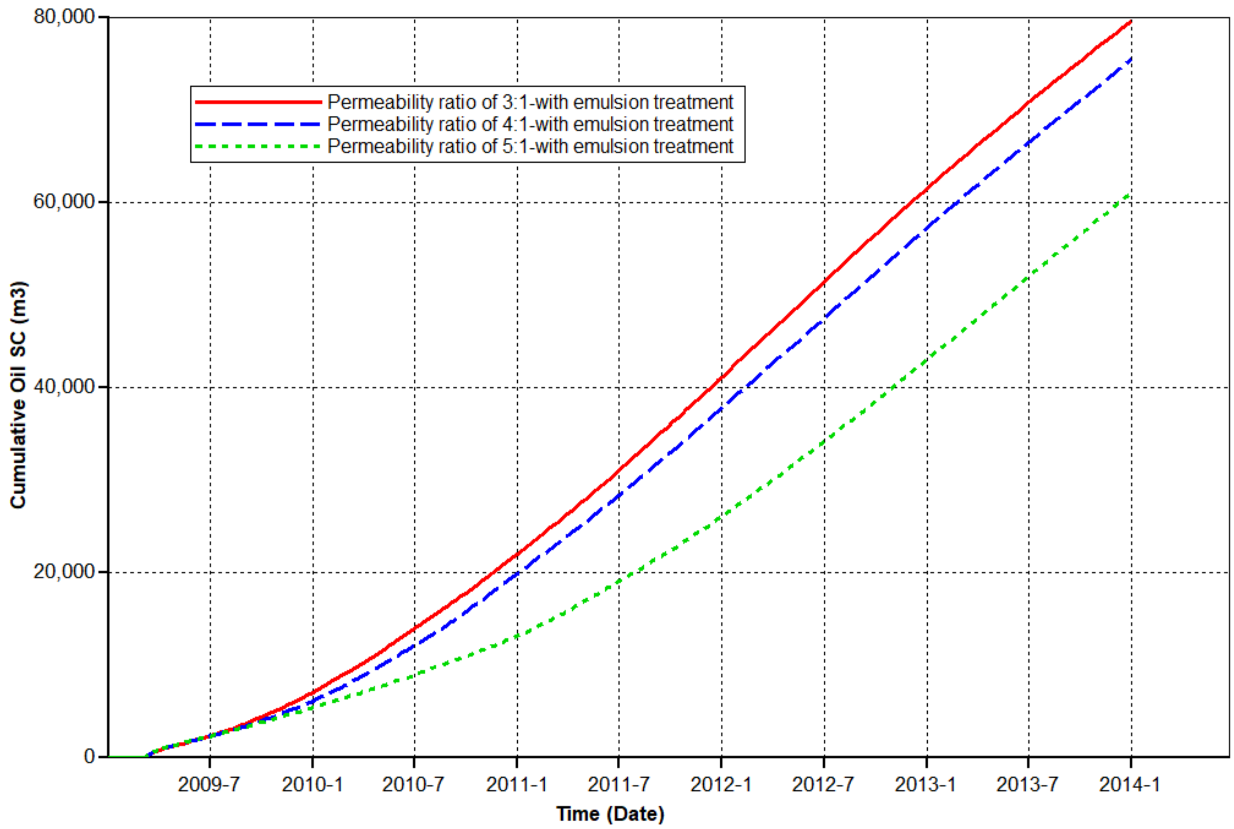

Figure 3.3.26. The cumulative oil production profile at different permeability ratios for case 1 with emulsion treatment.

Table 3.7. The cumulative oil production at different permeability ratios for case 1 without and with emulsion treatment.

Cumulative oil production, m^3			
Permeability ratio	3:1	4:1	5:1
Without emulsion treatment	63355	58366	53258
With emulsion treatment	79626	75417	61061
Increasing rate	20%	23%	13%

As shown in Figure 3.3.27, the cSOR increases as the permeability ratio increases because the injected emulsion is not able to provide sufficient plugging strength to block the high permeability zones (5000 mD), and leads to less dilation fluid flowing into the low permeability zones. If the low permeability zones are un-dilated, then it will take a longer time to build up an inter-well communication and thereby causing an increase in cSOR. The size of high permeability zones is not large enough can be concluded as a reason to explain the cSOR curves has a little difference between injecting the O/W emulsion into the simulation models with a permeability ratio of 3:1 and 4:1 at the post stage of SAGD normal production.

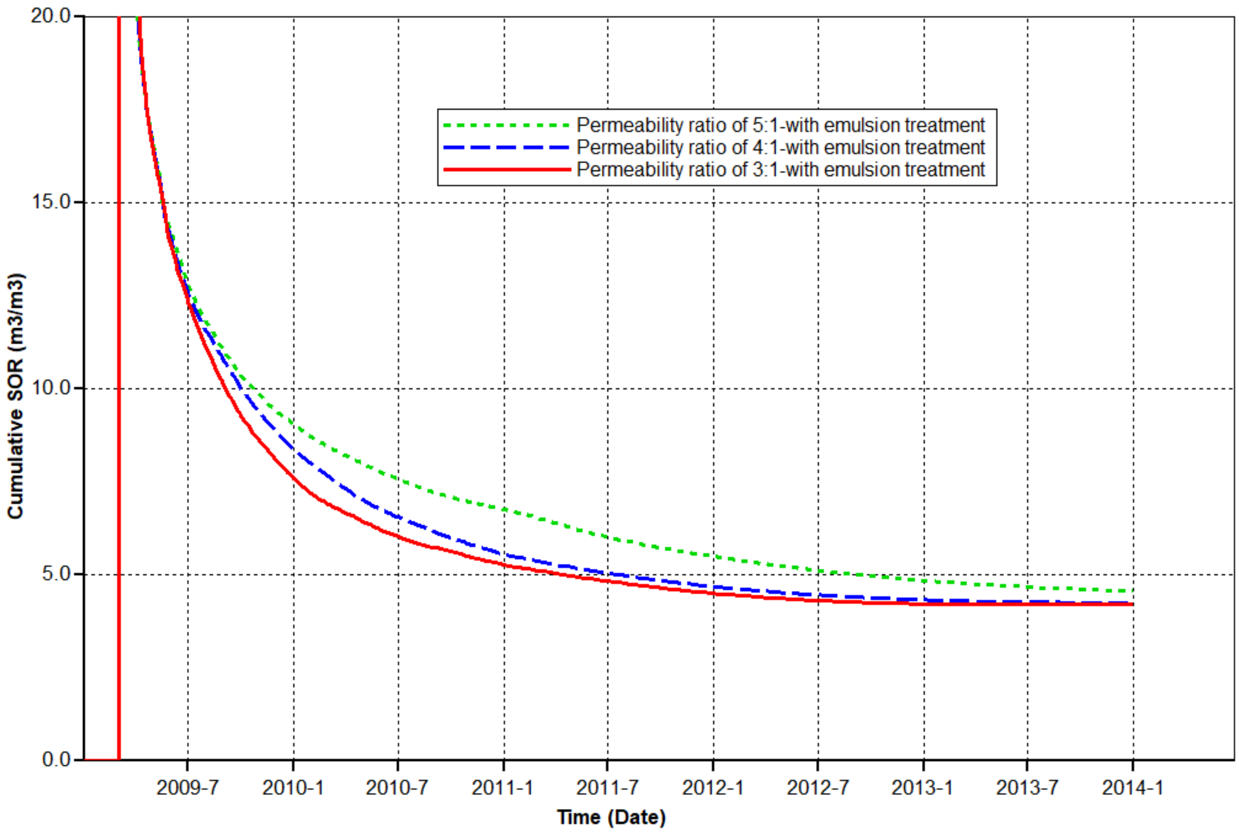

Figure 3.3.27. The cSOR profile at different permeability ratios for case 1 with emulsion treatment.

3.3.4 Sensitivity Tests on Permeability Ratio for Case 2

For the case 2, the high permeability zones are located above the injection well. The permeability ratio of the high permeability zones and the low permeability zones is 3:1. In this section, the permeability ratio will be changed to 4:1 (4000 mD:1000 mD) and 5:1 (5000 mD:1000 mD) in order to investigate the effects of higher permeability ratio on steam chamber growth, cSOR, and cumulative oil production for case 2 simulation model with and without emulsion treatment.

As shown in Figure 3.3.28, the cumulative production profile does not have a big change at different permeability ratios, which means the effectiveness of dilation start-up process does not affected by this type of reservoir heterogeneity (higher permeability zones placed above the injection well).

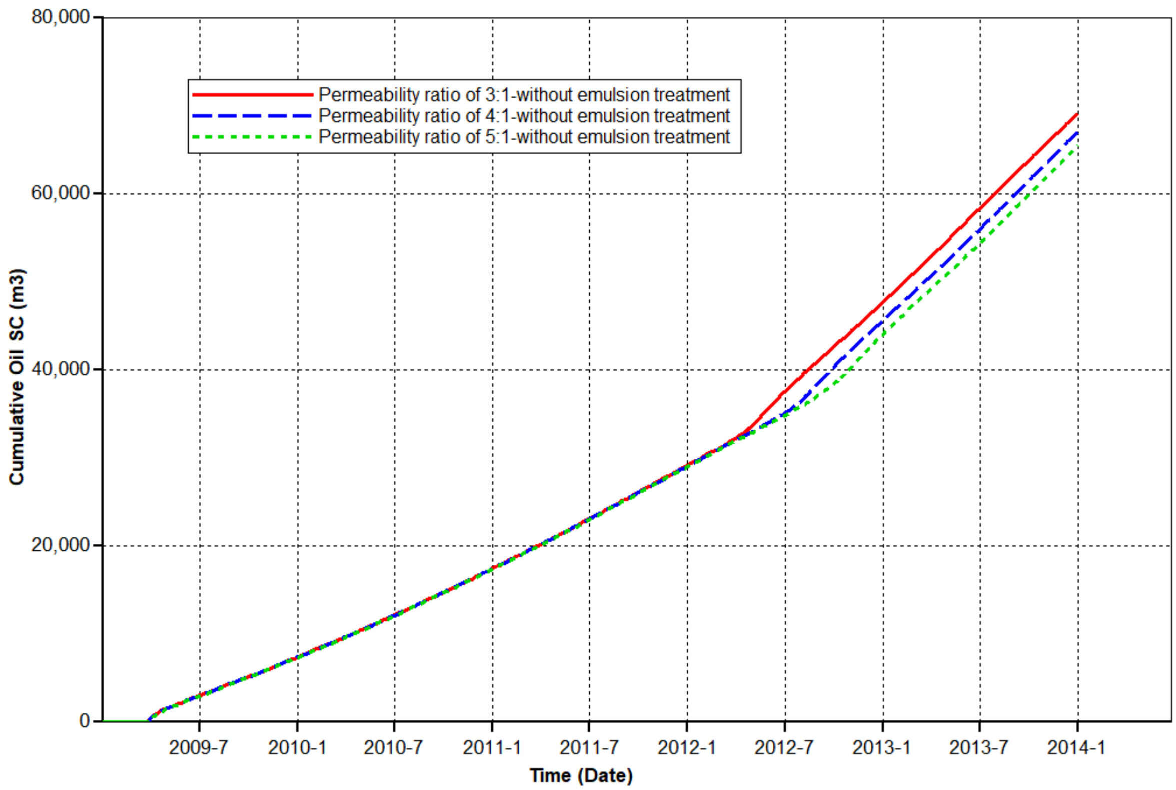

Figure 3.3.28. The cumulative oil production profile at different permeability ratios for case 2 without emulsion treatment.

The cSOR curve for each case is almost same which can be observed in Figure 3.3.29. The cSOR curve for the model with a permeability ratio of 3:1 drops earlier to reach its final value than the models with greater permeability ratios, which can be observed as the only difference between these cSOR curves.

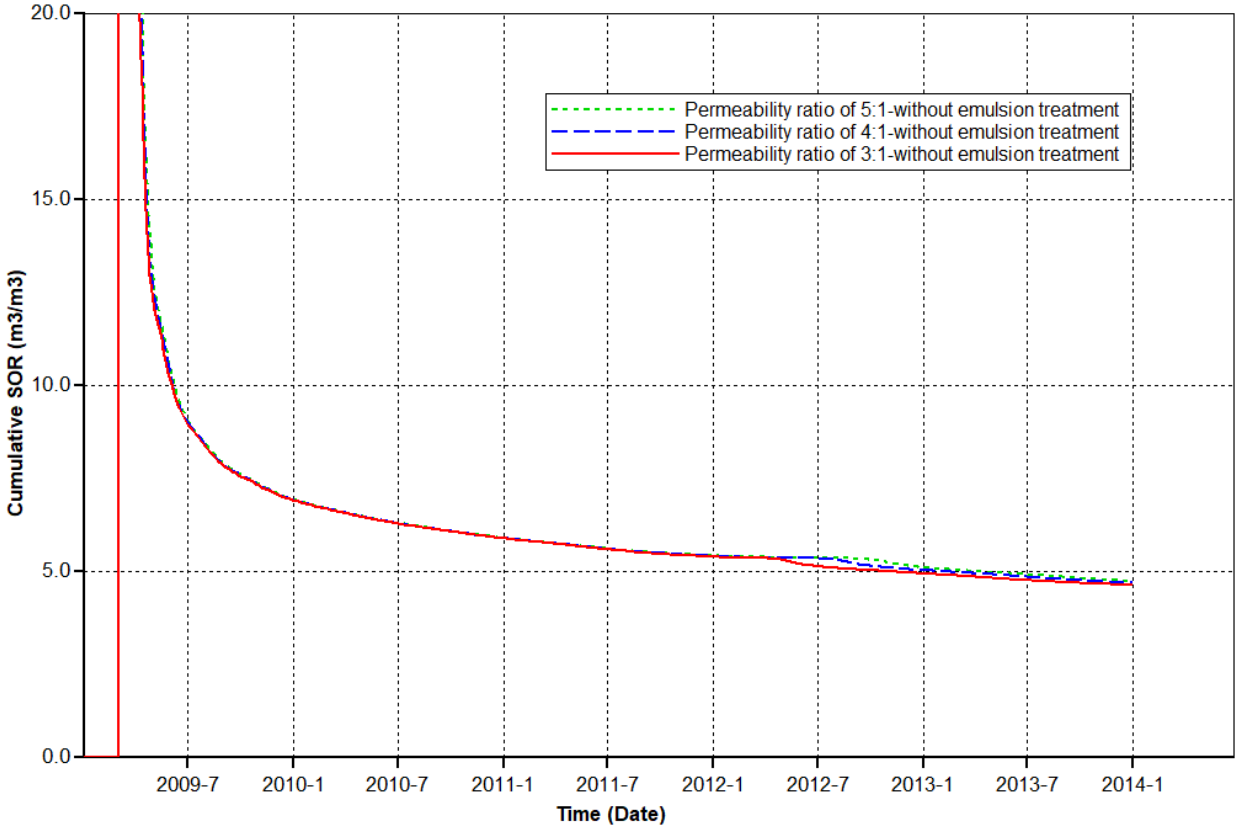

Figure 3.3.29. The cSOR profile at different permeability ratios for case 2 without emulsion treatment.

Figure 3.3.30 shows the cumulative oil production curves at different permeability ratios are almost same, because the injected O/W emulsion has sufficient plugging ability to block the zones with higher permeability (4000 mD and 5000 mD) and can divert the dilation fluid to dilate the low permeability zones. All in all, as the permeability ratio increased for case 1, it reduced the plugging strength caused by O/W emulsion to block the higher permeability zones, which leads to uneven steam chamber growth, cumulative oil production reduction, and increase in cSOR.

However, a greater permeability ratio tested in the case 2 model did not affect the performance of O/W emulsion treatment, which leads to similar cumulative oil production.

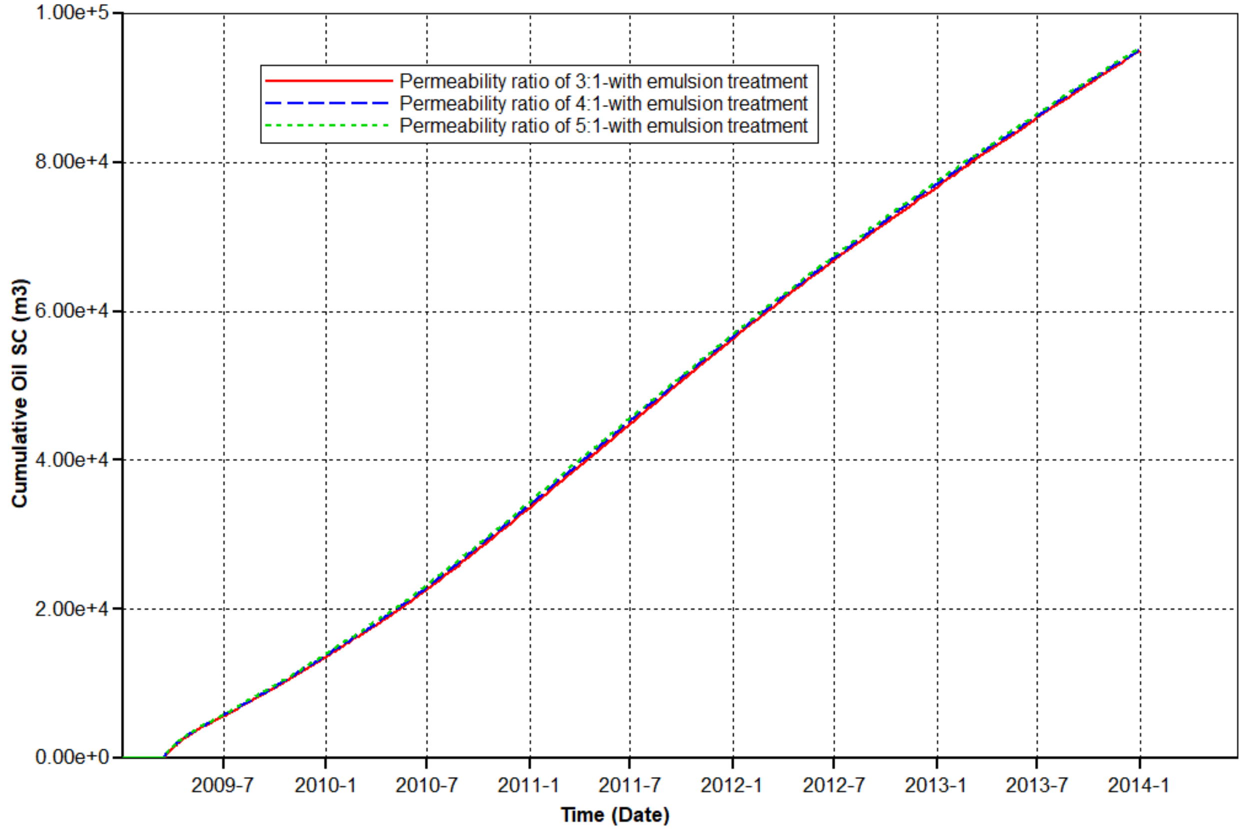

Figure 3.3.30. The cumulative oil production profile at different permeability ratios for case 2 with emulsion treatment.

Chapter 4. Conclusions and Recommendations

The simulation model was established based on the mechanism of a filtration model and can successfully model the experimental results of permeability reduction obtained in single sandpack tests and of conformance control obtained in parallel-sandpack models. Retention factor and capture coefficient were used in the simulation model. The correlations between the two parameters and different injection conditions were obtained through matching the results of emulsion injections in single sandpack tests at different oil qualities, sandpack permeabilities, emulsion slug sizes and injection flow rates. The obtained correlations were used to build up simulation models and successfully matched the fractional flow curves and pressure drops from parallel-sandpack tests.

It was found that good conformance control in the parellel-sandpack models can be achieved at moderate IFT and larger emulsion slug size. The injectivity needs to be taken into account when injecting O/W emulsion in sandpacks saturated with water and oil, due to the low effective permeability to water phase caused by the existing immobile oil. A simulation model was tested under this circumstance and it was found that a decrease in oil quality not only achieved good conformance control performance but also ensured the O/W emulsion can be injected into the sandpacks without creating tremendous increase in pressure drops. A critical combination of oil quality and emulsion slug size was determined by conducting sensitivity analysis on the parallel-sandpack simulation model using the O/W emulsion with a high oil viscosity.

In the conceptual field scale model, injection of O/W emulsion can effectively block high permeability zones and divert dilation fluid to low permeability zones, resulting in better steam chamber growth, lower cSOR, and higher cumulative oil production. This proved that O/W emulsion treatment can improve the performance of the dilation start-up process used for SAGD conformance control in heterogeneous oil sands reservoirs.

The emulsion droplet size can be considered to use in the simulation model to investigate the effect of droplet size on conformance control performance for the future work. The economic analysis of applying O/W emulsion treatment for SAGD conformance control is recommended to be conducted before the start of a real SAGD field work.

References

Bai, B., Zhang, H., (2011). Performed-particle-gel transport through open fractures and its effect on water flow. *SPE Journal*, 16(2), 388-400.

Borling, D., Chan, K., Hughes, T., Sydansk, R., (1994). Pushing out the oil with conformance control. *Oilfield Review*, 6(2), 44-58.

Butler, R. M., Stephens, D. J., (1981). The gravity drainage of steam-heated heavy oil to parallel horizontal wells. *Journal of Canadian Petroleum Technology*, 20(02).

Butler, R. M., (1987). Rise of interfering steam chambers. *Journal of Canadian Petroleum Technology*, 26(03).

Butler, R. M., (1998). SAGD Comes of Age. *Journal of Canadian Petroleum Technology*. 37(7), 9-12.

Dai, C., You, Q., Zhao, F., (2010). In-depth Profile Control Technologies in China—A Review of the State of the Art, *Petrol Sci Technol*, 28, 1307–1315.

Demikhova, I. I., Likhanova, N. V., Hernandez Perez, J. R., Lopez Falcon, D. A., Olivares-Xometl, O., Moctezuma Berthier, A. E., Lijanova. I. V., (2016). Emulsion flooding for enhanced oil recovery: Filtration model and numerical simulation. *Journal of Petroleum Science and Engineering*, 143, 235-244.

Ding, B., Yu, L., Dong, M., Gates, I. D., (2019). Study of Conformance control in oil sands by oil-in-water emulsion injection using heterogeneous parallel-sandpack models. *Fuel*, 244, 335-351.

Doan L. T., Baird H., Doan Q. T., Farouq-Ali S. M., (1999). An Investigation of the Steam-Assisted Gravity-Drainage Process in the Presence of a Water Leg. SPE-56545 presented at SPE Annual Technical Conference and Exhibition, Houston, Texas, 3-6.

Dong, M., Liu, Q., Li, A., (2012). Displacement mechanisms of enhanced heavy oil recovery by alkaline flooding in a micromodel, *Particuology*, 10, 298–305.

Edmunds, N., (1999). On the Difficult Birth of SAGD. *Journal of Canadian Petroleum Technology*, 38, 14-24.

Edmunds, N., Chhina, H., (2001). Economic Optimum Operating Pressure for SAGD Projects in Alberta. *Journal of Canadian Petroleum Technology*. 4, 13-17.

El-Karsani, K. S. M., Al-Muntasheri, G. A., Hussein, I. A., (2014). Polymer Systems for Water Shutoff and Profile Modification: A Review over the Last Decade. *SPE J*, 135-148.

Gates, I. D., Chakrabarty, N., (2008). Design of the steam and solvent injection strategy in expanding solvent steam-assisted gravity drainage. *Journal of Canadian Petroleum Technology*, 47(09).

Gotawala, D. R., Gates, I. D., (2010). On the Impact of Permeability Heterogeneity on SAGD Steam Chamber Growth. *Natural Resources Research*, 19(2), 151-164.

Gotawala, D. R., Gates, I. D., (2011). Stability of the Edge of a SAGD Steam Chamber in a Bitumen Reservoir. *Chemical Engineering Science*, 66, 1802-1809.

Gotawala, D. R., Gates, I. D., (2012). A basis for Automated Control of Steam Trap Subcool in SAGD. *SPE Journal*, 17(03), 1802-1809.

Imqam, A., Bai, B., (2015). Optimizing the strength and size of performed particle gels for better conformance control treatment. *Fuel*. 148, 178-185.

Ito, Y., Ipek, G., (2005). Steam fingering phenomenon during SAGD process. *SPE* 97729 presented at International Thermal Operations and Heavy Oil Symposium, Calgary, Alberta, Canada.

Jamin, J., (1860). Notes about equilibrium and flow of fluids in porous body. *Acad. Sci.* 50, 172.

Jennings, H. Y., Jr., Johnson, C. E., Jr., and McAuliffe, C. D. 1974. A caustic waterflooding process for heavy oils. *Journal of Petroleum Technology*, 26, 1344–1352.

Kabir, A. H., (2001). Chemical water & gas shutoff technology-An overview. *InSPE Latin Asia Pacific Improved Oil Recovery Conference.*

Liu, L., Xiang, W., Zhang, J., (2010). Study on the rheology of the crude oil emulsion of the Bohai oilfield. *Journal of southwest petroleum university (science & technology edition)*, 32(6), 143-146.

Liu, Q., Dong, M., Yue, X., Hou, J., (2006). Synergy of alkali and surfactant in emulsification of heavy oil in brine. *Colloids Surfaces A Physicochem Eng Asp*. 273, 219-228.

Liu, Z., Li, Y., Lv, J., Li, B., Chen, Y., (2017). Optimization of Polymer flooding design in conglomerate reservoirs. *Journal of Petroleum Science and Engineering*. 152, 267-274.

Mandal, A.; Samanta, A.; Bera, A.; Ojha, K., (2010). Characterization of Oil− Water Emulsion and Its Use in Enhanced Oil Recovery. *Industrial & Engineering Chemistry Research*. 49 (24), 12756−12761.

McAuliffe, C. D., (1973a). Oil-in-water emulsions and their flow properties in porous media. *Journal of Petroleum Technology*, 25, 727–733.

McAuliffe, C. D., (1973b). Crude-oil-in-water emulsions to improve fluid flow in an oil reservoir. *Journal of Petroleum Technology*, 25, 721–726.

Moradi-Araghi, A., (2010). A Review of Thermally Stable Gels for Fluid Diversion in Petroleum Production. *J Petrol Sci Eng*, 26 (1), 1–10.

Nasr, T.N., Ayodele, O.R., (2005). Thermal techniques for the recovery of heavy oil and bitumen, Society of Petroleum Engineering, *Alberta Research Council (ARC)*, Paper No- 97488.

Nasr T.N., Law D.H.S., Golbeck H., Korpany G., (2000). Counter-current Aspect of the SAGD Process. *Journal of Canadian Petroleum Technology*, 39, 41-47.

Parmar G., Zhao L., Graham, J., (2009). Start-up of SAGD Wells: History Match, Wellbore Design and Operation; *Journal of Canadian Petroleum Technology*, 48, 42-48.

Romero, L., Ziritt, J. L., Marin, A., Rojas, F., Mogollón, J. L., Paz, E. M. F., (1996). Plugging of high permeability-fractured zones using emulsions. *In SPE/DOE Improved Oil Recovery Symposium. Society of Petroleum Engineers*.

Sagitani, H., (1981). Making homogeneous and fine droplet O/W emulsion using nonionic surfactants. *Journal of the American Oil Chemists' Society.* 58(6), 738-743.

Sang, Q., Li, Y., Yu, L., Li, Z., Dong, M., (2014). Enhanced oil recovery by branched-performed particle gel injection in parallel-sandpack models. *Fuel*. 136, 295-306.

Shin, H., Choe, J., (2009). Shale barrier effects on the SAGD performance. Society of Petroleum Engineers: Houston, TX, USA.19-21.

Soo, H., Radke, C. J., (1984). Flow mechanism of dilute, stable emulsions in porous media. *Industrial & Engineering Chemistry Fundamentals*. 23(3), 342-347.

Soo, H., Radke, C. J., (1986). A filtration model for the flow of dilute, stable emulsions in porous media—I. Theory. *Chemical Engineering Science*. 41(2):263-272.

Vincent K. D., MacKinnon C. J., Palmgren C. T. S., (2004). Developing SAGD Operating Strategy using a Coupled Wellbore Thermal Reservoir Simulator. SPE-86970 presented at SPE International Thermal Operations and Heavy Oil Symposium and Western Regional Meeting, California, 16-18.

Wang, J., Dong, M., (2010). Simulation of O/W Emulsion Flow in Alkaline/Surfactant Flood for Heavy Oil Recovery. *Journal of Canadian Petroleum Technology*, 49(6), 46 – 52.

Wang J. Y., Ezeuko C. C., Gates I. D., (2012). Energy (Heat) Distribution and Transformation in the SAGD Process, SPE-157808 presented at SPE Heavy Oil Conference Canada, 12-14 June 2012, Calgary, Alberta, Canada.

Yu, L., Sang, Q., Dong, M., Yuan, Y., (2017). Effects of interfacial tension and droplet size on plugging performance of oil-in-water emulsions in porous media. *Industrial & Engineering Chemistry Research.* 56(32), 9237-9246.

Yu, L., Dong, M., Ding, B., Yuan, Y., (2018a). Emulsification of heavy crude oil in brine and its plugging performance in porous media. *Chemical Engineering Science*, 178, 335-347.

Yu, L., Dong, M.. Ding, B., Yuan, Y., (2018b). Experimental study on the effect of interfacial tension on the conformance control of oil-in-water emulsions in heterogeneous oil sands reservoirs. *Chemical Engineering Science*, 189, 165-178.

Yuan, Y., C., Yang, B., Xu, B., (2011). Fracturing in the Oil-Sands Reservoirs, Paper *GSUG/SPE* 149308 presented at the Canadian Unconventional Resources Conference, Calgary, Alberta, Canada, 15-17.

Yuan J. Y., McFarlane, R., (2009). Evaluation of Steam Circulation Strategies for SAGD Start-Up, *Paper CIPC* 2009-14 presented at the Canadian International Petroleum Conference, Calgary, Alberta, Canada, 16-18.

Yuan, X., Dou, S., Chen, S., Xu, B., (2013). Consideration of Geomechanics for In-situ Bitumen Recovery in Xinjiang, China. *SPE* 165414 presented at Heavy Oil Conference, Calgary, Alberta, Canada, 11-13.

Zhang, J., Fan, Y., Xu, B., Yuan, Y., (2016). Steam Circulation Strategies for SAGD Wells After Geomechanical Dilation Start-Up, Paper *SPE* 180705 presented at Canada Heavy Oil Technical Conference, Calgary, Alberta, Canada, 7-9.

Zhou, Y., Yin, D., Chen, W., Liu, B., Zhang, X., (2019). A comprehensive review of emulsion and its field application for enhanced oil recovery. *Energy Sci Eng*, 7, 1046-1058.

Appendix

Copyright Clearance Center Marketplace™

Society of Petroleum Engineers (SPE) - License Terms and Conditions

Order Date	19-Dec-2019
Order license ID	1009939-1
ISBN-13	978-1-61399-619-5
Type of Use	Republish in a thesis/dissertation
Publisher	International Petroleum Technology Conference
Portion	Chapter/article

LICENSED CONTENT

Publication Title	International Petroleum Technology Conference	Country	United States of America
Author/Editor	International Petroleum Technology Conference	Rightsholder	Society of Petroleum Engineers (SPE)
Date	12/31/2018	Publication Type	Conference Proceeding
Language	English		

REQUEST DETAILS

Portion Type	Chapter/article	Rights Requested	Main product
Page range(s)	1-21	Distribution	Worldwide
Total number of pages	21	Translation	Original language of publication
Format (select all that apply)	Electronic	Copies for the disabled?	No
Who will republish the content?	Academic institution	Minor editing privileges?	Yes
Duration of Use	Life of current edition	Incidental promotional use?	Yes
Lifetime Unit Quantity	Up to 499	Currency	CAD

NEW WORK DETAILS

Title	Conformance Control for SAGD Using Oil-in-Water Emulsions in Heterogeneous Oil Sands Reservoirs	Institution name	University of Calgary
		Expected presentation date	2019-12-18
Instructor name	Dr. Mingzhe Dong		

ADDITIONAL DETAILS

Order reference number	N/A	The requesting person / organization to appear on the license	Yidan Ni

REUSE CONTENT DETAILS

Title, description or numeric reference of the portion(s)	Conformance Control for SAGD Using Oil-in-Water Emulsions in Heterogeneous Oil Sands Reservoirs	**Title of the article/chapter the portion is from**	Conformance Control for SAGD Using Oil-in-Water Emulsions in Heterogeneous Oil Sands Reservoirs
Editor of portion(s)	N/A	**Author of portion(s)**	International Petroleum Technology Conference
Volume of serial or monograph	N/A	**Issue, if republishing an article from a serial**	N/A
Page or page range of portion	1-21	**Publication date of portion**	2018-12-18

PUBLISHER SPECIAL TERMS AND CONDITIONS

Person requesting republication permission is an author of IPTC-19079-MS.

CCC Republication Terms and Conditions

1. Description of Service; Defined Terms. This Republication License enables the User to obtain licenses for republication of one or more copyrighted works as described in detail on the relevant Order Confirmation (the "Work(s)"). Copyright Clearance Center, Inc. ("CCC") grants licenses through the Service on behalf of the rightsholder identified on the Order Confirmation (the "Rightsholder"). "Republication", as used herein, generally means the inclusion of a Work, in whole or in part, in a new work or works, also as described on the Order Confirmation. "User", as used herein, means the person or entity making such republication.

2. The terms set forth in the relevant Order Confirmation, and any terms set by the Rightsholder with respect to a particular Work, govern the terms of use of Works in connection with the Service. By using the Service, the person transacting for a republication license on behalf of the User represents and warrants that he/she/it (a) has been duly authorized by the User to accept, and hereby does accept, all such terms and conditions on behalf of User, and (b) shall inform User of all such terms and conditions. In the event such person is a "freelancer" or other third party independent of User and CCC, such party shall be deemed jointly a "User" for purposes of these terms and conditions. In any event, User shall be deemed to have accepted and agreed to all such terms and conditions if User republishes the Work in any fashion.

3. Scope of License; Limitations and Obligations.

    3.1. All Works and all rights therein, including copyright rights, remain the sole and exclusive property of the Rightsholder. The license created by the exchange of an Order Confirmation (and/or any invoice) and payment by User of the full amount set forth on that document includes only those rights expressly set forth in the Order Confirmation and in these terms and conditions, and conveys no other rights in the Work(s) to User. All rights not expressly granted are hereby reserved.

    3.2. General Payment Terms: You may pay by credit card or through an account with us payable at the end of the month. If you and we agree that you may establish a standing account with CCC, then the following terms apply: Remit Payment to: Copyright Clearance Center, 29118 Network Place, Chicago, IL 60673-1291. Payments Due: Invoices are payable upon their delivery to you (or upon our notice to you that they are available to you for downloading). After 30 days, outstanding amounts will be subject to a service charge of 1-1/2% per month or, if less, the maximum rate allowed by applicable law. Unless otherwise specifically set forth in the Order Confirmation or in a separate written agreement signed by CCC, invoices are due and payable on "net 30" terms. While User may exercise the rights licensed immediately upon issuance of the Order Confirmation, the license is automatically revoked and is null and void, as if it had never been issued, if complete payment for the license is not received on a timely basis either from User directly or through a payment agent, such as a credit card company.

    3.3.
    Unless otherwise provided in the Order Confirmation, any grant of rights to User (i) is "one-time" (including the editions and product family specified in the license), (ii) is non-exclusive and non-transferable and (iii)

is subject to any and all limitations and restrictions (such as, but not limited to, limitations on duration of use or circulation) included in the Order Confirmation or invoice and/or in these terms and conditions. Upon completion of the licensed use, User shall either secure a new permission for further use of the Work(s) or immediately cease any new use of the Work(s) and shall render inaccessible (such as by deleting or by removing or severing links or other locators) any further copies of the Work (except for copies printed on paper in accordance with this license and still in User's stock at the end of such period).

3.4. In the event that the material for which a republication license is sought includes third party materials (such as photographs, illustrations, graphs, inserts and similar materials) which are identified in such material as having been used by permission, User is responsible for identifying, and seeking separate licenses (under this Service or otherwise) for, any of such third party materials; without a separate license, such third party materials may not be used.

3.5. Use of proper copyright notice for a Work is required as a condition of any license granted under the Service. Unless otherwise provided in the Order Confirmation, a proper copyright notice will read substantially as follows: "Republished with permission of [Rightsholder's name], from [Work's title, author, volume, edition number and year of copyright]; permission conveyed through Copyright Clearance Center, Inc. " Such notice must be provided in a reasonably legible font size and must be placed either immediately adjacent to the Work as used (for example, as part of a by-line or footnote but not as a separate electronic link) or in the place where substantially all other credits or notices for the new work containing the republished Work are located. Failure to include the required notice results in loss to the Rightsholder and CCC, and the User shall be liable to pay liquidated damages for each such failure equal to twice the use fee specified in the Order Confirmation, in addition to the use fee itself and any other fees and charges specified.

3.6. User may only make alterations to the Work if and as expressly set forth in the Order Confirmation. No Work may be used in any way that is defamatory, violates the rights of third parties (including such third parties' rights of copyright, privacy, publicity, or other tangible or intangible property), or is otherwise illegal, sexually explicit or obscene. In addition, User may not conjoin a Work with any other material that may result in damage to the reputation of the Rightsholder. User agrees to inform CCC if it becomes aware of any infringement of any rights in a Work and to cooperate with any reasonable request of CCC or the Rightsholder in connection therewith.

4. Indemnity. User hereby indemnifies and agrees to defend the Rightsholder and CCC, and their respective employees and directors, against all claims, liability, damages, costs and expenses, including legal fees and expenses, arising out of any use of a Work beyond the scope of the rights granted herein, or any use of a Work which has been altered in any unauthorized way by User, including claims of defamation or infringement of rights of copyright, publicity, privacy or other tangible or intangible property.

5. Limitation of Liability. UNDER NO CIRCUMSTANCES WILL CCC OR THE RIGHTSHOLDER BE LIABLE FOR ANY DIRECT, INDIRECT, CONSEQUENTIAL OR INCIDENTAL DAMAGES (INCLUDING WITHOUT LIMITATION DAMAGES FOR LOSS OF BUSINESS PROFITS OR INFORMATION, OR FOR BUSINESS INTERRUPTION) ARISING OUT OF THE USE OR INABILITY TO USE A WORK, EVEN IF ONE OF THEM HAS BEEN ADVISED OF THE POSSIBILITY OF SUCH DAMAGES. In any event, the total liability of the Rightsholder and CCC (including their respective employees and directors) shall not exceed the total amount actually paid by User for this license. User assumes full liability for the actions and omissions of its principals, employees, agents, affiliates, successors and assigns.

6. Limited Warranties. THE WORK(S) AND RIGHT(S) ARE PROVIDED "AS IS". CCC HAS THE RIGHT TO GRANT TO USER THE RIGHTS GRANTED IN THE ORDER CONFIRMATION DOCUMENT. CCC AND THE RIGHTSHOLDER DISCLAIM ALL OTHER WARRANTIES RELATING TO THE WORK(S) AND RIGHT(S), EITHER EXPRESS OR IMPLIED, INCLUDING WITHOUT LIMITATION IMPLIED WARRANTIES OF MERCHANTABILITY OR FITNESS FOR A PARTICULAR PURPOSE. ADDITIONAL RIGHTS MAY BE REQUIRED TO USE ILLUSTRATIONS, GRAPHS, PHOTOGRAPHS, ABSTRACTS, INSERTS OR OTHER PORTIONS OF THE WORK (AS OPPOSED TO THE ENTIRE WORK) IN A MANNER CONTEMPLATED BY USER; USER UNDERSTANDS AND AGREES THAT NEITHER CCC NOR THE RIGHTSHOLDER MAY HAVE SUCH ADDITIONAL RIGHTS TO GRANT.

7. Effect of Breach. Any failure by User to pay any amount when due, or any use by User of a Work beyond the scope of the license set forth in the Order Confirmation and/or these terms and conditions, shall be a material breach of the license created by the Order Confirmation and these terms and conditions. Any breach not cured within 30 days of written notice thereof shall result in immediate termination of such license without further notice. Any unauthorized (but licensable) use of a Work that is terminated immediately upon notice thereof may be liquidated by payment of the Rightsholder's ordinary license price therefor; any unauthorized (and unlicensable) use that is not terminated immediately for any reason (including, for example, because materials containing the Work cannot reasonably be recalled) will be subject to all remedies available at law or in equity, but in no event to a payment of less than three times the Rightsholder's ordinary license price for the most closely analogous licensable use plus Rightsholder's and/or CCC's costs and expenses incurred in collecting such payment.

8. Miscellaneous.

    8.1. User acknowledges that CCC may, from time to time, make changes or additions to the Service or to these terms and conditions, and CCC reserves the right to send notice to the User by electronic mail or otherwise for the purposes of notifying User of such changes or additions; provided that any such changes or additions shall not apply to permissions already secured and paid for.

    8.2. Use of User-related information collected through the Service is governed by CCC's privacy policy, available online here: https://marketplace.copyright.com/rs-ui-web/mp/privacy-policy

    8.3. The licensing transaction described in the Order Confirmation is personal to User. Therefore, User may not assign or transfer to any other person (whether a natural person or an organization of any kind) the license created by the Order Confirmation and these terms and conditions or any rights granted hereunder; provided, however, that User may assign such license in its entirety on written notice to CCC in the event of a transfer of all or substantially all of User's rights in the new material which includes the Work(s) licensed under this Service.

    8.4. No amendment or waiver of any terms is binding unless set forth in writing and signed by the parties. The Rightsholder and CCC hereby object to any terms contained in any writing prepared by the User or its principals, employees, agents or affiliates and purporting to govern or otherwise relate to the licensing transaction described in the Order Confirmation, which terms are in any way inconsistent with any terms set forth in the Order Confirmation and/or in these terms and conditions or CCC's standard operating procedures, whether such writing is prepared prior to, simultaneously with or subsequent to the Order Confirmation, and whether such writing appears on a copy of the Order Confirmation or in a separate instrument.

    8.5. The licensing transaction described in the Order Confirmation document shall be governed by and construed under the law of the State of New York, USA, without regard to the principles thereof of conflicts of law. Any case, controversy, suit, action, or proceeding arising out of, in connection with, or related to such licensing transaction shall be brought, at CCC's sole discretion, in any federal or state court located in the County of New York, State of New York, USA, or in any federal or state court whose geographical jurisdiction covers the location of the Rightsholder set forth in the Order Confirmation. The parties expressly submit to the personal jurisdiction and venue of each such federal or state court.If you have any comments or questions about the Service or Copyright Clearance Center, please contact us at 978-750-8400 or send an e-mail to support@copyright.com.

v 1.1